UNIVERSITÀ DEGLI STUDI DI PADOVA

Dipartimento di Fisica e Astronomia "Galileo Galilei"

Master Degree in Physics

Final Dissertation

Prediction of optically-induced vibrations in large biomolecules

Thesis supervisor

Prof. Pier Luigi Silvestrelli

Thesis co-supervisor

Dr. Alberto Ambrosetti

Candidate

Leonardo Giammorcaro

Academic Year 2022/2023

Abstract

Non-covalent van Der Waals (vdW) forces are due to coupled-dipole oscillations, and with their long-range they play a key role in determining structural and mechanical properties of large molecules, thereby actively influencing the vibrational spectra. When molecules undergo optical excitation, non-local charge oscillation modes can be activated, causing a dramatic change of vdW interactions that introduces non-local stress in the molecular structure. Collective vibrational modes are thus expected to be activated by energy transfer from these optical charge-fluctuation modes.
Semi-classical and quantum-mechanical models for the interaction between charge oscillations and vibrational modes are proposed here, based on the many-body dispersion (MBD) model, where the electronic description is reduced to a set of coupled quantum harmonic oscillators.
The aim is to study the activation of vibrational modes, analyzing the transition between relevant quantum states within a perturbative framework, and to specifically analyze molecular systems such as photo-receptors and host-guest complexes. The activation of vibrational modes is first addressed within a semi-classical approach, where optical vdW forces are directly coupled to the available vibrational modes. Subsequently, a rigorous quantum-mechanical framework is developed to overcome the Born-Oppenheimer approximation, providing a quantum correction to the semi-classical approach.
Analysis of the combined optical and vibrational transitions in the benzene monomer, the C_{60}-catcher supramolecular complex, the 11-cis-retinal and the photoactive yellow protein consistently reveals that: i) only a few vibrational modes could be optically activated, which indicates the emergence effective selection rules; ii) quantum corrections to transition rates can be larger than the semi-classical predictions, which demonstrates the key role of a rigorous quantum approach; iii) the selectivity of the coupling mechanism with respect to both optical and vibrational modes is qualitatively compatible with recent experimental observations on bovine proteins, which indicate macroscopic energy conversion from absorbed light into a single vibrational mode.

Contents

Chapter 1

Introduction

One of the paradigms of sciences that delve into the study, concept, and origin of life, is the complexity and interconnection among systems, whether they be simple molecules or more intricate protein structures, or macromolecules of various kinds. This complexity is often embodied in phenomena that can be termed 'collective' or 'emergent'. The identification of a macromolecule by its function in relation to other systems, rather than as a mere sum of components, does not directly depend on the single chemical bonds and short-range interactions, but it rather involves mechanisms capable of influencing much larger scales. The duality between identity and function is certainly one of the guiding principles that sciences with non-reductionist approach tend to address. The global properties of a system are often connected to collective phenomena. Due to the ability to relate entities across a wide range of scales, collective phenomena provide precious information about macroscopic properties and functions, also in relation with other systems.
Currently, there is a growing interest in physical theories trying to address phenomena that have already been extensively characterized and are coherent within biological and chemical theories. This approach can create a solid bridge between disciplines, each of which is founded upon postulates and tenets that are not necessarily congruent with those of other disciplines.
We note that local descriptions, based on knowledge of all parameters involving each component of a physical system can be surpassed in predictivity and significance by a global approach, capable of encompassing emergent properties with fewer relevant parameters. In spite of all technical and computational advances, predicting the physical properties of biologically relevant systems, such as proteins, in a reductionist spirit remains energy and time-intensive – and often conceptually limiting.

An intriguing and largely unexplored feature of both biomolecules and nanostructures is the mechanical response to light absorption. When optical photons are absorbed, electrons can undergo photoexcitation, producing charge displacements that eventually cause the appearance of mechanical stress. The computation of all ionic forces caused by photoexcitation can be accomplished in principle [20] within the Bethe-Salpeter equation (BSE) framework. However, this approach is extremely demanding from the computational point of view, so that BSE force calculations are realistically limited to a few atoms, and cannot be presently extended to large-scale systems such as proteins or host-guest nanosystems. However, recent work [3] demonstrated that a more efficient coarse-grained approach (many-body dispersion [5] - or MBD), based on coupled quantum harmonic oscillators, can be exploited when only long-range optical van der Waals (vdW) forces are demanded. Optical vdW forces are due to collective charge displacements induced by photoexcitations, and can exhibit extremely non-local character. These forces can interest the whole structure, and are accordingly expected to cause non-local mechanical distortions, and collective vibrations. Within the MBD model, the dipole response of each atom is mapped into a charged quantum harmonic oscillator, bound to the atomic nucleus. The Coulomb coupling between all atom-centered oscillators implies a full many-body treatment of dipole oscillations, that are responsible for dispersion and optical vdW forces. The non-local features of long-range charge oscillations are thus naturally inbuilt in MBD.

The aim of this work is to investigate how the photoexcitation of collective charge-fluctuation modes, that are responsible for optical vdW forces, is eventually traduced into quantum mechanical vibrations. Molecular vibrations are thus explored in this thesis as induced by the interaction between electronic and ionic degrees of freedom. The significance of molecular vibrational modes is now well-established, as evidenced by recent findings linking theory to biologically relevant processes such as protein folding and intracellular signaling, as well as to properties involving the geometric structure of a molecular system in general.

This thesis will introduce a rigorous quantum mechanical theory for the quasi-electron–phonon coupling, beyond the Born-Oppenheimer approximation, and will be applied to large-scale systems that could not be addressed within the standard BSE framework. Despite the various contributions on electron-phonon interactions (EPI), (for an overview see F. Giustino, *Electron-phonon interactions from first principles* [10]), large-scale effects still pose major challenges, which we try to address here.

1.1 Main contribution to electron-phonon coupling

One of the most significant and pioneering contributions to electron-phonon interaction (EPI) or coupling (EPC) can be traced back to the works of Herbert Fröhlich [9], characterized by the introduction of the quasi-particle known as the 'polaron'. This quasi-particle denotes the polarization of the crystalline lattice that is created by a charge distortion. In Fröhlich's model, this distortion gives rise to lattice vibrations capable of propagating, undergoing scattering processes, and reciprocally influencing the motion and energy of electrons, all within a self-consistent process. Formally, Fröhlich's theory is founded on the 'Fröhlich Hamiltonian', from which, employing a second quantization formalism, the fundamental parameter representing the coupling strength between vibrations and electrons, known as the 'Fröhlich coupling constant', is derived. This constant depends on electronic masses, phonon frequency, and dielectric constants. The values of these constants are now established for several solids. Good for studying superconductivity, semiconductors, and charge transfer, it represents a simplified model that may not fully catch all aspects of the complex EPI that occur in real materials.
Another popular model, highly compatible with the study of systems amenable to 'ab initio' numerical simulations, is reported in [10]. The Kohn-Sham DFT formalism is identified here as the foundational framework for coupling electrons and phonons, which emerges by expanding the Kohn-Sham effective potential to first order for small atomic displacements. The result is a coupling Hamiltonian dependent on 'electron-phonon matrix elements'. Furthermore, building upon the Fröhlich and Kohn-Sham DFT frameworks, the Migdal-Eliashberg theory [22] provides a comprehensive approach to electron-phonon coupling in superconductors. While Fröhlich's theory mainly focuses on weak-coupling regimes, the Migdal-Eliashberg theory extends its applicability to the strong-coupling regime, where electron-phonon interactions are more significant. The focal point of this theory is the capability of prediction of the superconductive gap, i.e. the energy involved in the separation of electrons involved in the Cooper pair bounded state (see BCS theory), and the critical temperature for superconduction threshold. In quantum field theory, the electron-phonon coupling is instead based on the assumption of introducing Green's functions for electrons and ions, according to the following scheme [10]. The non-relativistic 'electron-phonon' Hamiltonian is defined using second quantization operators. Then the single-electron zero-temperature Green function G_{el} is introduced. Evaluating the thermal average of Schrödinger's equation, a new equation for G_{el} arises. Inside it, a new term appears, namely the scalar electric potential which couples to both electronic and ionic degrees of freedom. The latter is used as a perturbative term. Eventually, by studying both the time and space evolution of the system, the ionic 'displacement-displacement' correlation function is obtained. The displacement-displacement correlation function measures how the displacement of a particle is correlated with the displacement of another one, at different (or equal) times. Without going into details, this correlation function is used for calculating the screened Coulomb potential, which provides the interaction strength for the electron-phonon coupling.

1.2 Molecular vibrations in structural biology

Biological molecules are extremely complex systems, whose geometrical, dynamical, and functional features can be hardly predicted by a unified theory. However, despite the approximations necessarily introduced in their modeling, significant correlations are found between experimental results, theoretical insights, and numerical simulations. An intriguing, and yet largely unexplored aspect involves the conversion of light absorption into mechanical vibrations. When a normal vibrational mode [32] is excited, atoms coherently fluctuate along preferred directions around the equilibrium positions, sharing a frequency that pervades the entire system. Theoretical assessments of these vibrations often involve the harmonic approximation to the interatomic potential. From now on, molecular vibrations and phonons will be referred to interchangeably; the only distinction lies in the fact that in the case of molecular vibrations, the absence of periodic structure prevents propagation of vibrations, whereas, in the context of crystalline lattices, the phonon acquires quasi-particle properties.
The significance of molecular vibrations is evidenced by their role (not yet systematically understood) in biological phenomena. These phenomena include protein folding and misfolding [19], which are

understood as the processes by which a protein chain assumes or loses its three-dimensional structure, referred to as tertiary structure. The structure undergoes changes via energy minimization, implying the participation of the vibrational spectrum in this process.

The role of molecular vibrations has been also supposed in intracellular signaling, the process in which cell information is propagated to other ones with a signal transduction; molecular vibrations in the infrared frequency range play a pivotal role in the emission and resonance of electromagnetic patterns capable of activating enzymes [17]. This process implies the presence of some efficient EPC mechanism. Relevant EPC effects have also been confirmed in recent experiments [21], wherein following excitation induced by optical pumping, bovine serum albumin exhibited pronounced occupation of vibrational modes at a specific frequency (0.314 THz) [25].
Vibrational spectroscopy is also powerful in the inspection of the enzyme-carrier interactions [27].

This thesis will first investigate molecular vibrations in their theoretical and computational aspects as an independent phenomenon. Subsequently, it will propose models capable of predicting EPC. The focus will be on the activation of normal modes of vibration, due to excitation of collective electronic modes (excitons), within the MBD theoretical framework. As previously mentioned, long-range excitons activate optical van der Waals forces. These forces can be treated semi-classically or quantum mechanically, and facilitate the construction of rigorous models wherein the activation of vibrational modes is obtained by time-evolution of a suitable wavefunction within perturbation theory.
This thesis will also try to understand whether phenomena such as photoisomerization of photoreceptors can be explained (and to what extent). One of the macromolecules involved in human vision is rhodopsin. This molecules is found in the rods of the retina and it is composed of two substructures, opsin and retinal. The latter, also known as retinaldehyde or vitamin A aldehyde, is a small-sized molecule (49 atoms) bound to opsin. In its bound state, retinal is inactive and, in animal organisms, it exists in the 11-cis configuration. Upon absorption of a photon, the retinal undergoes isomerization to the all-trans structure. Assuming an all-trans configuration, rhodopsin sets off a signaling cascade, prompting the activation of enzymes and ion channels within the photoreceptor cell. This sequence of events culminates in the production of electrical signals (action potential) that get transmitted to the brain through the optic nerve. Another photoreceptor protein is the photoactive yellow protein (PYP), which is present in different bacteria. The p-coumaric acid, which is chemically bound within the protein, reacts to light absorption (around 446 nm, i.e. 2.77 eV) [15] by isomerization. This triggers structural changes in the protein, that influence its activity.
The number of atoms in rhodopsin is quite high (5068 [26]); therefore, retinal will be analyzed as an independent structure. Conversely, PYP has a number of atoms (1912) that allows for the comprehensive study of its entire structure with the available computational resources, and will be fully analyzed in this thesis.
However, the aforementioned structural changes imply rearrangements of chemical bonds, and such effects (being local and short-ranged) are poorly described a priori only in terms of vdW forces.
Nonetheless, it is still relevant to observe whether there are electronic excitations that could facilitate or contribute to the process. Furthermore, the role of molecular vibrations in the isomerization process is not entirely clear. There is a body of research from the early 2000s, which, however, does not appear to have yielded definitive answers; for the most significant contributions, reference can be made to [12].

Due to the long-range and non-local character of vdW interactions, the MBD theory is expected to mainly address large-scale collective phenomena. For instance, we will consider macromolecules and host-guest systems, where vdW forces can play a major role. Host-guest complexes are particularly relevant in supramolecular chemistry, having implications in several areas, such as molecular recognition, molecular delivery, and so on. More details are found in Ambrosetti et al. *Hard Numbers for Large Molecules: Toward Exact Energetics for Supramolecular Systems* [4]. This work indicates that the interaction energies of such complexes are extremely sensitive to many body effects, so that contributions beyond (standard) pairwise London dispersion and Axilrod-Teller terms are necessary for a reliable description. Molecular vibrations may also play a crucial role in the interaction between host and guest, since the structure of the 'host' molecule directly influences the van der Waals forces

experienced by the 'guest' molecule.

Chapter 2

Many body dispersion

2.1 Theory of Many body dispersion

2.1.1 Many body dispersion hamiltonian

The concept of many-body dispersion is associated to the collective interaction that emerges within atomic structures as a result of van der Waals (vdW) forces. The description of dispersion forces owes its development to various contributions in the field of computational chemistry and condensed matter physics, such as the TS method [30] by A. Tkatchenko and M. Scheffler, the D2 method by S. Grimme [13], the many-body dispersion (MBD) approach by A. Ambrosetti et al. [5], and many others. Their work has provided valuable insights into the role of quantum mechanical effects in intermolecular forces and has led to improved computational models for describing the properties of materials and molecules. In the context of many-body dispersion, vdW intermolecular forces are not solely limited to pairwise interactions between individual particles. Instead, they encompass interactions involving multiple particles simultaneously. This collective behavior arises due to the quantum mechanical nature of electrons and their distribution around atoms or molecules.
The Coupled Fluctuating Dipole Model (CFDM) provides a description of molecular systems by considering them as a collection of coupled three-dimensional quantum harmonic oscillators (QHOs). CFDM is primarily used for computing the many-body van der Waals (vdW) energy. Within CFDM, each atom is associated to a (charged) QHO, also called "quantum Drude oscillator" (QDO). By replacing the true set of electrons and protons of an atom with a single negatively charged light quasiparticle, harmonically bound to a positively charged heavy quasinucleus, the Drude oscillator model emulates the electronic response to applied electric fields. The "drudon", i.e. the quantum Drude "quasiparticle", has a negative charge $-q$, and is balanced by a classical particle, the Drude "nucleus" that is placed at the center of oscillation and is characterized by an opposite charge. The drudon mimics the effect of the electron cloud surrounding ions, and its characteristic parameters are the charge, the mass and the frequency, that are determined computationally in the framework of density functional theory (DFT), in such a way to exactly reproduce static atomic polarizabilities and homoatomic C_6 coefficients. All QDO's are coupled: the long range interactions between different electron clouds are described by the dipole-dipole interaction tensor $\boldsymbol{T}$, which depends on the atomic distances. The physical model describing a system of drudons and Drude nuclei is a set of interacting quantum harmonic oscillators [7].

The dipole moments of the atoms are considered to be the primary contributors to intermolecular dispersion interactions. This corresponds to the adoption of the dipole-dipole approximation, which is valid in the long range limit. By analyzing the distribution of dipole moments and their correlations, the CFDM offers valuable insights into various properties such as structural characteristics, dielectric response, and dynamical behavior. It allows for a comprehensive understanding of the system's behavior in all phases. Although the CFDM is an effective model that neglects certain intricate aspects of molecular interactions, such as higher-order multipolar interactions and explicit treatment of charge transfer effects, it remains a useful framework for predicting and comprehending long-range interactions in molecular systems and condensed phases.

The expressions "Many-Body Dispersion (MBD) Hamiltonian" and "Coupled Fluctuating Dipole Model (CFDM) Hamiltonian" can be used interchangeably. From now on, we will uniquely refer to the "MBD Hamiltonian" to indicate the following expression:

$$\hat{H}_{mbd} = -\frac{1}{2}\sum_{i=1}^{N}\frac{\nabla^2_{\boldsymbol{\zeta}_i}}{\tilde{m}_i} + \frac{1}{2}\sum_{i=1}^{N}\tilde{m}_i\omega_i^2\boldsymbol{\zeta}_i^2 + \frac{1}{2}\sum_{\substack{i,j=1\\ i\neq j}}^{N} e_i e_j \boldsymbol{\zeta}_i T_{ij}(d_{ij})\boldsymbol{\zeta}_j\,. \tag{2.1}$$

Here N is the number of atoms, $\boldsymbol{\zeta}_i = \tilde{\boldsymbol{r}}_i - \boldsymbol{r}_i$ is the displacement from i-th ionic position $\boldsymbol{r}_i$ for a Drude particle at position $\tilde{\boldsymbol{r}}_{\boldsymbol{i}}$, $\boldsymbol{T}$ is the dipole-dipole interaction tensor, depending on d_{ij}, the distance between atoms i and j.
$\tilde{m}_i$ and ω_i are respectively the mass of i-th Drude oscillator and the frequency associated fluctuations in the electronic charge distribution. Rescaling displacements with oscillator masses $\boldsymbol{\xi}_i = \sqrt{\tilde{m}_i}\boldsymbol{\zeta}_i$

and introducing the polarizability $\alpha_i = \frac{q_i^2}{\tilde{m}_i \omega_i^2}$ (q is the atomic charge), such that in Hartree units $\tilde{m}_i = q^2(\alpha_i \omega_i^2)^{-1}$ [30] is equal to one, Eq.2.1 reads:

$$\hat{H}_{mbd} = -\frac{1}{2}\sum_{i=1}^{N} \nabla^2_{\boldsymbol{\xi}_i} + \frac{1}{2}\sum_{i,j}^{N} \sum_{a,b=(x,y,z)} \boldsymbol{\xi}_i^a \omega_i \omega_j \left[\delta_{ij}^{ab} + \sqrt{\alpha_i \alpha_j} T_{ij}^{ab}(d_{ij})\right] \boldsymbol{\xi}_j^b \,. \tag{2.2}$$

The description is switched from N 3D harmonic oscillators to $3N$ independent 1D harmonic oscillators:

$$\hat{H}_{mbd} = -\frac{1}{2}\sum_{p=1}^{3N} \nabla^2_{\xi_p} + \frac{1}{2}\sum_{p,q}^{3N} \xi_p \omega_p \omega_q \left[\delta_{pq} + \sqrt{\alpha_p \alpha_q} T_{pq}(d_{ij})\right] \xi_q \,. \tag{2.3}$$

It is important to emphasize the relationship between indices: $p = 3(i-1) + a$, $q = 3(j-1) + b$, where $a, b = 1, 2, 3$ (accounting for x, y, z cartesian components). We define here the matrix $\boldsymbol{C}$, which contains the interactions between electron clouds in Eq. 2.2. This is reported according to both index sets:

$$C_{ij}^{ab} = \omega_i \omega_j \left[\delta_{ij}^{ab} + \sqrt{\alpha_i \alpha_j} T_{ij}^{ab}(d_{ij})\right] , \tag{2.4}$$

$$C_{pq} = \omega_p \omega_q \left[\delta_{pq} + \sqrt{\alpha_p \alpha_q} T_{pq}(d_{ij})\right] . \tag{2.5}$$

The dipole-dipole tensor $\boldsymbol{T}$ is obtained considering the Coulomb interaction between two spherical Gaussian charge densities, which leads to the introduction of a short-range damping [29] due to charge overlap $v_{ij} = \frac{erf(d_{ij}/\sigma_{ij})}{d_{ij}}$ (here $d_{ij} = |\mathbf{r}_i - \mathbf{r}_j|$ is the distance between atoms i and j). This short-range damping is compatible with the ground state wavefunction of quantum harmonic oscillator which has a gaussian form, where $\sigma_{ij} = \sqrt{\sigma_i^2 + \sigma_j^2}$ is the gaussian width of atoms i and j.

$$T_{ij}^{ab} = \nabla_{\mathbf{r_i}} \otimes \nabla_{\mathbf{r_j}} v_{ij}^{gg} = \nabla_{\mathbf{r_i}} \otimes \nabla_{\mathbf{r_j}} \left(\frac{erf(d_{ij}/\sigma_{ij})}{d_{ij}}\right) \tag{2.6}$$

$$= -\frac{3 r_a r_b - d_{ij}^2 \delta_{ab}}{d_{ij}^5} \left(erf\left(\frac{d_{ij}}{\sigma_{ij}}\right) - \frac{2}{\sqrt{\pi}} \frac{d_{ij}}{\sigma_{ij}} e^{-\left(\frac{d_{ij}}{\sigma_{ij}}\right)^2} \right) + \frac{4}{\sqrt{\pi}} \frac{1}{\sigma_{ij}^3} \frac{r_a r_b}{d_{ij}^2} e^{-\left(\frac{d_{ij}}{\sigma_{ij}}\right)^2} \quad , \tag{2.7}$$

where in the latter $r_a = r_{ia} - r_{ja}$, i.e. the a-th component of the vector $(\mathbf{r}_i - \mathbf{r}_j)$.
The energy spectrum of the MBD hamiltonian, Eq. 2.2, is obtained from the eigenvalues $\lambda_p = \tilde{\omega}_p^2$ of $\boldsymbol{C}$, which is a symmetric $3N \times 3N$ matrix. Eventually, $\hat{H}_{mbd}$ can be reduced to normal form [11]:

$$\hat{H}_{mbd} = -\frac{1}{2}\sum_{p=1}^{3N} \nabla^2_{\chi_p} + \frac{1}{2}\sum_{p}^{3N} \chi_p^2 \tilde{\omega}_p^2 \,, \tag{2.8}$$

where $\boldsymbol{\chi}$ is the set of collective coordinates depending on the fixed ionic configuration $\boldsymbol{r}$; for each normal mode n the transformation $\chi_n = \sum_p M_{np}^T \xi_p = \sum_p M_{np}^T \sqrt{\tilde{m}_p} \zeta_p$ holds, where the matrix $\boldsymbol{M}$ contains the eigenvectors of $\boldsymbol{C}$ as columns. In atomic units, $\tilde{\omega}_n$ is the vibrational frequency (i.e. energy) of the n-th Drude normal mode, given by the square root of the n-th eigenvalues of $\boldsymbol{C}$, λ_n, which depends on the space coordinates $\boldsymbol{r}$ of the atoms. The many-body dispersion energy is finally computed as the energy difference between the interacting Drude oscillators and the independent Drude oscillators:

$$E_{mbd} = \frac{1}{2}\sum_{i=1}^{3N} \tilde{\omega}_i - 3\sum_{i=1}^{N} \omega_i \,. \tag{2.9}$$

Fig.2.1 depicts the MBD spectrum for selected molecules, aimed at comprehending the energy range of collective excitations. The spectra are obtained by applying a variable Gaussian broadening around discrete frequency values and can be compared with those presented in Ref. [3].

2.1.2 van der Waals forces

By incorporating many-body dispersion effects, MBD provides an accurate description of vdW forces, beyond the two-body pairwise approximation. The force F_{lc} exerted by an atom l along the coordinate c, is evaluated through the gradient of the many-body dispersion energy

$$F_{lc}(\boldsymbol{r}) = -\frac{\partial E(\boldsymbol{r})}{\partial r_{lc}}\,, \tag{2.10}$$

and depends on the atomic configuration $\boldsymbol{r}$.
The energy spectrum of the MBD hamiltonian is that of a set of quantum oscillators with frequencies $\tilde{\omega}$. This can be expressed as:

$$E_{mbd} = \sum_{i=1}^{3N} \tilde{\omega}_i \left(\frac{1}{2} + n_i\right) = E_{mbd}^{(0)} + E_{mbd}^{(n)}\,, \tag{2.11}$$

where $E_{mbd}^{(0)}$ is the MBD ground state, while $E_{mbd}^{(n)}$ is the excitation energy term depending on the quantum numbers n_i different from zero and it is responsible for the "optical" van der Waals forces occuring inside the atomic complex. If a single excitation of the γ-th mode occurs, then $n_\gamma = 1$ is the only quantum number different from zero, and the (single-)excitation energy associated to the "optical" vdW forces is:

$$E_{vdw}^{(\gamma)} = \tilde{\omega}_\gamma\,. \tag{2.12}$$

The frequencies $\tilde{\omega}_\gamma$ relative to the collective MBD dipole modes provide a spectrum of "single" excitations for the MBD model. The MBD spectra for benzene monomer, 11-cis-retinal, C_{60}-clamp complex and PYP are reported for instance in Fig. 2.1.

$E_{mbd}^{(0)}$ is responsible for the dispersion forces that characterize the molecule in its ground state and can be absorbed by the ion-ion potential V, for which more detailed explanations will be provided in the subsequent chapters.
Instead, optical van der Waals forces, due to the extra energy term $\tilde{\omega}_\gamma$ can be computed as the gradient of the vdW energy. Hence the force exterted by atom l along c direction, given a ionic configuration $\boldsymbol{r}$ is

$$\begin{aligned} F_{lc}^{(\gamma)}(\boldsymbol{r}) = -\frac{\partial \tilde{\omega}_\gamma}{\partial r_{lc}} &= -\frac{\partial \sqrt{\left(\boldsymbol{M}^T\boldsymbol{C}\boldsymbol{M}\right)_{\gamma\gamma}}}{\partial r_{lc}} \\ &= -\frac{1}{2\sqrt{\left(\boldsymbol{M}^T\boldsymbol{C}\boldsymbol{M}\right)_{\gamma\gamma}}} \frac{\partial \left(\boldsymbol{M}^T\boldsymbol{C}\boldsymbol{M}\right)_{\gamma\gamma}}{\partial r_{lc}} \qquad (2.13) \\ &= -\frac{1}{2\tilde{\omega}_\gamma} \sum_j \sum_k M_{\gamma j}^T M_{k\gamma} \frac{\partial C_{jk}}{\partial r_{lc}}\,. \qquad (2.14) \end{aligned}$$

As already mentioned, matrix $\boldsymbol{M}$ contains the eigenvectors of $\boldsymbol{C}$ as columns, hence, adopting index notation for eigenvalue relation, $\sum_k C_{jk}M_{ki} = \lambda_i M_{ji}$, where $\lambda_i = \sum_{kj} M_{ij}^T C_{jk} M_{ki}$ is the i-th eigenvalue of $\boldsymbol{C}$ matrix.
A short demonstration, following the principles of the Hellmann-Feynman force theorem [8], is presented in Appendix A. This demonstration elucidates the mathematical steps that lead to the derivation of Eq. 2.14. The coordinates dependence in $\boldsymbol{C}$ arises from the $\boldsymbol{T}$ matrix. The derivation of $\frac{\partial C_{jk}}{\partial r_{lc}}$ is reported in Appendix B. The set of optical van der Waals forces is represented by a $3N \times 3N$matrix $\boldsymbol{F}$, in which the row index is associated with the oscillator upon which the force acts, and the column with the excited MBD mode. The derivatives of $\boldsymbol{C}$ are switched from atomic coordinates to QHO ones, recalling the relationship between the sets of indices: $p = 3(k-1) + a$, $q = 3(j-1) + b$,

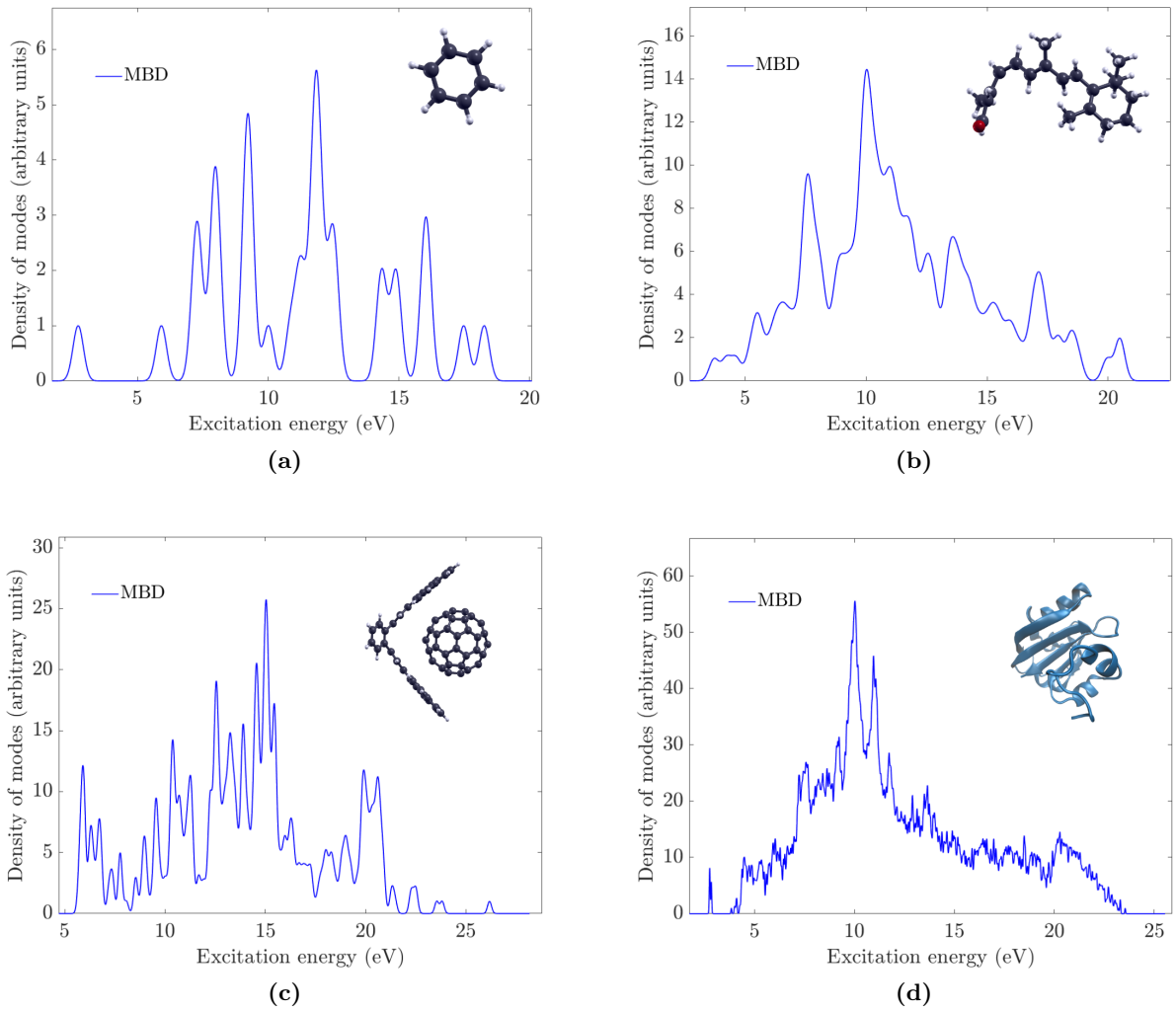

Figure 2.1: MBD exciton spectra. MBD spectrum of benzene molecule C_6H_6 **(a)**, 11-cis-retinal **(b)** and C_{60}-clamp complex **(c)**, all get with gaussian broadening of 0.2 eV around discrete frequencies. MBD spectrum for photoactive yellow protein (PYP) [6] [14] **(d)** with gaussian broadening of 0.02 eV.

$a, b = 1, 2, 3$, $\sigma = 3(l-1) + c$, and a compact form is adopted $\dfrac{\partial C_{jk}}{\partial r_\sigma} \equiv C'_{\sigma jk}$.
Hence exploiting QHO indices one has:

$$F_\sigma^\gamma = -\frac{1}{2\tilde{\omega}_\gamma} \sum_j \sum_k M_{\gamma j}^T M_{k\gamma} C'_{\sigma jk} \,. \tag{2.15}$$

Since $\boldsymbol{C}'$ is a tensor with three indices (and $(3N)^3$ elements), the numerical evaluation of the forces matrix could be computationally demanding, especially for large systems. Throughout the thesis, tensor calculations are frequently employed, which is why index notation is commonly adopted. This notation intuitively conveys the type of tensor contractions involved and quickly adapts to the numerical computation methods employed in this thesis. Specifically, a high-performing and user-friendly algorithm has been identified within the pre-implemented *tensorprod* function in MATLAB [16].

The aim of the thesis is to investigate the primary effects arising from the excitation of MBD modes on atom dynamics and, above all, to comprehend the theoretical regime within which the model finds successful application and where it reveals limitations. We are dealing with an approximation that facilitates the efficient assessment of long-range interactions, and this is expected to provide best description of systems with a substantial number of atoms. Of clear relevance is the energy range within

which such modes can be excited. It is evident that in biology and biophysics, the visible spectrum represents the most pertinent energy window, given its association with photoreceptor activation. The effect of optical excitations is explored through two distinct models. In the first, van der Waals forces are treated as a perturbation to atomic dynamics, following a 'semiclassical' approach. In the second, a rigorous coupling between atomic and electronic degrees of freedom is theorized, employing a quantum approach rooted in the premises of the Born-Oppenheimer approximation. In this latter case, van der Waals forces are embedded within the coupling.

In addition to energy spectra, an intuitive interpretation of MBD modes is provided through the geometric patterns of forces and dipole oscillation directions, whose relationship is found in Eq. 2.15. Particularly for complex systems, MBD modes can both give rise to "localized" and "highly delocalized" forces, depending on the corresponding MBD exciation (see Figs.2.2c, 2.2d, 2.2e and 2.2f). It will be demonstrated later that these geometries adhere to certain symmetries, which play a key role in understanding the reciprocal compatibility between optical excitations and ion dynamics.

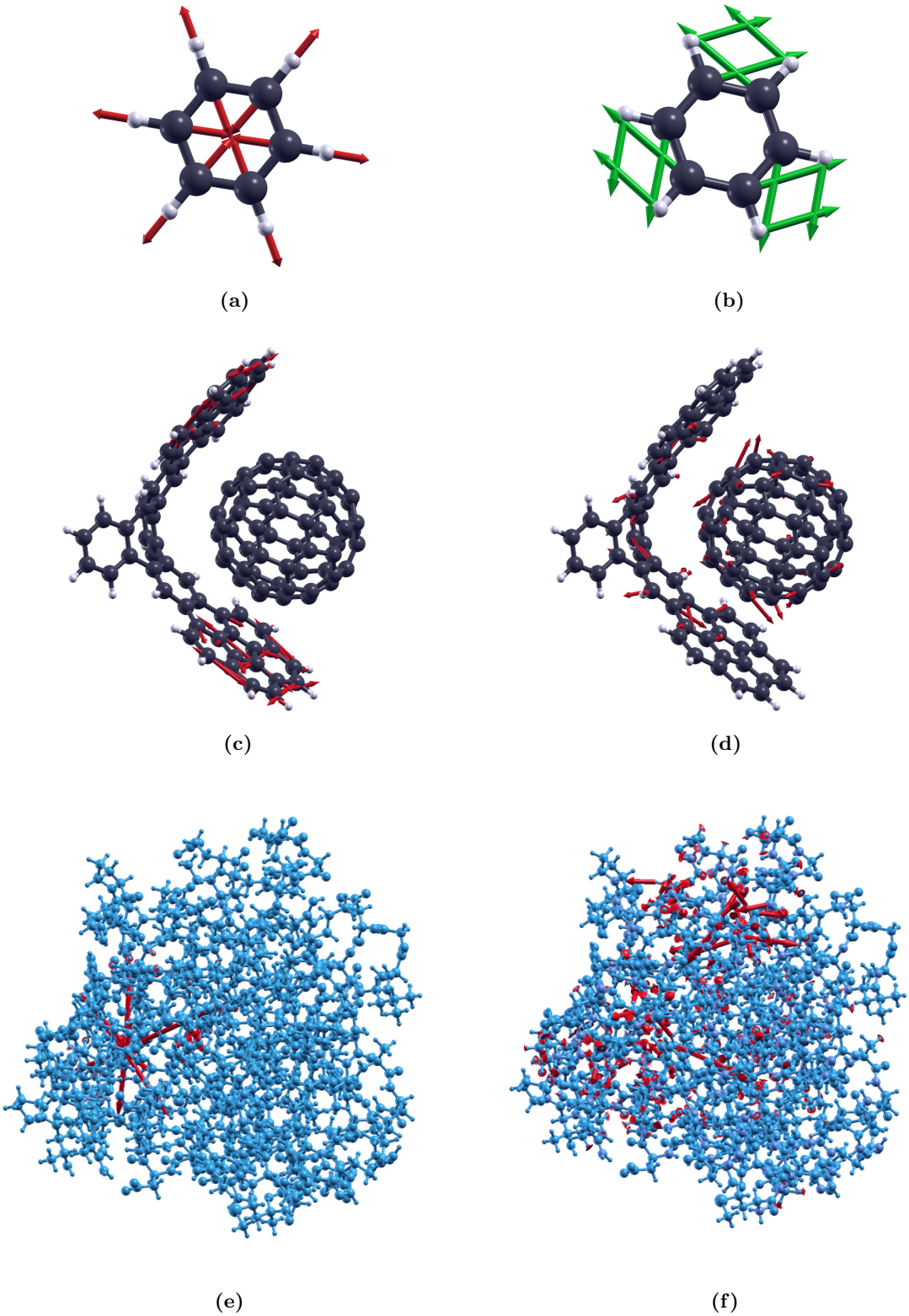

(a) **(b)** **(c)** **(d)** **(e)** **(f)**

Figure 2.2: Geometrical visualization of MBD modes. Optical vdW forces and dipole oscillation directions are reported for systems of interest. Benzene monomer's 34-th exciton mode is reported in vdW forces **(a)** (red arrows) and dipole oscillations **(b)** (green arrows).
Localization properties of MBD modes are visualized in the Buckminsterfullerene-clamp complex and PYP. Forces are depicted for low frequencies excitations and high energies. In particular, for Buckminsterfullerene-clamp modes 15 **(c)** and 412 **(d)**; for PYP modes 5 **(e)** and 4000 **(f)**. Modal indices are reported in ascending order of frequency.

Chapter 3

Molecular vibrations and normal mode analysis

3.1 Molecular vibrations and phonons

Molecular vibrations refer to the oscillatory motion of atomic ions within a molecule. Within the quadratic approximation, a molecule is described as a system of N atoms connected by chemical bonds acting like springs. This allows atoms to vibrate around their equilibrium positions, denoted as $\boldsymbol{R}$. A pattern of atomic displacements, all oscillating with the same frequency is called "normal mode" (NM).
The number of physical NMs for molecules is usually $3N - 6$, since translations and rotations are excluded from the counting. Structure, dynamical and thermodynamical properties of molecules are strongly affected by these collective vibrations. In the context of condensed matter, it is common to refer interchangeably to 'phonons' and NMs; however, phonons are quasiparticles arising on a periodic lattice, while the case of molecular vibrations is simpler and does not involve Fourier analysis due to the lack of periodicity.
Both phonons and NM are associated to quantized, discrete energy levels, but in the second case it is the potential energy surface of the molecule to determine vibrations, implying dependence on bond strengths, bond angles, and other molecular properties. The molecular vibrational properties are therefore described by a wavefunction, whose state is related to the probability to find the molecule in a particular vibrational mode.

The harmonic oscillator model is the fundamental concept used to describe NMs. In this model one assumes that the bonds between atoms behave like simple springs, each obeying Hooke's law. The vibrational spectrum is given by the characteristic frequencies at which all atoms in the whole molecule oscillate, following a different trajectory for each mode. The strength of the bonds connecting atoms, the masses and also the van der Waals forces between atoms determine the frequency spectrum.
At this stage, the harmonic approximation for the atom-atom interaction potential is assumed, while higher-order corrections are neglected. However, molecular vibrations can be anharmonic, meaning that they can deviate from the simple harmonic oscillator model. Anharmonicity can arise due to the non-quadratic nature of the potential energy surface, which affects the bond strength when atoms move far away from their equilibrium positions.

Suppose atoms to move within a potential $V(\boldsymbol{r})$ ($\boldsymbol{r}$, without any index represent the whole set of coordinates) depending only on atomic positions. At this stage we assume that electronic effects simply determine the the inter-ionic potential, hence vibrational properties are only related to the dynamics of ions.

$$\hat{H}_{ions} = \sum_i \frac{\nabla^2_{\boldsymbol{r_i}}}{2m_i} + V(\{\boldsymbol{r}\})\,. \tag{3.1}$$

Ions are free to oscillate around their equilibrium positions $\boldsymbol{R}$, and when oscillations are small, the potential is approximated by the harmonic [32] term:

$$\begin{aligned} V(\boldsymbol{r}) &\simeq V(\boldsymbol{R}) + \frac{1}{2}\sum_{ij} \frac{\partial^2 V}{\partial \boldsymbol{r}_i \partial \boldsymbol{r}_j}(\boldsymbol{R}) d\boldsymbol{r}_i d\boldsymbol{r}_j \\ &= V(\boldsymbol{R}) + \frac{1}{2}\sum_{ij} d\boldsymbol{r}_i H_{ij} d\boldsymbol{r}_j\,. \end{aligned} \tag{3.2}$$

Here $\boldsymbol{H}$ is the Hessian matrix relative to the ionic potential, evaluated at the equilibrium configuration. Shifting the potential energy in order to incorporate the constant term $V(\{\boldsymbol{R}\})$, $\hat{H}_{ions}$ reads:

$$\hat{H}_{ions} = -\sum_i \frac{\nabla^2_{\boldsymbol{r_i}}}{2m_i} + \frac{1}{2}\sum_{ij} d\boldsymbol{r}_i H_{ij} d\boldsymbol{r}_j\,. \tag{3.3}$$

Rescaling also the ionic positions by the corresponding atomic mass, and switching the description

from positions to displacements $\boldsymbol{q}$, $\boldsymbol{r}'_i = \sqrt{m_i}\boldsymbol{r}_i$, $\boldsymbol{q}_i = \sqrt{m_i}(\boldsymbol{r}_i - \boldsymbol{R}_i)$ one has:

$$\begin{aligned}\hat{H}_{ions} &= -\frac{1}{2}\sum_i \nabla^2_{\boldsymbol{r}'_i} + \frac{1}{2}\sum_{ij} d\boldsymbol{r}'_i \frac{H_{ij}}{\sqrt{m_i m_j}} d\boldsymbol{r}'_j \\ &= -\frac{1}{2}\sum_i \nabla^2_{\boldsymbol{q}_i} + \frac{1}{2}\sum_{ij} \boldsymbol{q}_i \mathcal{H}_{ij} \boldsymbol{q}_j \,, \end{aligned} \tag{3.4}$$

where $\boldsymbol{\mathcal{H}}$ is a symmetric matrix, namely the so-called mass-weighted Hessian. $\hat{H}_{ions}$ describes a set of N $3D$ harmonic oscillators. Diagonalization leads to a collection of $3N$ $1D$ independent harmonic oscillators, so, globally, the system can be viewed as a set of $3N$ independent one dimensional harmonic oscillators:

$$\hat{H}_{ions} = -\frac{1}{2}\sum_{i=1}^{3N} \nabla^2_{q_i} + \frac{1}{2}\sum_{ij=1}^{3N} q_i \mathcal{H}_{ij} q_j \,. \tag{3.5}$$

Denoting by $\boldsymbol{S}$ the rotation matrix such that $\boldsymbol{D} = \boldsymbol{S}^{-1}\boldsymbol{\mathcal{H}}\boldsymbol{S}$ is the diagonal matrix whose elements are the eigenvalues of $\boldsymbol{\mathcal{H}}$ ($D_{ij} = \delta_{ij}\lambda_{ij}$) , one can recast $\hat{H}_{ions}$ in the normal form:

$$\hat{H}_{ions} = -\frac{1}{2}\sum_{i=1}^{3N} \nabla^2_{Q_i} + \frac{1}{2}\sum_{ij=1}^{3N} Q_i \lambda_i Q_i \,. \tag{3.6}$$

The transformation from the initial basis to the eigenvectors is:

$$Q_j = \sum_i S^T_{ji} q_i = \sum_i S^T_{ji}\sqrt{m_i}\; dr_i \,, \tag{3.7}$$

while the inverse transformation is $q_i = \sum_j S_{ij} Q_j$. Regarding the laplacian operator, since $\boldsymbol{S}^{-1} = \boldsymbol{S}^T$, $\boldsymbol{S}^T\boldsymbol{S} = \mathbb{1}$ i.e. $\delta_{ij} = \sum_k S^T_{ik} S_{kj}$.

$$\sum_i \nabla^2_{q_i} f = \sum_i \frac{\partial}{\partial q_i} \sum_k \frac{\partial}{\partial Q_k}\frac{\partial Q_k}{\partial q_i} f \tag{3.8}$$

$$= \sum_i \frac{\partial}{\partial q_i} \sum_k \frac{\partial}{\partial Q_k} S^T_{kj}\delta_{ij} f \tag{3.9}$$

$$= \sum_k \sum_i S^T_{ki} \sum_l \frac{\partial}{\partial Q_l}\left(\frac{\partial Q_l}{\partial q_i} f\right) \tag{3.10}$$

$$= \sum_k \sum_i S^T_{ki} \sum_l \frac{\partial}{\partial Q_l} S^T_{li} f \tag{3.11}$$

$$= \sum_{kl} \frac{\partial}{\partial Q_k}\frac{\partial}{\partial Q_l} f \underbrace{\sum_i S^T_{ki} S^T_{li}}_{\delta_{kl}} \tag{3.12}$$

$$= \sum_k \frac{\partial^2}{\partial Q_k^2} f \tag{3.13}$$

$$= \sum_k \nabla^2_{Q_k} f \,. \tag{3.14}$$

About the potential energy term:

$$\sum_{ij} q_i \mathcal{H}_{ij} q_j = \sum_{ij} \sum_{l} S_{il} Q_l \mathcal{H}_{ij} \sum_{k} S_{jk} Q_k \tag{3.15}$$

$$= \sum_{lk} Q_l Q_k \sum_{ij} S_{il} \mathcal{H}_{ij} S_{jk} \tag{3.16}$$

$$= \sum_{lk} Q_l Q_k \sum_{ij} S^T_{li} \mathcal{H}_{ij} S_{jk} \tag{3.17}$$

$$= \sum_{lk} Q_l Q_k \lambda_k \delta_{lk} \tag{3.18}$$

$$= \sum_{k} Q_k Q_k \lambda_k \,. \tag{3.19}$$

The square root of the $\boldsymbol{\mathcal{H}}$ eigenvalues are the collective frequencies of the NMs, $\sqrt{\lambda_i} = \Omega_i$. These only depend on ionic positions in the equilibrium configuration: $\Omega = \Omega(\boldsymbol{R})$.

$$\hat{H}_{ions} = -\frac{1}{2} \sum_i \nabla^2_{Q_i} + \frac{1}{2} \sum_i Q_i^2 \Omega_i^2(\{\boldsymbol{R}\}) \,. \tag{3.20}$$

Here $\boldsymbol{Q}$ represents the set of collective ion coordinates called 'normal coordinates'. The newly defined coordinates $\boldsymbol{Q}$ have the dimensions of a distance multiplied by the square root of a mass; to obtain pure collective coordinates, it is necessary to introduce an effective mass μ for each ionic harmonic oscillator. For this purpose, a new set of coordinates $\boldsymbol{\rho}$ is defined, such that for i-th harmonic ionic oscillator $\rho_i = \dfrac{Q_i}{\sqrt{\mu_i}}$. Following this approach the goal is to find a unitary transformation from the ionic displacements $d\boldsymbol{r}$ to $\boldsymbol{\rho}$ sets, starting from the definition of $\boldsymbol{Q}$, finding a suitable expression for the phononic effective masses.

$$\rho_i = \frac{Q_i}{\sqrt{\mu_i}} = \sum_j S^T_{ij} \frac{\sqrt{m_j}}{\sqrt{\mu_i}} dr_j \tag{3.21}$$

$$\equiv \sum_j S'^T_{ij} \, dr_j \,, \tag{3.22}$$

where matrix $\boldsymbol{S'}$ is the transformation from ionic coordinates to collective ones $S'_{ij} = S_{ij} \sqrt{\dfrac{m_i}{\mu_j}}$.
The orthonormality of matrix $\boldsymbol{S}$ is reflected in the relation $\sum_k S^T_{ik} S_{kj} = \delta_{ij}$. By imposing the same for $\boldsymbol{S'}$, the effective masses are found, hence:

$$1 = \sum_k S'^T_{ik} S'_{ki} \tag{3.23}$$

$$= \sum_k S^T_{ik} \sqrt{\frac{m_k}{\mu_i}} S_{ki} \sqrt{\frac{m_k}{\mu_i}} \tag{3.24}$$

$$= \frac{1}{\mu_i} \sum_k m_k S^T_{ik} S_{ki} \,. \tag{3.25}$$

The effective mass for the i-th ionic normal mode is

$$\mu_i = \sum_k m_k S^2_{ki} \,, \tag{3.26}$$

in this way the ionic hamiltonian reads:

$$\hat{H}_{ions} = -\frac{1}{2} \sum_i \frac{\nabla^2_{\rho_i}}{\mu_i} + \frac{1}{2} \sum_i \rho_i^2 \mu_i \Omega_i^2 = \sum_i \hat{H}^i_{ions} \,. \tag{3.27}$$

Since we are also willing to investigate which processes can induce a system to alter its conformation towards a desired structure, a filter is applied to all potential modes of vibration to discern which of them can generate a geometry compatible with the intended configuration. A unitary motion along the normal coordinate ρ_k corresponds to a displacement $dr_i^{(k)}$ for each i-th quantum harmonic oscillator:

$$dr_i^{(k)} = \sum_j S'_{ij}\rho_j\delta_{jk} = S'_{ik}\,. \tag{3.28}$$

In order to understand which of the normal modes makes the molecule oscillate towards a certain spatial configuration $\boldsymbol{R}^{(c)}$, a displacement vector $\Delta\boldsymbol{r}$ joining the equilibrium position $\boldsymbol{R}$ to the desired molecular configuration $\boldsymbol{R}^{(c)}$ is obtained: $\Delta R_i = R_i^{(c)} - R_i$. For each normal mode k the overlap is defined as:

$$O^{(k)} = \frac{1}{N}\sum_i \frac{|\Delta\boldsymbol{R}_i \cdot d\boldsymbol{r}_i^{(k)}|}{\|\Delta\boldsymbol{R}_i\|\ \|d\boldsymbol{r}_i^{(k)}\|}\,. \tag{3.29}$$

In the latter $\cdot$ denotes the scalar product between 3D atomic coordinates and the sum is performed over all atoms. $O^{(k)}$ is a parameter ranging from 0 to 1, that quantifies how the k-th normal mode's vibration displaces atoms toward the target configuration $\boldsymbol{R}^{(c)}$.
Eq.3.29 is valid only if each atom occupies a different position in $\boldsymbol{R}$ and $\boldsymbol{R}^{(c)}$ configurations. If position of atom i is unchanged $\|\Delta\boldsymbol{R}_i\| = 0$, hence singularity occurs. To address this issue, the overlap parameter can be defined as follows:

$$O^{(k)} = \frac{1}{N}\sum_i \frac{|\left(\Delta\boldsymbol{R}_i - d\boldsymbol{r}_i^{(k)}\right)\cdot d\boldsymbol{r}_i^{(k)}|}{\|\Delta\boldsymbol{R}_i - d\boldsymbol{r}_i^{(k)}\|\ \|d\boldsymbol{r}_i^{(k)}\|}\,. \tag{3.30}$$

The range for the overlap value is kept between zero and one. In addition to avoiding singularities, the advantage is that if there are atoms occupying the same position between the initial and target configurations, the highest overlap will correspond to modes that induce the least displacement of the atoms.

3.1.1 Second quantization of the phonon wave function

As already observed, the harmonic approximation for the motion of ions allows for a description of the molecular system in terms of $3N$ independent degrees of freedom (referred to as collective coordinates or normal coordinates).
The global motion of the system along one of these coordinates indicates that one of the $3N$ possible normal modes of oscillation has been excited. The system is now described by $3N$ independent harmonic oscillators, with frequency Ω and mass μ. The remaining task is to solve the problem of calculating the energy spectrum, which has already been extensively addressed within the framework of "second quantization".
The energy spectrum of the ionic system is evaluated solving the Schrödinger equation for the Hamiltonian H_{ions} (Eq.3.27). Since this hamiltonian is approximated by a quadratic form, it will be referred to hereafter as the "phononic" Hamiltonian H_{ph}. Its diagonalization yields a wave function Φ, which describes a set of independent 1-dimensional harmonic oscillators. In general, the state m satisfies

$$\hat{H}_{ph}\Phi^m = E_m^{ph}\Phi^m\,. \tag{3.31}$$

The independence of the harmonic oscillators is reflected into the factorization of an arbitrary many-body eigenstate Φ, which globally depends on the entire set of coordinates $\boldsymbol{\rho}$, but can be expressed as a product of functions, each depending only on one of the $3N$ collective coordinates [31].

$$\Phi(\rho) = \Phi(\rho_1,\ldots,\rho_{3N}) = \phi_1(\rho_1)\otimes\phi_2(\rho_2)\otimes\ldots\otimes\phi_{3N}(\rho_{3N})\,. \tag{3.32}$$

More precisely, an arbitrary eigenstate Φ^m corresponds to a set of quantum numbers of each single-particle wave function, $m = \{m_1,\ldots,m_{3N}\}$, hence

$$\Phi^m(\rho) = \phi_1^{m_1}(\rho_1)\otimes\phi_2^{m_2}(\rho_2)\otimes\ldots\otimes\phi_{3N}^{m_{3N}}(\rho_{3N})\,, \tag{3.33}$$

and satisfies, for each $i = 1, \dots, 3N$

$$-\frac{1}{2}\frac{\nabla^2_{\rho_i}}{\mu_i}\phi_i^{m_i}(\rho_i) + \frac{1}{2}\rho_i^2\mu_i\Omega_i^2\phi_i^{m_i}(\rho_i) = E_{ph,i}^{m_i}\phi_i^{m_i}(\rho_i)\,. \tag{3.34}$$

If $\phi_i^{m_i}(\rho_i)$ corresponds to

$$\phi_i^{m_i}(\rho_i) = \frac{1}{\sqrt{2^{m_i}m_i!}}\left(\frac{\mu_i\Omega_i}{\pi}\right)^{1/4} e^{-\frac{\mu_i\Omega_i\rho_i^2}{2}} H_{m_i}\left(\sqrt{\mu_i\Omega_i}\rho_i\right)\,,\ m_i = 0, 1, 2, \dots\,, \tag{3.35}$$

where $H_{m_i}(z) = (-1)^{m_i}e^{z^2}\dfrac{d^{m_i}}{dz^{m_i}}\left(e^{-z^2}\right)$ is the m_i-th Hermite polynomial, the energy eigenvalue $E_{ph,i}^{m_i}$ is (half-integer) multiple of the frequency of the i-th vibrational normal mode Ω_i, i.e. $E_{ph,i}^{m_i} = \Omega_i\left(m_i + \frac{1}{2}\right)$, and the total energy of state m is the sum of the energies of each oscillator $E_{ph}^{m} = \sum_i \Omega_i\left(m_i + \frac{1}{2}\right)$.
The integer value m_i can be interpreted as the number of excitations of the i-th harmonic oscillator. It is thus conveninent to adopt a compact Dirac bra-ket notation.

Given an arbitrary wavefunction $\phi_i(\rho_i)$, this can be expressed as as a linear combination of eigenstates $|m\rangle$ (denoting the multiplicity of the single QHO excitations), $\phi_i(\rho_i) = \sum_m c_m\varphi_m(\rho_i)\,|m\rangle$. More explicitly, the state Φ^m is depicted as

$$\Phi^m = |m_1\rangle \otimes |m_2\rangle \otimes \dots \otimes |m_{3N}\rangle \equiv |m\rangle\ , \tag{3.36}$$

and Schrödinger's equation then reads

$$\hat{H}_{ph}\,|m\rangle = E_m^{ph}\,|m\rangle\ . \tag{3.37}$$

From now on, to simplify the notation, the wave function will be labelled with the indices of the excited harmonic oscillators: for example the ground state, in which $n_i = 0\ \forall\ i$ is $|0\rangle$, and the state $|1_\gamma\rangle$ is the one with $n_i = \delta_{n_\gamma,1}\delta_{\gamma i}$, in other words vibrational excitation γ as occurred.

$$|1_\gamma\rangle = |0, \dots, 1_\gamma, \dots, 0\rangle\ . \tag{3.38}$$

Each collective single-oscillator Hamiltonian $H_{ph,i}$ can be re-expressed introducing ladder operators. Recalling that in space-representation the momentum operator is $\hat{P}_{\rho_i} = -i\nabla_{\rho_i}$:

$$\hat{b}_i^\dagger = \frac{1}{\sqrt{2\mu_i\Omega_i}}(\mu_i\Omega_i\rho_i - iP_{\rho_i})\,, \tag{3.39}$$

$$\hat{b}_i = \frac{1}{\sqrt{2\mu_i\Omega_i}}(\mu_i\Omega_i\rho_i + iP_{\rho_i})\,. \tag{3.40}$$

These operators are well defined, and one has:

$$\hat{b}_i^\dagger\hat{b}_i = \frac{1}{2\Omega_i\mu_i}\left(-\nabla^2_{\rho_i} + \mu_i\Omega_i\left[\rho_i, \nabla_{\rho_i}\right] + \mu_i^2\rho_i^2\Omega_i^2\right) \tag{3.41}$$

Using a generic auxiliary wave function ψ, the commutator is:

$$[\rho_i, \nabla_{\rho_i}]\psi = -(\nabla_{\rho_i}\rho_i)\psi = -\psi \tag{3.42}$$

The Hamiltonian $\hat{H}_{ph}$ can be written in terms of these operators:

$$\hat{b}_i^\dagger\hat{b}_i = \frac{1}{2\mu_i\Omega_i}\left(-\nabla^2_{\rho_i} + \mu_i^2Q_i^2\Omega_i^2 - \mu_i\Omega_i\right) = \frac{1}{\Omega_i}\left(\hat{H}_{ph,i} - \frac{\Omega_i}{2}\right)\ , \tag{3.43}$$

$$\hat{H}_{ph,i} = \Omega_i \left(\hat{b}_i^\dagger \hat{b}_i + \frac{1}{2} \right) , \tag{3.44}$$

$$\hat{H}_{ph} = \sum_i \Omega_i \left(\hat{b}_i^\dagger \hat{b}_i + \frac{1}{2} \right) . \tag{3.45}$$

It is also expedient to report the effect of $\hat{b}$ operators on the phononic wave function:

$$\begin{aligned} \hat{H}^{ph} \left(\hat{b}_\gamma^\dagger |n\rangle \right) &= \sum_i \Omega_i \left(\hat{b}_i^\dagger \hat{b}_i + \frac{1}{2} \right) \left(\hat{b}_\gamma^\dagger |n\rangle \right) \\ &= \Omega_\gamma \hat{b}_\gamma^\dagger \left(\hat{b}_\gamma^\dagger \hat{b}_\gamma + 1 + \frac{1}{2} \right) |n\rangle \ + \sum_{i \neq \gamma} \Omega_i \left(\hat{b}_i^\dagger \hat{b}_i \hat{b}_\gamma^\dagger |n\rangle + \frac{1}{2} \hat{b}_\gamma^\dagger |n\rangle \right) \qquad (3.46) \\ &= \hat{b}_\gamma^\dagger \sum_i \hat{H}_{ph}^i |n\rangle + \Omega_\gamma \hat{b}_\gamma^\dagger |n\rangle \\ &= \hat{b}_\gamma^\dagger \left(E_n^{ph} + \Omega_\gamma \right) |n\rangle \\ &= \left(E_n^{ph} + \Omega_\gamma \right) \hat{b}_\gamma^\dagger |n\rangle \ . \qquad (3.47) \end{aligned}$$

Following the definitions of $\hat{b}_i$ and $\hat{b}_i^\dagger$:

$$\rho_i = \frac{1}{\sqrt{2\mu_i \Omega_i}} \left(\hat{b}_i + \hat{b}_i^\dagger \right) \tag{3.48}$$

$$, \nabla_{\rho_i} = \sqrt{\frac{\mu_i \Omega_i}{2}} \left(\hat{b}_i - \hat{b}_i^\dagger \right) . \tag{3.49}$$

3.2 Force field and "ab initio" approaches

The evaluation of the vibrational spectrum for a molecule is related to the correct diagonalization of the mass-weighted hessian matrix (sometimes called 'dynamical matrix') $\mathcal{H}$, that requires the determination of the molecular potential V. The more accurate the potential, the more reliable will be the energetic spectrum. In computational chemistry two main classes of methods are normally adopted, depending on the size of the explored systems, on the available computational power, and on the required precision: these are "ab initio" and "force fields" approaches. In this work, both methods are tested, and force fields are adopted in the most demanding calculations.
Softwares based on "ab initio" methods provide an approximate solution of the electronic Schrödinger equation, using quantum mechanical principles, and avoiding the introduction of empirical parameters. Once the electronic structure of the molecule is computed, the ionic vibrational frequencies are determined from the potential energy surface.
High accuracy is reached at the price of a high computational cost, due to the need to solve the all-electron Schrödinger equation numerically, including electronic correlation effects. This class of approaches is thus well suited for addressing NM's of small molecules. Instead, larger systems composed by many atoms will be addressed via force fields.
Force fields rely on suitably parameterized effective potentials, that model the interatomic interactions in molecules and are based on classical mechanics and do not explicitly consider the electronic structure, but only the effective interaction between atoms. The ionic potential, from which the Hessian matrix is computed, is of a classical nature and therefore is directly calculated as the negative gradient of the forces acting on the atoms. For this reason, the problem boils down to the force calculation, which is profoundly different in the two computational approaches.

3.2.1 Vibrational spectra

Since a prerequisite of this thesis is a reliable methodology capable to obtain vibrational spectra at affordable computational cost, even in large nanoscale systems, "force field' methods will be preferred.

Nonetheless, before proceeding with large-scale calculations, we explicitly tested the vibrational spectra obtained from "force fields" against "ab-initio" methods for a set of small molecules, where the latter (more demanding) approach is applicable. A comparison is performed in order to assess the reliability of the force fields method that will be used in the following chapters.

A finite-difference evaluation of the Hessian matrix is performed starting from ouput forces, computed via density functional theory, with Perdew-Burke-Ernzerhof (PBE) exchange-correlation functional. The Quantum Espresso package is exploited in order to perform calculations. This benchmarking enables to analyze the limits beyond which the two methods start to diverge and the range of modes where similar results are instead obtained.

As a start, we need to clarify that every NM analysis implies the evaluation of the potential energy surface at its minimum, i.e. in the equilibrium configuration. Different approaches can lead to different equilibrium configurations. For this reason, geometrical relaxation is performed for each molecule and each method, before computing NM's. The only inputs needed by QE are the atomic coordinates, the pseudopotentials (ultrasoft here) [2] and the masses. Moreover, one needs to provide some parameters such as the energy cutoff for the plane-wave expansion of the electronic wavefunctions and the kinetic energy cutoff for charge density, that are respectively fixed here to 30 Ry and 180 Ry.

In QE, the optimal molecular structure $\boldsymbol{R}$ is reached by a relaxation process (routine `relax`) that iteratively adjusts atomic positions until a minimum in the energy landscape is reached. Forces acting on atoms are then evaluated in the equilibrium configuration using the "self-consistent field" (`scf`) calculation. After these two steps, $\boldsymbol{F}_{eq}$ and $\boldsymbol{R}$ are obtained and saved. By displacing a single atom, along one direction at a time, and re-evaluating atomic forces in the new configuration, the so-call 'dynamical' or 'hessian' matrix is obtained numerically, with a simple algorithm that we call `NDM` (numerical dynamical matrix):

$$H_{ij}^{ab} = \frac{\partial^2 V}{\partial r_i^a \partial r_j^b} = -\frac{\partial F_j^b}{\partial r_i^a} = -\frac{F_j^b\ (\boldsymbol{R}+d\boldsymbol{r}_i^a) - F_j^b(\boldsymbol{R})}{d\boldsymbol{r}_i^a}\,, \tag{3.50}$$

where bold $d\boldsymbol{r}_i^a$ denotes a small displacement of atom i along axis a. To take into account the inertial nature of each harmonic oscillator, one needs to rescale the $\boldsymbol{H}$ matrix by atomic masses, obtaining the mass-weighted hessian matrix $\mathcal{H}_{ij}^{ab} = \frac{H_{ij}^{ab}}{\sqrt{m_i m_j}}$. The diagonalization of the $3N \times 3N$ matrix $\boldsymbol{\mathcal{H}}$ is performed with the MatLAB routine `eig` [16] (based on `LAPACK` libraries), and yields the NM spectrum on output.

In order to compute the vibrational spectrum with GROMACS, it is imperative to possess specific input files. While Quantum Espresso only necessitated atomic positions, an approach based on force fields requires prior knowledge of certain chemical properties of the system. Consequently, two primary files are essential: a `.pdb` file and a `.top` file.

A PDB (Protein Data Bank) file conforms to a standardized file format utilized for storing atomic coordinates and molecular data. It encompasses a structured representation of the molecule's three-dimensional structure, including atom positions and types, connectivity details, chemical bonds, charges and supplementary annotations such as secondary protein structure and ligand binding sites. NMR (Nuclear magnetic resonance) spectroscopy and X-ray crystallography are the main experimental techniques to obtain PDB parameters. The correct units in a PDB file are: Å for gometrical coordinates and bond lengths, and degrees (°) for bond angles and dihedral angles. Conversely, a topology file (`.top`) in GROMACS includes comprehensive details concerning the force field parameters employed to describe interactions between atoms within the system. It specifies atom types, their charges, bond parameters (bond lengths and force constants), angle parameters, dihedral parameters, as well as non-bonded interaction parameters (including van der Waals and electrostatic interactions). The topology file provides essential input for the molecular dynamics simulation by defining the force field parameters indispensable for calculating the system's potential energy. In summary, a PDB file supplies initial atomic coordinates and connectivity information for the molecular system, while the GROMACS topology file (`.top`) delineates the force field parameters requisite for modeling atom interactions during molecular dynamics simulations. These files collectively facilitate the configuration

and simulation of molecular systems employing GROMACS. Both `.top` and `.pdb` files were obtained from the ATB website [1], that provides also a custom force field package as extension of the `GROMOS 54A7 forcefield`. GROMACS reads `.mdp` files in which the simulation parameters are reported. For our aim just two of them are required: one specifies the energy-minimization algorithm, choosing between Steepest Descent `steep`, Conjugate Gradient `cg`, `L-BFGS` and others, and the other are related to the NM analysis (method `nm`) that evaluates the hessian matrix, which is then postprocessed by GROMACS routines `nmeig` and `anaeig`. The other significant parameters of an .mdp file include the type of boundary conditions, the van der Waals radius, the Coulomb radius, and the cutoff scheme, that determine how interactions between atoms are treated beyond a certain distance, known as the cut-off distance. It is important to mention the appropriate units in which the spectra will be reported; due to different energy scales, vibrational spectra are indicated in cm^{-1}, while MBD spectra are indicated in eV. In all graphs representing vibrational spectra, an additional axis is included to display the values in electronvolts. Spectra for selected molecules, ranging in atom numbers from 3 (water) to 60 (Buckminsterfullerene) are reported in Fig.3.1, while tables with results are reported in Appendix C.

Overall, we observe fair qualitative agreement between vibrational spectra of the selected molecules, which encompass different size, chemical composition, structure and topology. Ab-initio frequencies are not always closer to experimental data with respect to force fields. The main challenge for force field calculations is reproducing the "higher peaks", that correspond to degenerate or closely spaced modes. We stress in any case that slight frequency shifts are not expected to imply a major deficiency for quasielectron-phonon couplings. In fact, vibrational frequencies only cause a renormalization of the coupling factors.

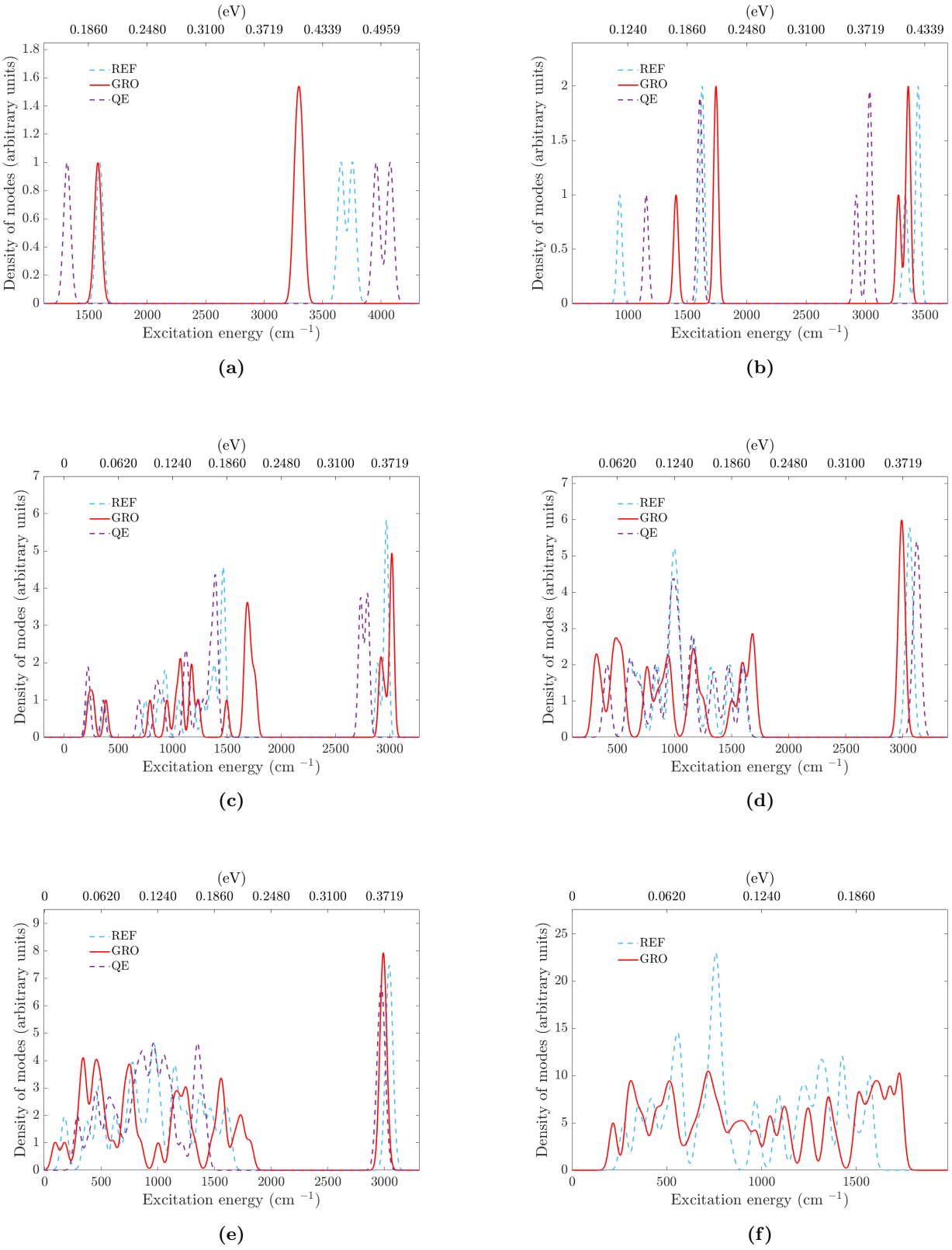

Figure 3.1: Vibrational spectra. Comparison between vibrational spectra of reference molecules obtained from: i) GROMACS (GRO) `nm` analysis, ii) Quantum espresso (QE) `scf+NDM`, and iii) reference data (experimental, theorical or numerical, depending on availability) (REF) – **a)** Water (H_2O); **b)** Ammonia (NH_3); **c)** Propane (C_3H_8); **d)** Benzene (C_6H_6); **e)** Naphtalene ($C_{10}H_8$); **f)** Buckminsterfullerene (C_{60}). The discrete spectra are converted into continuous spectra using a Gaussian broadening with variable width (from 20 to 30 cm^{-1}) and presented in cm^{-1}, which is the common unit of measurement for IR and Raman spectroscopy, and in eV, consistently with the different energy scale of MV and MBD spectra, reported in the previous chapter. All molecular structures and topologies are obtained from the repository ATB (Automated Topology Builder) [1], while the involved pseudopotentials used in QE `relax` and `scf` are reported in Appendix C. REF data sources too are reported in Appendix C.

Chapter 4

Coupling between many-body dispersion and vibrational modes

4.1 Semi-classical coupling between phonons and optical vdW forces

Our aim here is to address the effect of "optical vdW forces" on ionic dynamics. Upon photon absorption, a system can undergo electronic excitation, and this will imply the emergence of interatomic forces and possible excitation of vibrational modes. Since MBD provides a reliable many-body description of polarizability and non-covalent forces, this will be adopted as a reference method for the quantum mechanical description of "optical vdW forces". Short-range optical forces may also arise upon electron excitation, but will not be considered in this thesis. As a starting point, we thus assume that short-range electron correlations can be approximated by a semi-classical potential V_{ions}, while long-range correlations are treated from a quantum-mechanical point of view, via the MBD model. The total hamiltonian can thus be expressed as:

$$\begin{aligned}\hat{H} &= \hat{H}_{mbd} + \hat{H}_{ions} \\ &= -\frac{1}{2}\sum_{p=1}^{3N} \nabla^2_{\chi_p(\boldsymbol{r})} + \frac{1}{2}\sum_{p}^{3N} \chi(\boldsymbol{r})^2_p \tilde{\omega}^2_p(\boldsymbol{r}) - \sum_{i}^{N} \frac{\nabla^2_{\boldsymbol{r}_i}}{2m_i} + V_{ions}(\boldsymbol{r})\,. \end{aligned} \tag{4.1}$$

This hamiltonian describes two sets of quantum harmonic oscillators, coupled to each other. In fact, ions move subject to a potential energy surface which is influenced by the MBD modes. We already note here that the Born-Oppenheimer approximation should be eventually overcome in order to rigorously treat this problem, but this will be fully addressed in the next chapters.

We now assume that the γ-th collective MBD mode is excited by phonon absorption; then the MBD energy is expressed as:

$$E^{(\gamma)}_{mbd} = E^{(0)}_{mbd} + \tilde{\omega}_\gamma\,. \tag{4.2}$$

The groundstate-energy term $E^{(0)}_{mbd}$ is absorbed in the inter-ionic potential $V(\boldsymbol{r}) = V_{ions}(\boldsymbol{r}) + E^{(0)}_{mbd}$, that can be treated as a harmonic potential so that the total hamiltonian becomes the sum of a phononic hamiltonian $\hat{H}_{ph}$ and an energy term due to photoexcitation:

$$\hat{H} = \hat{H}_{mbd} - E^{(0)}_{mbd} - \sum_i \frac{\nabla^2_{\boldsymbol{r_i}}}{2m_i} + V(\boldsymbol{r}) = \hat{H}_{mbd} - E^{(0)}_{mbd} + \hat{H}_{ph}\,. \tag{4.3}$$

Henceforth, this method will be referred to as the 'semiclassical method' (**SC**), to distinguish it from a fully quantum model that will be presented later on. The extra energy term can be interepreted as a perturbation of the phononic hamiltonian.

The unperturbed spectrum of $\hat{H}_{ph}$ is exactly known and following the formalism of the second quantization it is possible to understand the effect of the perturbation due to optical vdW forces on the vibrational state.

Coming back to the total hamiltonian (Eq.4.3), it will be clear why a second quantization turns out to be a good choice. The MBD excitation energy $\tilde{\omega}_\gamma$ (which depends on $\mathbf{r}$) can be expanded to first order in the displacement operators, in the following way:

$$\begin{aligned}\tilde{\omega}_\gamma(\boldsymbol{r}) &= \tilde{\omega}_\gamma(\boldsymbol{R}) - \boldsymbol{F}^{(\gamma)} \cdot d\boldsymbol{r}\,, \\ &= const - \sum_\sigma F^{(\gamma)}_\sigma dr_\sigma\,. \end{aligned} \tag{4.4}$$

where dr_σ is the displacement of oscillator σ, and $F^{(\gamma)}_\sigma$ is the van der Waals force acting on it due to excitation of the MBD γ-th mode, while the constant term is irrelevant and will be neglected hereafter. Recalling the transformation from cartesian to collective coordinates and the second quantization

expression for collective displacement (Eq. 3.49), one has:

$$\tilde{\omega}_\gamma(\boldsymbol{r}) = -\sum_{\sigma i} F_\sigma^{(\gamma)} S'_{\sigma i} \rho_i \tag{4.5}$$

$$= -\sum_{\sigma i} F_\sigma^{(\gamma)} \frac{S_{\sigma i}}{\mu_i} \sqrt{\frac{m_\sigma}{2\Omega_i}} \left(\hat{b}_i + \hat{b}_i^\dagger\right) \tag{4.6}$$

$$= -\sum_{\sigma i} \frac{F_\sigma^{(\gamma)} S'_{\sigma i}}{\sqrt{2\mu_i \Omega_i}} \left(\hat{b}_i + \hat{b}_i^\dagger\right) \tag{4.7}$$

Now, the hamiltonian Eq. 4.3 (where the constant term has been neglected) can be expressed in terms of ladder operators,

$$\hat{H} = \sum_i \Omega_i \left(\hat{b}_i^\dagger \hat{b}_i + \frac{1}{2}\right) - \sum_{\sigma i} \frac{F_\sigma^{(\gamma)} S'_{\sigma i}}{\sqrt{2\mu_i \Omega_i}} \left(\hat{b}_i + \hat{b}_i^\dagger\right) , \tag{4.8}$$

and within a perturbative framework, it is possible to identify the preferred phononic transitions of the system and the corresponding amplitudes.

A short mathematical derivation is provided here for the quantum mechanical transitions due to the coupling between MBD forces and vibrational modes. More specifically, transitions between vibrational states are described as due to a perturbation $\hat{H}'(t)$ of the (phononic) Hamiltonian that describes the system in the unperturbed state. Obviously, this perturbative term is identified with the first term in Eq.(4.8),

A global time-dependent wavefunction $|\Psi(t)\rangle$, built as superposition of the unperturbed eigenstates $|\Psi_n(t)\rangle$ (see Eq.3.37), is written as

$$|\Psi(t)\rangle = \sum_n c_n(t) \, |\Psi_n(t)\rangle = \sum_n c_n(t) \, |n\rangle \, e^{-iE_{ph}^n t} . \tag{4.9}$$

By following mathematical steps that mirror the derivation of the so-called Fermi's golden rule in the framework of perturbation theory [18], the expansion coefficients c_f, related to the transition from an initial state $|i\rangle$, to a final one $|f\rangle$ are:

$$c_f(t) = -\frac{i}{\hbar} \int_0^t dt' \;\; \langle f| \, H' \, |i\rangle \, e^{-i(E_i - E_f)t'} . \tag{4.10}$$

Here, we will restrict to very short time-intervals, after photoexcitation. The main reason is that the induced dynamics would eventually bring our geometrical conformation far away from the equilibrium structure, where vibrational modes are well defined. We will thus investigate the first instants of the dynamics, unveiling how energy is transferred to vibrational modes.

Time integration will thus be avoided, considering only evolution for small time steps. The probability to observe the system in the state $|f\rangle$ is $c_f^* c_f = |c_f|^2$. In our case E_i and E_f in Eq.4.10 denote the unperturbed energy eigenvalues in the initial and final states, respectively, and the 'perturbative' term is:

$$\hat{H}' = -\sum_{\sigma i} \frac{F_\sigma^{(\gamma)} S'_{\sigma i}}{\sqrt{2\mu_i \Omega_i}} \left(\hat{b}_i + \hat{b}_i^\dagger\right) \tag{4.11}$$

This perturbative term enables excitation or annihilation of single vibrational modes due to optical vdW forces, hence it produces an effective coupling between electronic excitations and ion dynamics.

If the initial state corresponds to the vibrational vacuum $|0\rangle$, the matrix element in Eq.4.10, can be expressed as:

$$\langle f|\, H' \,|i\rangle = -\sum_{\sigma n} \frac{F_\sigma^{(\gamma)} S'_{\sigma n}}{\sqrt{2\mu_n \Omega_n}} \langle f|\, \hat{b}_n^\dagger + \hat{b}_n \,|0\rangle \tag{4.12}$$

$$= -\sum_{\sigma n} \frac{F_\sigma^{(\gamma)} S'_{\sigma n}}{\sqrt{2\mu_n \Omega_n}} \underbrace{\langle f|1_n\rangle}_{\delta_{f,1_n}} . \tag{4.13}$$

It is clear that under these assumptions the final state will be characterized by the excitation of a single vibrational mode, such as $|1_k\rangle$ or $|k\rangle$:

$$\langle 1_k|\, \hat{H}' \,|0\rangle = -\frac{1}{\sqrt{2\mu_k \Omega_k}} \sum_\sigma F_\sigma^{(\gamma)} S'_{\sigma k} \tag{4.14}$$

$$= -\frac{1}{\sqrt{2\mu_k \Omega_k}} \boldsymbol{F}^{(\gamma)} \cdot \boldsymbol{S}'^{(k)} . \tag{4.15}$$

According to the present model, the "transition amplitude" P (proportional to the transition probablility but not normalized) from the ground state $\phi^{(0)} = |0\rangle$ to state $\phi_k = |1_k\rangle$, due to the optical excitation γ is:

$$P_{0\to k}^\gamma = |\, \langle k|\, H' \,|0\rangle \,|^2$$

$$= \frac{1}{2\mu_k \Omega_k} \left| \boldsymbol{F}^{(\gamma)} \cdot \boldsymbol{S}'^{(k)} \right|^2 . \tag{4.16}$$

$\boldsymbol{F}^{(\gamma)}$ is the $3N$-dimensional vector of vdW forces due to excitation of γ-th MBD mode, and $\boldsymbol{S}'^{(k)}$ is the k-th ($3N$-dimensional) eigenvector of the mass-weighted hessian matrix (Eq. 3.4), rescaled by effective masses in order to ensure normalization (Eq. 3.22). The SC transition probability for phonon states, due optical vdW forces (within the MBD framework), depends on the scalar product between vdW forces and excited phonon geometries. According to Eq. 4.16 larger transition rates are expected when optical vdW forces are "aligned" with the direction of collective vibrational modes, expecially when the vibrational frequency is low. Conversely, when forces and vibrations are orthogonal, no transition will occur.

4.1.1 Semi-Classical approach: results

Transition amplitudes in Eq.4.16 are the main results for the SC approach: they are represented by a heatmap, whose abscissa corresponds to the initial MBD state (representing van der Waals forces between atoms), while the ordinate labels the excited vibrational state (NM) in the final outcome. The entries of the heatmap are the transition amplitudes.
As from Fig.4.1a, most vibrational modes cannot be excited semi-classically by optical vdW forces, so that no signal is present in the heatmap. Since the number of modes (both vibrational and MBD) is three times the number of atoms, for clearer visualization one can select only those vibrational modes that admit finite transition amplitudes, and can compute the overlap of the vibrational mode with a sought configuration.
While benzene, given its planar structure, lacks vibrational modes that can significantly alter its atomic configuration, some more complex structures may exhibit interesting structures induced by certain vibrational modes.
For example, an interesting system is a complex formed by a buckminsterfullerene C_{60} and a carbon-oxygen structure shaped like a clamp. One may search for MBD excitations capable of exciting vibrational modes that could open or close the 'clamp' and hold the C_{60}, molding the structure until it becomes compatible with the one shown in Fig.4.4. Among other structural transformations, there is the isomerization of retinal from 11-cis to all-trans, as shown in Figs.4.4a and 4.4c. However, a substantial difference exists between the two structural changes. In the case of C_{60}-clamp, the chemical bonds within the structure remain roughly unaltered. On the other hand, the process involving

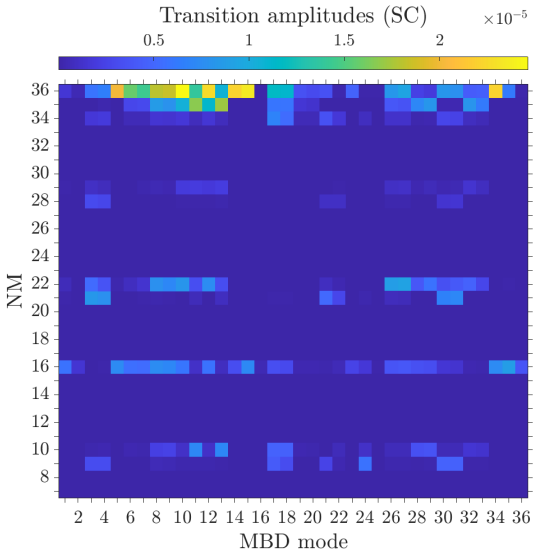

(a)

initial MBD	final NM	P ($\times 10^{-5}$)
10	36	2.47
15	36	2.34
12	36	2.26
14	36	2.21
34	36	2.21
5	36	2.02
9	36	1.85
8	36	1.81
13	35	1.72
11	35	1.67

(b)

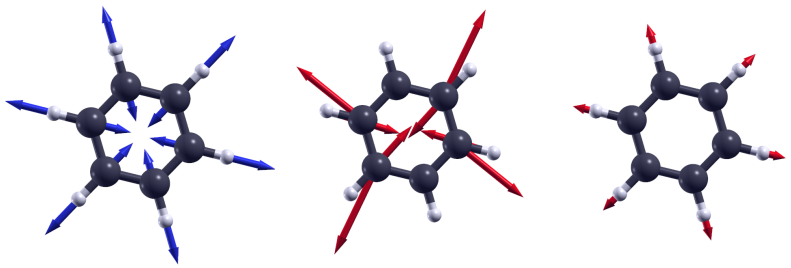

(c) **(d)** **(e)**

Figure 4.1: Transition amplitudes for the C_6H_6 monomer (SC). Visual representation of **(a)** transition amplitudes for vibrational states (y-axis) triggered by excitation of individual MBD modes (x-axis). Pairs of indices (MBD and NM) associated with the highest amplitudes P are reported **(b)** in descending order. Geometric visualization of the modes involved in preferred transitions, using blue arrows for phonon displacements and red arrows for vdW forces: vibrational normal mode 36 **(c)**, exciton MBD modes 10 **(d)** and 15 **(e)**.

retinal entails the breaking and subsequent formation of covalent chemical bonds, which transition between double and single bonds or vice versa. Since MBD only accounts for non covalent vdW forces we anticipate that we cannot expect an accurate description of covalent bonding effects. We rather expect to correctly reproduce large-scale geometry deformations that do not directly depend on covalent bonding.

Moreover, even the molecular size is of interest. In fact, complex structures can exhibit attractive or repulsive optical vdW forces acting non-locally between different parts of the molecule. These non-local forces can influence dynamical geometry rearrangements, as observed in various proteins - a phenomenon unlikely to occur in a stiff and small molecule such as benzene. Another relevant and crucial aspect is that the existence of a vibrational mode with a high overlap with structural changes of interest is not guaranteed a priori. There are fortunate cases, such as the C_{60}-clamp, where the overlap with clamp-opening deformation is complete, and others, like the case of 11-cis-retinal, where no oscillation exists that could entirely lead to the final "all-trans" isomer. Nevertheless, one should consider that the transition to the "all-trans" conformer implies a large rotation of a molecular segment. A much smaller rotation along the same axis could in principle better overlap with a few vibrational modes, and this could still suggest which modes can facilitate the transformation onset.
The interpretation of the SC model is straightforward: the larger the alignment between phonon displacements and van der Waals forces, the higher the transition rate for the excitation of the corresponding phonon. Hence, when willing to deform a system by optical absorption, the challenge is to

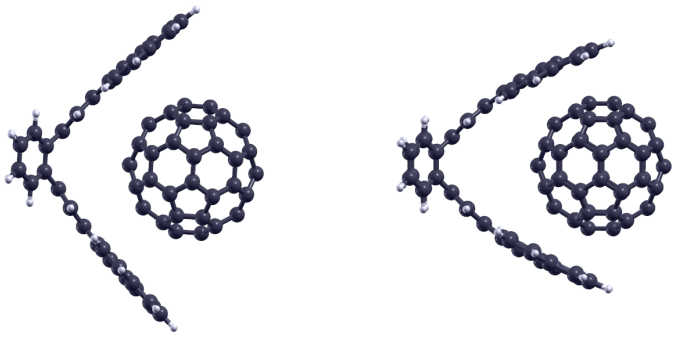

(a) **(b)**

Figure 4.2: Geometrical structure of the 'C_{60}-clamp' complex. The equilibrium configuration from GROMACS energy minimization **(a)**, the 'closed clamp' configuration **(b)**, which is used to calculate the overlap with the vibrational modes.

find the appropriate vibrational mode (and a compatible MBD mode). The SC model preditcs moderate transition amplitudes for the opening/closure of the C_{60}-clamp complex, since the vdW forces tend to be oriented parallel to the planes formed by the carbon 'clamps'. As can be observed in Figs. 4.1d and 4.1e, the MBD modes that admit opening/closure are those in which the forces primarily act on the tail of the structure. Based on these premises, it is nevertheless evident that the coupling between phonons and MBD modes depends on the symmetries of the considered system. Somewhat larger transition amplitudes can be found for vibrational modes that are compatible with the initial step of the conformational change of retinal. One can conclude that the semi-classical exciton-phonon coupling term is relevant only when phonon geometries satisfy the symmetry relationships that characterize van der Waals interactions.

4.1.2 Symmetries

The SC coupling between MBD oscillations and phononic degrees of freedom provides a possible estimate of the transition coefficients. The heatmaps presented in this section (Figs.4.1a, 4.3a, 4.5a, 4.6) exhibit a pronounced dependence on the excited vibrational mode, displaying a 'striped' appearance. Dark colors indicate that for some of these phonon modes, the transition is improbable, regardless of the initial MBD state. This suggests that the favored phononic geometries should exhibit some geometrical properties that are compatible with optical van der Waals forces. For instance, since the MBD model is characterized by certain symmetries, these could play a role in the coupling. It is evident that the system energy is invariant under translation. Envisioning a rigid translation of the molecule along a direction represented by $\boldsymbol{r}' = (a, b, c)$, the energy must remain constant $E(\boldsymbol{r}_1, \ldots, \boldsymbol{r}_N) = E(\boldsymbol{r}_1 + \boldsymbol{r}', \ldots, \boldsymbol{r}_N + \boldsymbol{r}')$. Hence, the relationship $\sum_{i=1}^{N} \nabla_{\boldsymbol{r}_i} E(\boldsymbol{r}) \cdot d\boldsymbol{r}_i = 0$ holds, from which we deduce that

$$-\sum_i \boldsymbol{F}_i^{vdW} \cdot d\boldsymbol{r}_i = -\sum_i \left(F_{i,x}^{vdW} a + F_{i,y}^{vdW} b + F_{i,z}^{vdW} c \right) = 0 \,. \tag{4.17}$$

For each MBD mode γ, adopting QDO indexing one has:

$$\sum_{i=1}^{N} \boldsymbol{F}_i^{(\gamma)} = 0 \,. \tag{4.18}$$

Since the sum of forces is zero, the variation of linear momentum is also zero: $\Delta \boldsymbol{p} = \boldsymbol{F}^{(\gamma)} \Delta t = 0$, and the center of mass cannot be displaced by vdW forces. Since transition amplitudes in Eq.4.16 are higher when forces align with the geometries of vibrational modes, one expects that admitted phonon transitions should be best compatible with this symmetry.

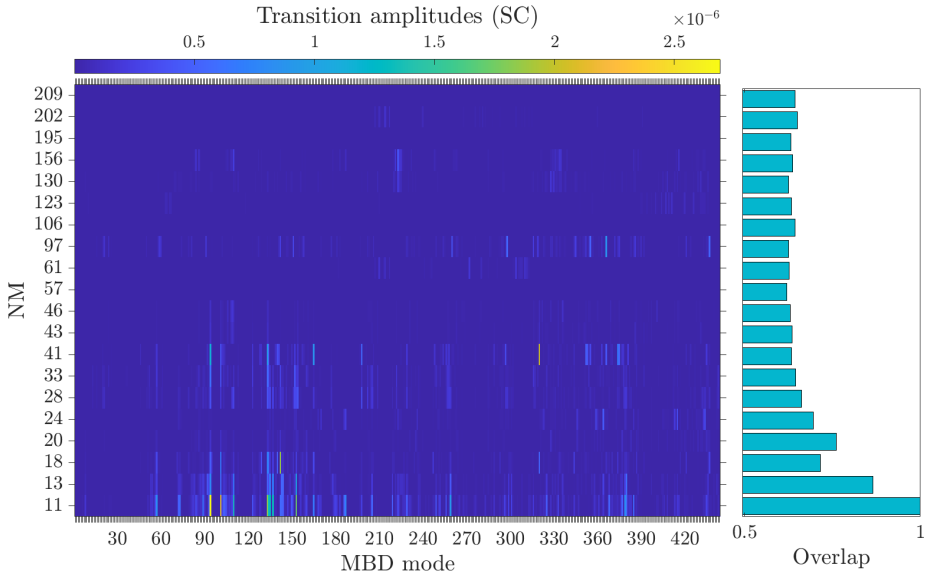

(a)

initial MBD	final NM	P ($\times 10^{-6}$)
94	11	2.69
101	11	2.11
320	41	2.04
142	18	1.87
133	11	1.83
153	11	1.73
110	11	1.35
134	11	1.34
137	11	1.32
135	11	1.27

(b)

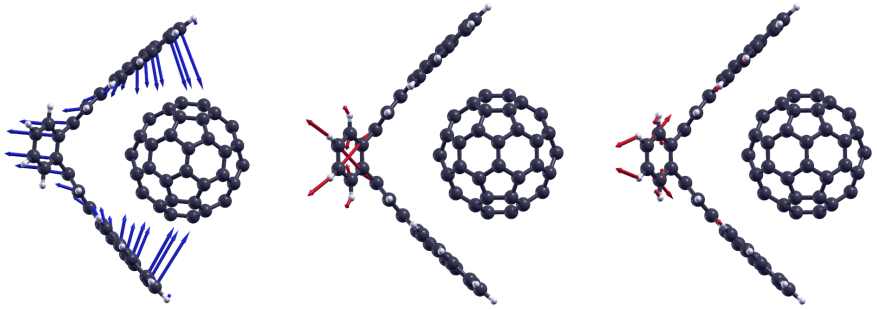

(c) **(d)** **(e)**

Figure 4.3: Transition amplitudes for the C_{60}-clamp complex (SC) . Visual representation **(a)** of transition amplitudes to vibrational state (y-axis) due to excitation of MBD modes (x-axis). The normal modes under consideration are the top 20 modes with the highest overlap with the structural deformation of Fig.4.2b (closed clamp), as indicated by the values reported to the right. Pairs of indices associated with the highest amplitudes P **(b)**, are reported in descending order. Geometric visualization of the modes involved in the preferred transitions, using blue arrows for phonon displacements and red arrows for vdW forces: vibrational mode 7 **(c)**, MBD exciton modes 94 **(d)** and 101 **(e)**.

We thus compute the displacement of the center of mass:

$$\sum_{i=1}^{N} \frac{\boldsymbol{S}_i'^{(k)} m_i}{\sum_j m_j} \equiv \boldsymbol{v}^{(k)} = \boldsymbol{0}\,. \tag{4.19}$$

In this case $\boldsymbol{S}_i'^{(k)}$ is a 3D vector that denotes the displacement direction of i-th atom in k-th vibrational mode (as well as $\boldsymbol{S}'$ matrix is defined in Eq.3.22 in quantum harmonic oscillators indices), furthermore the vector $\boldsymbol{v}^k$ is just defined as the sum of all $\boldsymbol{S}_i'$ of the mode k, weighted by atomic masses. For each vibrational mode we evaluated the norm of the $\boldsymbol{v}^{(k)}$ vector: comparing Fig.4.7a and heatmap of Fig.4.1a for the benzene molecule. It becomes clear that the modes for which the transition amplitudes are non-zero satisfy the condition $|\boldsymbol{v}| = 0$.

Similar considerations can also apply to rotational symmetries. If a rotation matrix $R(\theta)$ is applied to position vectors, the MBD energy does not change, as in the translational case; in fact, the energy

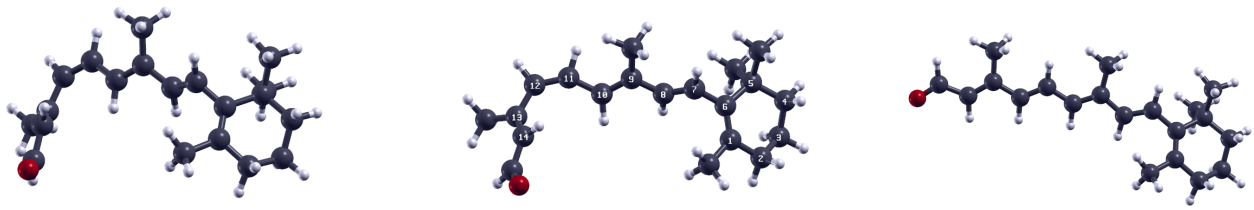

(a) **(b)** **(c)**

Figure 4.4: Geometrical structure of the retinal molecule. Equilibrium configurations obtained by GROMACS energy minimization for the 11-cis isomer (**a**) and all-trans isomer (**c**), i.e. the configuration reached after light absorption in animals. Configuration (**b**) is and intermediate structure obtained by partially rotating the 11-cis-retinal tail around 11-th carbon, by an angle of $\pi/8$ rad.

only depends on the interatomic distances, encoded in the dipole tensor.

$$E(\boldsymbol{r}_1, \ldots, \boldsymbol{r}_N) = E(R(\theta)\boldsymbol{r}_1, \ldots, R(\theta)\boldsymbol{r}_N)\,. \tag{4.20}$$

In a molecular system the torque is the sum of the cross products between forces exerted by atoms and position vectors, and its norm is the derivative of the total energy with respect to rotation angle:

$$|\boldsymbol{M}| = \left|\sum_i \boldsymbol{r}_i \times \boldsymbol{F}_i\right| = \left|\frac{\partial E}{\partial \theta}\right| = 0\,. \tag{4.21}$$

This is zero due to the rotational symmetry. After confirming that the relationship in Eq.4.21 is compatible with each set of vdW forces generated by MBD modes, the same analysis can be carried out for phonon displacements. Hence, the phonon k modes compatible with the property

$$\tau^{(k)} \equiv \left|\sum_i \frac{m_i \boldsymbol{r}_i}{\sum_j m_j} \times \boldsymbol{S}_i'^{(k)}\right| = 0\,, \tag{4.22}$$

are expected to better couple with vdW forces.

The case of the benzene molecule is taken as an example, given that its planar nature allows for a simplification of the analysis. The benzene molecule lies in the xy plane and has its center of mass set as the origin of the coordinates. The vector $\boldsymbol{\tau}$ is evaluated with respect to the axis perpendicular to the molecular plane and passing through its center of mass. As from Fig.4.7b, the condition $\boldsymbol{\tau} = 0$ is respected in approximate form on active modes (small vector products are found there). We expect this is due to the numerical approximations introduced in the geometrical structure and hessian, which are eventually reflected in phonon modes.

We also note that additional symmetries are present in benzene: for instance, discrete rotation of the molecular plane by multiples of 30° introduce neither energy change nor configurational variation. Inspection of the individual phonon modes of benzene for which finite transition probability is found reveals that: i) all phonon modes that are compatible with excitation exhibit a discrete rotational symmetry (either by 30 or 180 degrees); ii) phonon modes that involve displacements that are orthogonal to the molecular plane are incompatible with excitation; iii) some phonon modes have in-plane geometry, but are still incompatible with excitation; these modes are antisymmetric either by rotation by 30, 60, or 180 degrees. We expect analogous conclusions to hold also for other molecules. Detection of molecular symmetries should enable the predictivity of allowed phonon excitations.

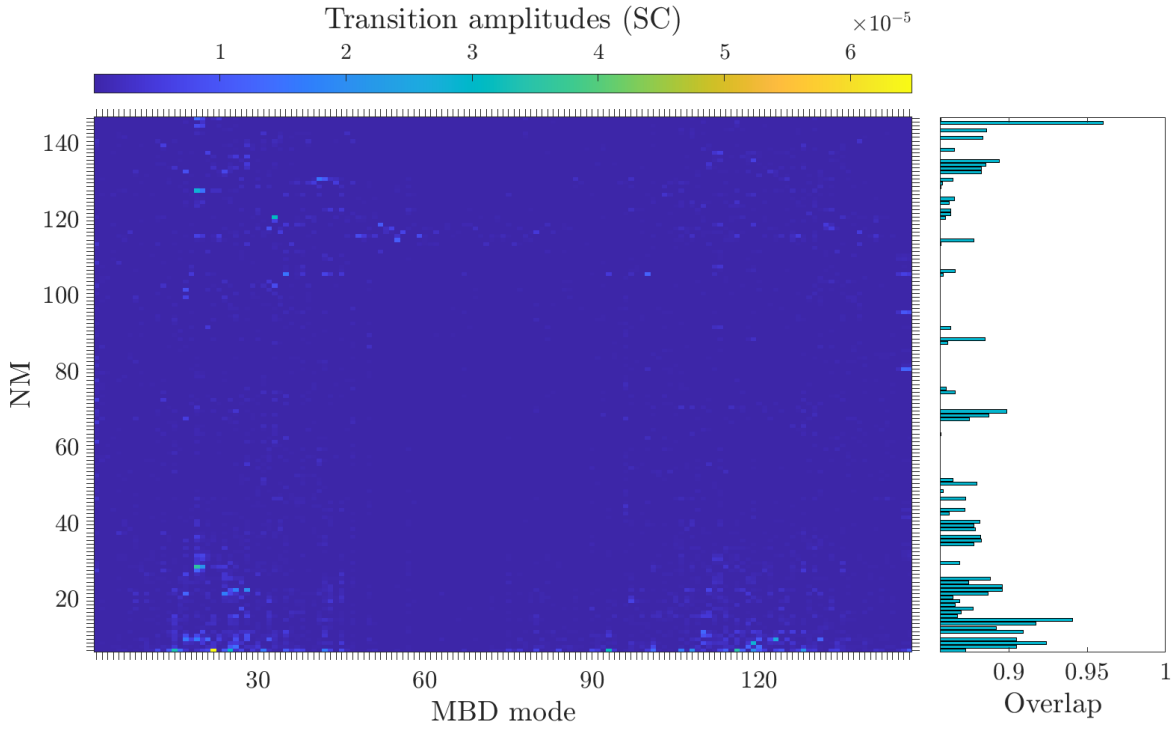

(a)

initial MBD	final NM	P ($\times 10^{-5}$)
22	7	6.49
116	7	3.47
15	7	3.32
93	7	3.15
25	7	3.06
128	7	2.16
108	7	2.04
119	7	2.00
106	7	1.64
42	7	1.63

(b)

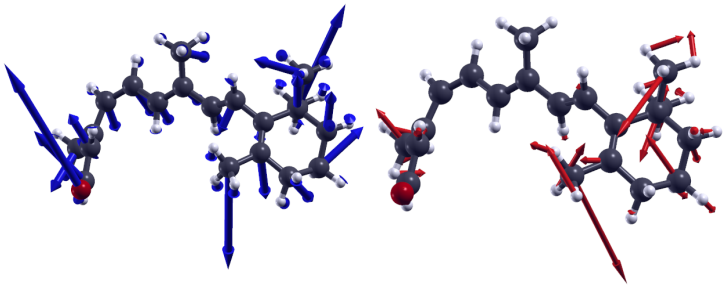

(c) **(d)**

Figure 4.5: Transition amplitudes for the retinal molecule (SC). Visual representation **(a)** of the transition amplitude for given vibrational modes (y-axis, in ascending order in frequency) due to excitation of an individual MBD mode (x-axis, in ascending order in frequency). For each normal mode, the overlap with the structural deformation of 4.4b is on the right side of the heatmap. Pairs of indices associated with the highest amplitudes P **(b)** are reported in descending order. Geometric representation of the modes involved in higher-amplitude transition, using blue arrows for phonon displacements and red arrows for vdW forces: vibrational normal mode 7 **(c)**, exciton MBD mode 22 **(d)**.

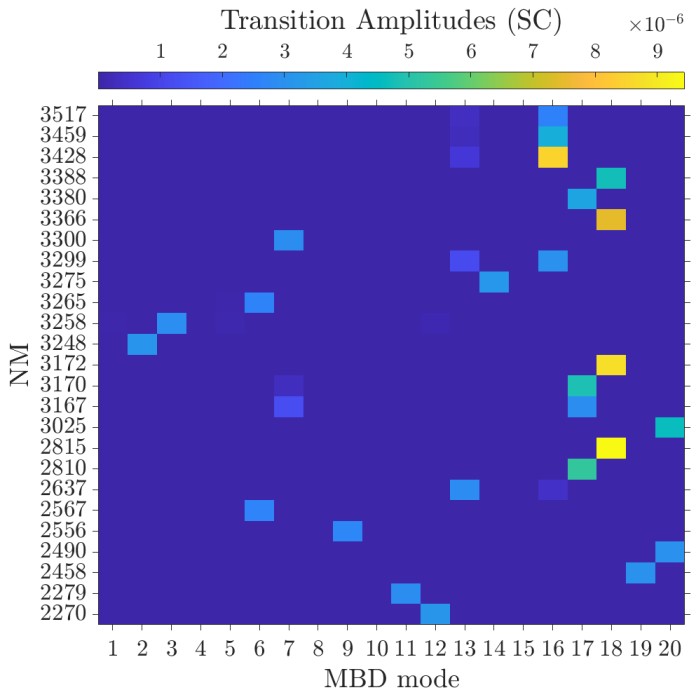

(a)

initial MBD	eV	final NM	P ($\times 10^{-6}$)
18	4.025	2815	9.4
18	4.025	3172	8.7
16	3.835	3428	8.4
18	4.025	3366	7.5
17	3.991	2810	5.3
17	3.991	3170	4.8
18	4.025	3388	4.7
20	4.087	3025	4.6
16	3.835	3459	3.9
17	3.991	3380	3.6

(b)

Figure 4.6: Transition amplitudes for PYP (SC). Visual representation **(a)** of the transition amplitude P for given vibrational normal mode (y-axis, in ascending order in frequency), due to excitation of an individual MBD mode (x-axis, in ascending order in frequency). Pairs of indices associated with the highest amplitudes **(b)** are reported in descending order with the energy of the matching MBD mode (in eV).

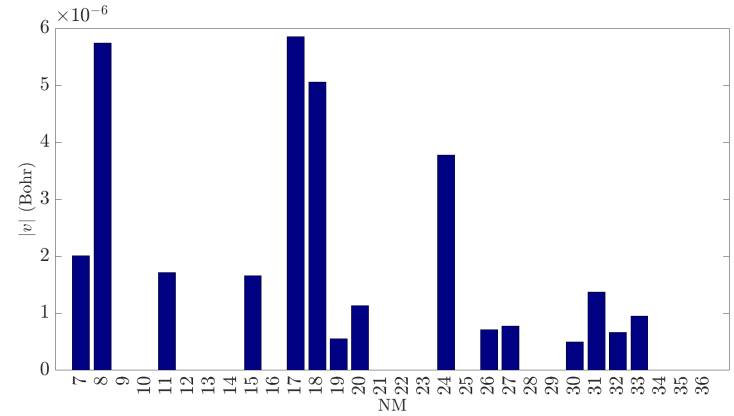

(a)

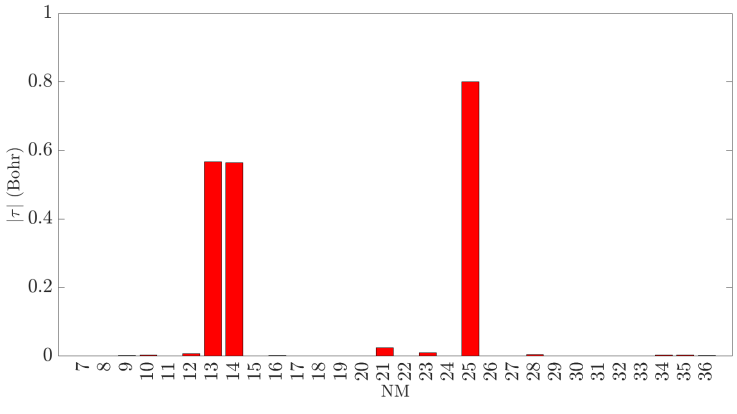

(b)

Figure 4.7: Symmetry analysis. Norm of $\boldsymbol{v}$ **(a)** and $\boldsymbol{\tau}$ **(b)** vectors for each vibrational mode of the benzene.

4.2 Theory of quasielectron-phonon coupling beyond the Born-Oppenheimer approximation

A comprehensive description of a molecular system entails the intricate interplay between electrons and ions, and requires a solution of the Schrödinger equation associated with the global wave function. This endeavor would enable in principle the determination of an energy spectrum that fully accounts for coupled electronic and ionic contributions within the molecular structure of choice. However, solving such a problem is computationally and analytically demanding, especially when dealing with large molecules. The total Hamiltonian depends on both electronic and ionic degrees of freedom. However, within the framework of the Many-Body Dispersion approach, electron clouds are mapped into quasiparticles (referred to as "drudons") that oscillate around the ionic positions and interact with each other through dipole-dipole tensors. This model circumvents the need to explicitly consider the kinetic energy of individual electrons but does not guarantee an independent description of ionic and electronic phenomena.

To simplify the problem, the Born-Oppenheimer (BO) approximation is widely adopted in electronic structure calculations. This approximation implies the separation of ionic and electronic degrees of freedom and facilitates the overall analysis. Shortly, with the BO approximation, one assumes that the electrons are so fast that their wavefunction can instantaneously "adapt" to the ionic configuration. On the other hand, ions should be so slow that they simply determine the external potential of the electrons, and can thus be treated as "frozen" parameters in the electronic wavefunction.

In our specific case, MBD provides an explicit quantum mechanical description of vdW forces, whereas short-range interactions are treated semiclassically. Then, the total Hamiltonian can be expressed as:

$$\begin{aligned}\hat{H} &= \hat{H}_{mbd} + \hat{H}_{ions} \\ &= -\frac{1}{2}\sum_{i=1}^{N}\nabla^2_{\boldsymbol{\xi}_i} + \frac{1}{2}\sum_{i,j}^{N}\boldsymbol{\xi}_i\omega_i\omega_j\left[\delta^{ab}_{ij} + \sqrt{\alpha_i\alpha_j}T^{ab}_{ij}(d_{ij})\right]\boldsymbol{\xi}_j - \frac{1}{2}\sum_{i=1}^{N}\frac{\nabla^2_{\boldsymbol{r_i}}}{m_i} + V_{ions}(\{\boldsymbol{r}\})\,. \end{aligned} \tag{4.23}$$

We recall that $\boldsymbol{\xi}_i$ is the mass-weighted drudon displacement, while d_{ij} is the distance between ions i and j. It is clear that $\hat{H}$ depends on both "electronic" (QDO) $(p_{\tilde{r}}, \tilde{r})$ and ionic (ionic quantum harmonic oscillators IQHO) (p_r, r) degrees of freedom. Hence, the Schrödinger equation for a state $\Phi^i(\tilde{\boldsymbol{r}}, \boldsymbol{r})$, depending on all ionic and electronic coordinates should be:

$$\hat{H}\Phi^i(\tilde{\boldsymbol{r}}, \boldsymbol{r}) = E^i_{tot}\Phi^i(\tilde{\boldsymbol{r}}, \boldsymbol{r})\ . \tag{4.24}$$

Given the much larger masses of the ions compared to electrons, within the BO approximation one neglects the ionic kinetic energy. Ions are thus treated as "fixed" at their positions $\boldsymbol{r}$. This assumption is the first premise of the Born-Oppenheimer approximation. Once ions are "fixed", a new Hamiltonian, referred to as the "electronic" Hamiltonian $\hat{H}_{el}$, is obtained, where only QHO's (electronic degrees of freedom) are treated quantum mechanically:

$$\hat{H}_{el} = -\frac{1}{2}\sum_{i=1}^{N}\nabla^2_{\boldsymbol{\xi}_i} + \frac{1}{2}\sum_{i,j}^{N}\boldsymbol{\xi}_i\omega_i\omega_j\left[\delta^{ab}_{ij} + \sqrt{\alpha_i\alpha_j}T^{ab}_{ij}(d_{ij})\right]\boldsymbol{\xi}_j + V_{ions}(\{\boldsymbol{r}\})\,. \tag{4.25}$$

Here, the term $V_{ions}(\{\boldsymbol{r}\})$ could be neglected since it solely depends on the positions of the ions and only contributes with a constant shift to the MBD energy spectrum. Under this assumption, $\hat{H}_{el}$ equals $\hat{H}_{mbd}$. We observe that $\hat{H}_{mbd}$ depends both on QDO coordinates, and on ionic positions $\boldsymbol{r}$, but the latter are only treated as external parameters. This is the "clamped-nuclei" Schrödinger equation:

$$\hat{H}_{mbd}\psi^n_{\boldsymbol{r}}(\tilde{\boldsymbol{r}}) = E^n_{mbd}(\boldsymbol{r})\psi^n_{\boldsymbol{r}}(\tilde{\boldsymbol{r}})\ . \tag{4.26}$$

Here, the so called "electronic" wave function ψ inherits the "parametric" dependence on ionic positions. Under the assumptions of the adiabatic approximation, a continuous change in the parameters

$\boldsymbol{r}$ enables instantaneous rearrangement of the electronic degrees of freedom (for instance into the updated groundstate). Switching to (quasi-electron) harmonic oscillators' indices (d_{ij} is left in atomic indices) one has:

$$\hat{H}_{mbd} = -\frac{1}{2}\sum_{p=1}^{3N}\nabla^2_{\xi_p} + \frac{1}{2}\sum_{p,q}^{3N}\xi_p\omega_p\omega_q\left[\delta_{pq} + \sqrt{\alpha_p\alpha_q}T_{pq}(d_{ij})\right]\xi_q\,. \tag{4.27}$$

Diagonalization of $\hat{H}_{mbd}$ will produce a set of orthogonal set of eigenstates $\psi^n_{\boldsymbol{r}}(\tilde{\boldsymbol{r}})$ with energies $E^n_{mbd}(\boldsymbol{r})$ depending on ionic positions $\boldsymbol{r}$. Each electronic state n that solves Eq.4.26 is the product of $3N$ independent harmonic oscillator wave functions, each of which depends on a single component of the collective coordinate set $\boldsymbol{\chi}$, as defined in Eq.2.8. The state index n summarizes the set of quantum numbers describing the state of each QDO, $n = \{n_1, n_2, \ldots, n_{3N}\}$.

$$\psi^{\boldsymbol{n}}_{\boldsymbol{r}}(\boldsymbol{\chi}) = \psi^{n_1}_{1,\boldsymbol{r}}(\chi_1)\otimes\ldots\otimes\psi^{n_{3N}}_{3N,\boldsymbol{r}}(\chi_{3N})\,. \tag{4.28}$$

It is important to clarify how the introduced wave functions depend on the different sets of coordinates relevant to a global description of the system. The MBD hamiltonian describes a set of interacting QDO through the dipole-dipole tensor $\boldsymbol{T}$, that depends on the ionic distances (i.e. positions). Diagonalization of the MBD Hamiltonian means to find a set of collective coordinates $\boldsymbol{\chi}$ depending on the whole ionic configuration $\boldsymbol{r}$ present within $\boldsymbol{T}$ itself. The interacting QDO set is transformed into a new set of non interacting QDO, each one characterized by frequency $\tilde{\omega}_i$ and coordinate χ_i. Both of them do not depend on the initial "drudon positions" but still depend on the ionic configuration, hence all components of MBD collective coordinates depend on $\boldsymbol{r}$: $\boldsymbol{\chi}(\boldsymbol{r}) = \chi_1(\boldsymbol{r}), \ldots, \chi_{3N}(\boldsymbol{r})$.
The global wave function Φ^i corresponding to the arbitrary i-th electro-nuclear eigenstate can thus be conveniently expanded as $\Phi^i(\boldsymbol{\chi}, \boldsymbol{r}) = \sum_n c^i_n(\boldsymbol{r})\psi^n_{\boldsymbol{r}}(\boldsymbol{\chi})$. The expansion coefficients c^i_n depend on the ionic configuration, so they are renamed for convenience as $\phi^i_n(\boldsymbol{r})$. The global wave function is thus factorized, partially separating ionic and electronic degrees of freedom. After re-introducing the ionic kinetic energy and the semi-classical potential, Schrödinger's equation for the total Hamiltonian becomes:

$$\hat{H}\sum_n \psi^n_{\boldsymbol{r}}(\boldsymbol{\chi})\,\phi^i_n(\boldsymbol{r}) = E^i_{tot}\sum_n \psi^n_{\boldsymbol{r}}(\boldsymbol{\chi})\,\phi^i_n(\boldsymbol{r}) \tag{4.29}$$

Left-multiplying by $\overline{\psi}^{n'}_{\boldsymbol{r}}(\boldsymbol{\chi})$ (bar denotes complex conjugate) and integrating with respect to the QDO coordinates one obtains:

$$\sum_n \int \overline{\psi}^{n'}_{\boldsymbol{r}}(\boldsymbol{\chi})\,(\hat{H}_{mbd} + \hat{H}_{ions})\psi^n_{\boldsymbol{r}}(\boldsymbol{\chi})\,\phi^i_n(\boldsymbol{r})d\boldsymbol{\chi} = \sum_n \int \overline{\psi}^{n'}_{\boldsymbol{r}}(\boldsymbol{\chi})\,E^i_{tot}\psi^n_{\boldsymbol{r}}(\boldsymbol{\chi})\,\phi^i_{n'}(\boldsymbol{r})d\boldsymbol{\chi}\,. \tag{4.30}$$

Recalling Eq. 4.26, and splitting the many body dispersion energy into $E^{n'}_{mbd}(\boldsymbol{r}) = E^0_{mbd}(\boldsymbol{r}) + \Delta E^{0n'}_{mbd}(\boldsymbol{r})$ (for sake of notation the dependence on $\boldsymbol{r}$ and $\boldsymbol{\chi}$ is now omitted):

$$\sum_n \int \left(\overline{\psi}^{n'}_{\boldsymbol{r}}\hat{H}_{mbd}\psi^n_{\boldsymbol{r}} + \overline{\psi}^{n'}_{\boldsymbol{r}}\hat{T}_{ions}\psi^n_{\boldsymbol{r}} + \overline{\psi}^{n'}_{\boldsymbol{r}}\hat{V}_{ions}\psi^n_{\boldsymbol{r}}\right)\phi^i_n d\boldsymbol{\chi} = E^i_{tot}\phi^i_{n'}\,, \tag{4.31}$$

$$\left(E^0_{mbd}(\boldsymbol{r}) + \Delta E^{0n'}_{mbd}(\boldsymbol{r}) + \hat{V}_{ions}\right)\phi^i_{n'} + \sum_n \int \overline{\psi}^{n'}_{\boldsymbol{r}}\hat{T}_{ions}\psi^n_{\boldsymbol{r}}\phi^i_n d\boldsymbol{\chi} = E^i_{tot}\phi^i_{n'}\,. \tag{4.32}$$

The term $\int \overline{\psi}^{n'}_{\boldsymbol{r}}\hat{T}_{ions}\psi^n_{\boldsymbol{r}}\phi^i_n d\boldsymbol{\chi}$ needs to be carefully analyzed. The operations regarding electronic states $\psi^n_{\boldsymbol{r}}(\boldsymbol{\chi})$ are recast following Dirac's bra-ket notation, for two states $\psi^n_{\boldsymbol{r}}(\boldsymbol{\chi})$ and $\psi^{n'}_{\boldsymbol{r}}(\boldsymbol{\chi})$ and an operator $\hat{\boldsymbol{A}}$, both parametrically depending on the same ionic configuration $\boldsymbol{r}$. We accordingly define $\langle n'_{\boldsymbol{r}}|\,\hat{\boldsymbol{A}}\,|n_{\boldsymbol{r}}\rangle = \int \overline{\psi}^{n'}_{\boldsymbol{r}}\hat{\boldsymbol{A}}\psi^n_{\boldsymbol{r}}d\boldsymbol{\chi} = \int \overline{\psi}^{n'}_{\boldsymbol{r}}\hat{\boldsymbol{A}}\psi^n_{\boldsymbol{r}}d\chi_1\ldots\chi_{3N}$. Obviously, the final integral will still depend on

$\boldsymbol{r}$.

$$\begin{aligned}\int \overline{\psi}^{n'}_{\boldsymbol{r}} \hat{T}_{ions} \psi^{n}_{\boldsymbol{r}} \phi^{i}_{n} d\boldsymbol{\chi} &= -\frac{1}{2}\sum_{p}\frac{1}{m_p}\int \overline{\psi}^{n'}_{\boldsymbol{r}} \nabla^2_{r_p}\left(\psi^{n}_{\boldsymbol{r}}\phi^{i}_{n}\right) d\boldsymbol{\chi} \\ &= -\frac{1}{2}\sum_{p}\frac{1}{m_p}\int \overline{\psi}^{n'}_{\boldsymbol{r}} \left(\left(\nabla^2_{r_p}\psi^{n}_{\boldsymbol{r}}\right)\phi^{i}_{n} + 2(\nabla_{r_p}\psi^{n}_{\boldsymbol{r}})(\nabla_{r_p}\phi^{i}_{n}) + \psi^{n}_{\boldsymbol{r}}\nabla^2_{r_p}\phi^{i}_{n}\right) d\boldsymbol{\chi} \\ &= -\frac{1}{2}\sum_{p}\frac{1}{m_p}\int \left(\overline{\psi}^{n'}_{\boldsymbol{r}} \left(\nabla^2_{r_p}\psi^{n}_{\boldsymbol{r}}\right)\phi^{i}_{n} + 2\overline{\psi}^{n'}_{\boldsymbol{r}} \left(\nabla_{r_p}\psi^{n}_{\boldsymbol{r}}\right)\left(\nabla\phi^{i}_{n}\right) + \overline{\psi}^{n'}_{\boldsymbol{r}} \left(\nabla^2_{r_p}\phi^{i}_{n}\right)\psi^{n}_{\boldsymbol{r}}\right) d\boldsymbol{\chi} \\ &= -\frac{1}{2}\sum_{p}\frac{1}{m_p}\left(\langle n'_{\boldsymbol{r}}|\,\nabla^2_{r_p}\,|n_{\boldsymbol{r}}\rangle\,\phi^{i}_{n} + 2\,\langle n'_{\boldsymbol{r}}|\,\nabla_{r_p}\,|n_{\boldsymbol{r}}\rangle\,\nabla_{r_p}\phi^{i}_{n} + \delta_{nn'}\nabla^2_{r_p}\phi^{i}_{n}\right). \end{aligned} \tag{4.33}$$

Plugging this result into the Eq. 4.32 one has:

$$\begin{aligned}&\left(E^{0}_{mbd}(\boldsymbol{r}) - \frac{1}{2}\sum_{p}\frac{\nabla^2_{r_p}}{m_p} + \hat{V}_{ions} + \Delta E^{0n'}_{mbd}(\boldsymbol{r})\right)\phi^{i}_{n'} \\ &-\sum_{pn}\frac{1}{m_p}\left(\frac{1}{2}\,\langle n'_{\boldsymbol{r}}|\,\nabla^2_{r_p}\,|n_{\boldsymbol{r}}\rangle + \langle n'_{\boldsymbol{r}}|\,\nabla_{r_p}\,|n_{\boldsymbol{r}}\rangle\,\nabla_{r_p}\right)\phi^{i}_{n} \\ &= E^{i}_{tot}\phi^{i}_{n'}\,. \end{aligned} \tag{4.34}$$

The functions $\phi^{i}_{n}(\boldsymbol{r})$ will be related to the nuclear dynamics. Expanding in vibrational eigenstates φ_a one finds:

$$\phi^{i}_{n}(\boldsymbol{r}) = \sum_{a} C^{i}_{na}\varphi_a(\boldsymbol{r})\,, \tag{4.35}$$

$$\left(E^{0}_{mbd}(\boldsymbol{r}) - \frac{1}{2}\sum_{p}\frac{\nabla^2_{r_p}}{m_p} + \hat{V}_{ions} + \Delta E^{0n'}_{mbd}(\boldsymbol{r})\right)\sum_{a} C^{i}_{n'a}\varphi_a \tag{4.36}$$

$$\begin{aligned}&-\sum_{pn}\frac{1}{m_p}\left(\frac{1}{2}\,\langle n'_{\boldsymbol{r}}|\,\nabla^2_{r_p}\,|n_{\boldsymbol{r}}\rangle + \langle n'_{\boldsymbol{r}}|\,\nabla_{r_p}\,|n_{\boldsymbol{r}}\rangle\,\nabla_{r_p}\right)\sum_{a} C^{i}_{na}\varphi_a \\ &= E^{i}_{tot}\sum_{a} C^{i}_{n'a}\varphi_a\,. \end{aligned} \tag{4.37}$$

Since $V(\boldsymbol{r}) = E^{0}_{mbd}(\boldsymbol{r}) + \hat{V}_{ions}(\boldsymbol{r})$ is a potential involving both the short-range inter-ionic potential and (groundstate) dispersion interactions, the term $-\frac{1}{2}\sum_{p}\frac{\nabla^2_{r_p}}{m_p} + V(\boldsymbol{r})$ is commonly interpreted as the quantum mechanical Hamiltonian $\hat{H}_{ph}$ for the nuclei. Adopting the harmonic approximation for $V(\boldsymbol{r})$ (which is appropriate at the overall equilibrium geometry and will be adopted hereafter), one obtains the same Hamiltonian introduced in Chapter 3 to describe molecular vibrations:

$$\hat{H}_{ph}(\boldsymbol{r}) = -\frac{1}{2}\sum_{p=1}^{3N}\nabla^2_{q_p} + \frac{1}{2}\sum_{pq=1}^{3N} q_p\mathcal{H}_{pq}q_q\,. \tag{4.38}$$

Here q_i is the mass-weighted i-th ionic QHO displacement operator and $\dfrac{\nabla^2_{r_p}}{m_p} = \nabla^2_{q_p}$. The nuclear vibrational spectrum is obtained by diagonalizing the mass-weighted Hessian matrix $\boldsymbol{\mathcal{H}}$, and it only depends on the equilibrium configuration $\boldsymbol{R}$. In this case as well, as shown in Section 3.1.1, it is convenient to adopt an ionic wave function that is a product of single-particle functions. To achieve this, the description of ion dynamics is shifted from Cartesian positions $\boldsymbol{r}$ to collective coordinates $\boldsymbol{\rho}$, defined in Eq. 3.22. Hence the ionic wave function in Eq.4.35 becames

$$\phi^{i}_{n}(\boldsymbol{r}) = \phi^{i}_{n}(\boldsymbol{\rho}) = \sum_{a} C^{i}_{na}\varphi_a(\boldsymbol{\rho})\,, \tag{4.39}$$

$$\varphi_a(\boldsymbol{\rho}) = \varphi_{1,a_1}(\rho_1)\otimes\ldots\otimes\varphi_{3N,a_{3N}}(\rho_{3N})\,, \tag{4.40}$$

where in Eq. 4.40 the ionic state index a describes a set of quantum numbers for single QHO, $a = \{a_1, \ldots, a_{3N}\}$. The vibrational eigenstates φ_a are chosen to diagonalize $\hat{H}_{ph}$

$$\int \overline{\varphi}_b(\boldsymbol{\rho}) \hat{H}_{ph}(\boldsymbol{\rho}) \varphi_a(\boldsymbol{\rho}) d\boldsymbol{\rho} = \delta_{ab} E_a^{ph}(\boldsymbol{R}) \,. \tag{4.41}$$

For an arbitrary ionic operator $\hat{B}$ we now extend the bra-ket notation introduced above $\langle \varphi_b | \hat{B} | \varphi_a \rangle = \int \varphi_b(\boldsymbol{\rho}) \hat{B} \varphi_a(\boldsymbol{\rho}) d\boldsymbol{\rho}$. Then, after left multiplication for $\overline{\varphi}_b$ and integration with respect to ionic collective coordinates one has:

$$\begin{aligned}
\sum_a C_{n'a}^i \int \overline{\varphi}_b E_a^{ph} \varphi_a d\boldsymbol{\rho} \;\; + \;\; \sum_a C_{n'a}^i \int \overline{\varphi}_b \Delta E_{mbd}^{0n'}(\boldsymbol{r}) \varphi_a d\boldsymbol{\rho} \\
- \frac{1}{2} \int \sum_{pna} \frac{1}{m_p} C_{na}^i \overline{\varphi}_b(\boldsymbol{\rho}) \langle n'_{\boldsymbol{r}} | \nabla_{r_p}^2 | n_{\boldsymbol{r}} \rangle \varphi_a(\boldsymbol{\rho}) d\boldsymbol{\rho} \\
- \sum_{pna} \frac{1}{m_p} C_{na}^i \int \overline{\varphi}_b \langle n'_{\boldsymbol{r}} | \nabla_{r_p} | n_{\boldsymbol{r}} \rangle \nabla_{r_p} \varphi_a \; d\boldsymbol{\rho} \\
= \sum_a E_{tot}^i C_{n'a}^i \underbrace{\int \overline{\varphi}_b \varphi_a d\boldsymbol{\rho}}_{\delta_{ab}} \,.
\end{aligned} \tag{4.42}$$

In Eq. 4.42 the presence of 'electronic' matrix elements of the kind $\langle n'_{\boldsymbol{r}} | \hat{\boldsymbol{A}} | n_{\boldsymbol{r}} \rangle$ make the integration with respect to ionic coordinates not trivial since the interdependence between $\boldsymbol{r}$ and $\boldsymbol{\rho}$ coordinates' sets, hence some approximations is introduced. The term $\Delta E_{mbd}^{0n'}(\boldsymbol{r})$ is expanded in Taylor series for small displacements around the equilibrium configuration $\boldsymbol{R}$:

$$\Delta E_{mbd}^{0n'}(\boldsymbol{r}) \simeq \Delta E_{mbd}^{0n'}(\boldsymbol{R}) + \sum_\sigma \frac{\partial \Delta E_{mbd}^{0n'}}{\partial r_\sigma}\Big|_{\boldsymbol{r}=\boldsymbol{R}} (r_\sigma - R_\sigma) \tag{4.43}$$

$$= \Delta E_{mbd}^{0n'}(\boldsymbol{R}) - \sum_\sigma F_\sigma^{n'}(\boldsymbol{R}) dr_\sigma \,. \tag{4.44}$$

Then, the electronic states are assumed to be nearly constant, given the small oscillations of the ions:

$$\langle n'_{\boldsymbol{r}} | \nabla_{r_p} | n_{\boldsymbol{r}} \rangle \simeq \langle n'_{\boldsymbol{R}} | \nabla_{r_p} | n_{\boldsymbol{R}} \rangle \;, \tag{4.45}$$

$$\langle n'_{\boldsymbol{r}} | \nabla_{r_p}^2 | n_{\boldsymbol{r}} \rangle \simeq \langle n'_{\boldsymbol{R}} | \nabla_{r_p}^2 | n_{\boldsymbol{R}} \rangle \;. \tag{4.46}$$

In this way $\langle n'_{\boldsymbol{R}} | \nabla_{r_p} | n_{\boldsymbol{R}} \rangle$ and $\langle n'_{\boldsymbol{R}} | \nabla_{r_p}^2 | n_{\boldsymbol{R}} \rangle$ depend only on $\boldsymbol{R}$ and are taken out of the integral:

$$\begin{aligned}
\sum_a C_{n'a}^i E_a^{ph}(\boldsymbol{R}) \underbrace{\langle \varphi_b | \varphi_a \rangle}_{\delta_{ab}} \;\; + \sum_a C_{n'a}^i \Delta E_{mbd}^{0n'}(\boldsymbol{R}) \underbrace{\langle \varphi_b | \varphi_a \rangle}_{\delta_{ab}} - \sum_a C_{n'a}^i \sum_\sigma F_\sigma^{n'}(\boldsymbol{R}) \langle \varphi_b | dr_\sigma | \varphi_a \rangle \\
- \frac{1}{2} \sum_{pna} \frac{1}{m_p} C_{na}^i \langle n'_{\boldsymbol{R}} | \nabla_{r_p}^2 | n_{\boldsymbol{R}} \rangle \underbrace{\langle \varphi_b | \varphi_a \rangle}_{\delta_{ab}} \\
- \sum_{pna} \frac{1}{m_p} C_{na}^i \langle n'_{\boldsymbol{R}} | \nabla_{r_p} | n_{\boldsymbol{R}} \rangle \langle \varphi_b | \nabla_{r_p} | \varphi_a \rangle \\
= \sum_a E_{tot}^i C_{n'a}^i \underbrace{\langle \varphi_b | \varphi_a \rangle}_{\delta_{ab}} \,.
\end{aligned} \tag{4.47}$$

Therefore, after contraction with MBD and ionic states, Schrödiger's equation takes the following form:

$$\begin{aligned}
C_{n'b}^i E_b^{ph}(\boldsymbol{R}) + C_{n'b}^i \Delta E_{mbd}^{0n'}(\boldsymbol{R}) - \sum_a C_{n'a}^i \sum_\sigma F_\sigma^{n'}(\boldsymbol{R}) \langle \varphi_b | dr_\sigma | \varphi_a \rangle \\
- \frac{1}{2} \sum_{pn} \frac{1}{m_p} C_{nb}^i \langle n'_{\boldsymbol{R}} | \nabla_{r_p}^2 | n_{\boldsymbol{R}} \rangle - \sum_{pna} \frac{1}{m_p} C_{na}^i \langle n'_{\boldsymbol{R}} | \nabla_{r_p} | n_{\boldsymbol{R}} \rangle \langle \varphi_b | \nabla_{r_p} | \varphi_a \rangle \\
= E_{tot}^i C_{n'b}^i \,.
\end{aligned} \tag{4.48}$$

One can now assume that at some initial time the system occupies well defined vibrational and MBD states, i.e. the tensor product of $|\varphi_a\rangle$ and $|n_{\boldsymbol{R}}\rangle$, associated to the vibrational and MBD energies $E_a^{ph}(\boldsymbol{R})$ and $\Delta E_{mbd}^{0n'}(\boldsymbol{R})$, respectively. According to Eq. (4.48) the system has the possibility to transition from one state to another, due to the presence of non-diagonal "electron-phonon" coupling terms, that effectively act as perturbations. In the framework of perturbation theory the transition amplitude is obtained from the square modulus of the bra-ket product of the operator describing the perturbation $\hat{H}'$ and the initial and final states, in the unperturbed picture: $P\left(a \to b\right) = \left|\langle a|\, \hat{H}'\, |b\rangle\right|^2$. In our case:

$$\begin{aligned}\langle\varphi_b|\, \langle n'_{\boldsymbol{R}}|\, \hat{H}'\, |n_{\boldsymbol{R}}\rangle\, |\varphi_a\rangle = \delta_{nn'} \sum_\sigma F_\sigma^{n'}(\boldsymbol{R})\, \langle\varphi_b|\, dr_\sigma\, |\varphi_a\rangle - \frac{\delta_{ab}}{2} \sum_p \frac{1}{m_p}\, \langle n'_{\boldsymbol{R}}|\, \nabla^2_{r_p}\, |n_{\boldsymbol{R}}\rangle \\ - \sum_p \frac{1}{m_p}\, \langle n'_{\boldsymbol{R}}|\, \nabla_{r_p}\, |n_{\boldsymbol{R}}\rangle\, \langle\varphi_b|\, \nabla_{r_p}\, |\varphi_a\rangle\ . \end{aligned} \tag{4.49}$$

To simplify the overall notation, we introduce the following definitions:

$$\begin{aligned}\sum_\sigma F_\sigma^{n'}(\boldsymbol{R})\, \langle\varphi_b|\, dr_\sigma\, |\varphi_a\rangle = U_{n'}\left(a \to b\right)\ , \\ \sum_p \frac{1}{m_p}\, \langle n'_{\boldsymbol{R}}|\, \nabla_{r_p}\, |n_{\boldsymbol{R}}\rangle\, \langle\varphi_b|\, \nabla_{r_p}\, |\varphi_a\rangle = V\left(a \to b, n \to n'\right)\ , \\ \sum_p \frac{1}{m_p}\, \langle n'_{\boldsymbol{R}}|\, \nabla^2_{r_p}\, |n_{\boldsymbol{R}}\rangle = W\left(n \to n'\right)\ . \end{aligned} \tag{4.50}$$

The term $U_{n'}\left(a \to b\right)$ leaves the MBD state unchanged, thus it is different from zero only if $|n'\rangle = |n\rangle$, while it implies a single vibrational excitation/de-excitation. $V\left(a \to b, n \to n'\right)$ involves both vibrational and MBD transitions, while $W\left(n \to n'\right)$ only introduces MBD transitions.

Since our aim is to investigate the photoinduced energy transfer from electronic to vibrational modes, we will only focus on terms enabling vibrational transitions. In computing the transition probability from a vibrational state to another, we will ignore at the moment which final MBD state is eventually reached, and $W\left(n \to n'\right)$ will be neglected. Conversely, $U_{n'}\left(a \to b\right)$ and $V\left(a \to b, n \to n'\right)$ will be explicitly evaluated for an initial state corresponding to the vibrational groundstate, accompanied by a single γ excitation, induced after light absorbtion: $\Phi^{in} = |\varphi_0\rangle \otimes |1_{\gamma\boldsymbol{R}}\rangle$. Under this assumption one has:

$$U_{1_\gamma}\left(0 \to b\right) = \sum_\sigma F_\sigma^{1\gamma}(\boldsymbol{R})\, \langle\varphi_b|\, dr_\sigma\, |\varphi_0\rangle\ . \tag{4.51}$$

The displacement for the i-th harmonic oscillator $dr_i = r_i - R_i$ is a linear combination of the collective normal coordinates $\boldsymbol{\rho}$, $dr_i = \sum_j S'_{ij}\rho_j$, with $\rho_i = \frac{1}{\sqrt{2\mu_i\Omega_i}}\left(\hat{b}_i + \hat{b}_i^\dagger\right)$, with $\hat{b}_i$,$\hat{b}_i^\dagger$ respectively annihilation and destruction operators for i-th quantum of vibrational state.

$$\begin{aligned} U_{1_\gamma}\left(0 \to b\right) &= -\sum_{pj} F_p^{(1_\gamma)} S'_{pj}\, \langle\varphi_b|\, \rho_j\, |\varphi_0\rangle \\ &= -\sum_{pj} F_p^{(1_\gamma)} \frac{S'_{pj}}{\sqrt{2\mu_j\Omega_j}} \underbrace{\langle\varphi_b|\, \hat{b}_j + \hat{b}_j^\dagger\, |\varphi_0\rangle}_{\delta_{bj}} \\ &= -\frac{1}{\sqrt{2\mu_b\Omega_b}} \sum_p F_p^{(1_\gamma)} S'_{pb} \qquad (4.52) \\ &= -\frac{1}{\sqrt{2\mu_b\Omega_b}} \boldsymbol{F}^{(1_\gamma)} \cdot \boldsymbol{S}'^{(b)}\ . \qquad (4.53) \end{aligned}$$

$\boldsymbol{F}^{(1_\gamma)}$ is the force vector which arises upon excitation of the 1_γ MBD state, and $\boldsymbol{S}'^{(b)}$ is the b-th column of the atomic to normal coordinates transformation matrix $\boldsymbol{S}'$. We note that this term exactly matches

that obtained in Eq. (4.15) from semi-classical considerations. This semi-classical coupling term is commonly expected to provide the leading-order contribution to the photoexcitation of vibrational modes.

The coefficient $V^{ba}_{n'n}$, instead, is a quantum correction (QC), which involves a change in both vibrational and MBD states. This can be evaluated as:

$$V\left(0 \to b, 1_\gamma \to n'\right) = \sum_p \frac{1}{m_p} \langle n'_{\boldsymbol{R}}| \nabla_{r_p} |1_{\gamma \boldsymbol{R}}\rangle \langle \varphi_b| \nabla_{r_p} |\varphi_0\rangle \ . \tag{4.54}$$

In particular, considering that

$$\begin{aligned} \langle n'_{\boldsymbol{R}}| \left[H_{mbd}, P_p\right] |n_{\boldsymbol{R}}\rangle &= \langle n'_{\boldsymbol{R}}| H_{mbd} P_p |n_{\boldsymbol{R}}\rangle - \langle n'_{\boldsymbol{R}}| P_p H_{mbd} |n_{\boldsymbol{R}}\rangle \\ &= \left(E^{n'}_{mbd}(\boldsymbol{R}) - E^{n}_{mbd}(\boldsymbol{R})\right) \langle n'_{\boldsymbol{R}}| P_p |n_{\boldsymbol{R}}\rangle \ , \end{aligned} \tag{4.55}$$

and since momentum operators and space derivatives are related by $P_p = -i\nabla_{r_p}$, one finds:

$$\langle n'_{\boldsymbol{R}}| P_p |n_{\boldsymbol{R}}\rangle = \frac{\langle n'_{\boldsymbol{R}}| \left[H_{mbd}, P_p\right] |n_{\boldsymbol{R}}\rangle}{\left(E^{n'}_{mbd}(\boldsymbol{R}) - E^{n}_{mbd}(\boldsymbol{R})\right)} \ . \tag{4.56}$$

Exploiting now the expression for the commutator $[H_{mbd}, P_p] = i\nabla_{r_p} H_{mbd}$ one can write

$$\begin{aligned} \langle n'_{\boldsymbol{R}}| \nabla_{r_p} |n_{\boldsymbol{R}}\rangle &= i \frac{\langle n'_{\boldsymbol{R}}| \left[H_{mbd}, P_p\right] |n_{\boldsymbol{R}}\rangle}{\left(E^{n'}_{mbd}(\boldsymbol{R}) - E^{n}_{mbd}(\boldsymbol{R})\right)} \\ &= -\frac{\langle n'_{\boldsymbol{R}}| \left(\nabla_{r_p} H_{mbd}\right) |n_{\boldsymbol{R}}\rangle}{\left(E^{n'}_{mbd}(\boldsymbol{R}) - E^{n}_{mbd}(\boldsymbol{R})\right)} \ . \end{aligned} \tag{4.57}$$

Finally, exploiting the above relations, $V\left(0 \to b, 1_\gamma \to n'\right)$ can be computed as:

$$V\left(0 \to b, 1_\gamma \to n'\right) = -\sum_p \frac{\langle n'_{\boldsymbol{R}}| \left(\nabla_{r_p} H_{mbd}\right) |1_\gamma\rangle}{\left(E^{n'}_{mbd}(\boldsymbol{R}) - E^{1_\gamma}_{mbd}(\boldsymbol{R})\right)} \frac{\langle \varphi_b| \nabla_{r_p} |\varphi_0\rangle}{m_p} \ . \tag{4.58}$$

In order to explicitly evaluate this expression and to understand the allowed transitions, it is necessary to clearly emphasize the operatorial nature of $\nabla_{r_p} H_{mbd}$. Since the dipole-dipole tensor $\boldsymbol{T}$ depends on atomic distances, the analytic computation is performed in atomic indices ($p = 3(l-1) + c$):

$$\begin{aligned} \frac{\partial \hat{H}_{mbd}}{\partial r^c_l} &= \frac{\partial \hat{T}_{mbd}}{\partial r^c_l} + \frac{\partial \hat{V}_{mbd}}{\partial r^c_l} \qquad (4.59) \\ &= \frac{1}{2} \sum_{j,k} \sum_{a,b} \frac{\partial}{\partial r^c_l} \left[\xi^a_k C^{ab}_{kj}(d_{kj}) \xi^b_j\right] \\ &= \frac{1}{2} \sum_{j,k} \sum_{a,b} \left(\frac{\partial \xi^a_k \xi^b_j}{\partial r^c_l} C^{ab}_{kj}(d_{kj}) + \xi^a_k \xi^b_j \frac{\partial C^{ab}_{kj}(d_{kj})}{\partial r^c_l} \right) \\ &= \frac{1}{2} \sum_{j,k} \sum_{a,b} \left(\left(\xi^b_j \delta^{ac}_{lk} + \xi^a_k \delta^{bc}_{lj}\right) C^{ab}_{kj} + \xi^a_k \xi^b_j \frac{\partial C^{ab}_{kj}}{\partial r^c_l} \right) \\ &= \sum_{jkab} \xi^b_j \delta^{ca}_{lk} C^{ab}_{kj} + \frac{1}{2} \sum_{jkab} \xi^a_k \xi^b_j \frac{\partial C^{ab}_{kj}(d_{kj})}{\partial r^c_l} \qquad (4.60) \\ &= \sum_{jb} \xi^b_j C^{cb}_{lj} + \frac{1}{2} \sum_{jkab} \xi^a_k \xi^b_j \frac{\partial C^{ab}_{kj}}{\partial r^c_l} \ . \qquad (4.61) \end{aligned}$$

The step in Eq.4.59 is elaborated upon in the Appendix D, where it is demonstrated that the derivative with respect to the ionic coordinates of the MBD kinetic term is zero. Switching again to

QHO indices ($s = 3(k-1)+a$, $q = 3(j-1)+b$), after the transformation $\xi_q = \sum_\mu M_{q\mu}\chi_\mu = \sum_\mu M_{q\mu}\frac{1}{\sqrt{2\tilde{\omega}_\mu}}\left(\hat{a}_\mu + \hat{a}_\mu^\dagger\right) \equiv \sum_\mu \overline{M}_{q\mu}\left(\hat{a}_\mu + \hat{a}_\mu^\dagger\right)$, where annihilation and creation operators for the i-th MBD mode $\hat{a}_i$, $\hat{a}_i^\dagger$ satisfy $\chi_i = \frac{1}{\sqrt{2\tilde{\omega}_i}}\left(\hat{a}_i + \hat{a}_i^\dagger\right)$, Eq.4.61 becomes:

$$\frac{\partial \hat{H}_{mbd}}{\partial r_p} = \sum_q \xi_q C_{pq} + \frac{1}{2}\sum_{qs}\xi_s\xi_q\frac{\partial C_{sq}}{\partial r_p} \tag{4.62}$$

$$= \sum_{q\mu}\overline{M}_{q\mu}C_{pq}\left(\hat{a}_\mu + \hat{a}_\mu^\dagger\right) + \frac{1}{2}\sum_{qs\mu\nu}\overline{M}_{q\mu}\overline{M}_{s\nu}C'_{psq}\left(\hat{a}_\mu + \hat{a}_\mu^\dagger\right)\left(\hat{a}_\nu + \hat{a}_\nu^\dagger\right). \tag{4.63}$$

Hence, the derivative of a function $F(\boldsymbol{r})$, with respect to the ionic displacement is in this manner transformed:

$$\nabla_{r_p}F(r_1,\ldots,r_{3N}) = \sum_i \frac{\partial F}{\partial \rho_i}\frac{\partial \rho_i}{\partial r_p} = \sum_i \frac{\partial F}{\partial \rho_i}\frac{\partial\left(\sum_j S'^T_{ij} r_j\right)}{\partial r_p}$$

$$= \sum_i \frac{\partial F}{\partial \rho_i}\sum_j \delta_{jp}S'^T_{ij} = \sum_i S'^T_{ip}\nabla_{\rho_i}F\,. \tag{4.64}$$

Vibrational ladder operators also satisfy $\nabla_{\rho_i} = \sqrt{\frac{\mu_i\Omega_i}{2}}\left(\hat{b}_i - \hat{b}_i^\dagger\right)$, therefore

$$\nabla_{r_p} = \sum_i S'^T_{ip}\nabla_{\rho_i} = \sum_i S'_{pi}\sqrt{\frac{\mu_i\Omega_i}{2}}\left(\hat{b}_i - \hat{b}_i^\dagger\right). \tag{4.65}$$

Briefly, the bra-ket product involving phonon states and gradient coordinates is

$$\langle\varphi_b|\,\nabla_{r_p}\,|\varphi_0\rangle = -S'_{pb}\sqrt{\frac{\mu_b\Omega_b}{2}}\,. \tag{4.66}$$

Therefore, combining Eq. 4.61, Eq. 4.66 and Eq. 4.58, defining for sake of notation $\boldsymbol{\Lambda}$ and $\boldsymbol{\Pi}$ tensors as

$$\Lambda_{b\mu} = \sqrt{\frac{\mu_b\Omega_b}{2}}\sum_{pq}\frac{\overline{M}_{q\mu}C_{pq}S'_{pb}}{m_p}\,, \tag{4.67}$$

$$\Pi_{b\mu\nu} = \sqrt{\frac{\mu_b\Omega_b}{8}}\sum_{pqs}\frac{\overline{M}_{q\mu}\overline{M}_{s\nu}C'_{psq}S'_{pb}}{m_p}\,, \tag{4.68}$$

the V coefficient is

$$V\left(0\to b, 1_\gamma\to n'\right) = \sum_\mu \frac{\langle n'|\left(\hat{a}_\mu + \hat{a}_\mu^\dagger\right)|1_\gamma\rangle}{\left(E^{n'}_{mbd}(\boldsymbol{R}) - E^{1_\gamma}_{mbd}(\boldsymbol{R})\right)}\Lambda_{b\mu} + \sum_{\mu\nu}\frac{\langle n'|\left(\hat{a}_\mu + \hat{a}_\mu^\dagger\right)\left(\hat{a}_\nu + \hat{a}_\nu^\dagger\right)|1_\gamma\rangle}{\left(E^{n'}_{mbd}(\boldsymbol{R}) - E^{1_\gamma}_{mbd}(\boldsymbol{R})\right)}\Pi_{b\mu\nu}\,, \tag{4.69}$$

where MBD states are always assumed to be parametrically dependent on $\boldsymbol{R}$, thus $|n'\rangle = |n'_{\boldsymbol{R}}\rangle$.
To understand which quantum transitions are allowed, it is necessary to calculate bra-ket products of Eq. 4.69:

$$\langle n'|\,\hat{a}_\mu + \hat{a}_\mu^\dagger\,|1_\gamma\rangle = \begin{cases} \langle n'|0\rangle + \sqrt{2}\,\langle n'|2_\gamma\rangle & \mu = \gamma \\ \langle n'|1_\gamma, 1_\mu\rangle & \mu \neq \gamma\,, \end{cases} \tag{4.70}$$

$$\langle n'|\,\hat{a}_\mu \hat{a}_\nu\,|1_\gamma\rangle = \Big\{ 0 \quad \forall\ \mu, \nu\,, \tag{4.71}$$

$$\langle n'|\,\hat{a}_\mu \hat{a}_\nu^\dagger\,|1_\gamma\rangle = \begin{cases} 2\,\langle n'|1_\gamma\rangle & \mu = \nu = \gamma \\ \langle n'|1_\nu\rangle & \mu = \gamma\ ,\ \mu \neq \nu\,, \end{cases} \tag{4.72}$$

$$\langle n'|\,\hat{a}_\mu^\dagger \hat{a}_\nu\,|1_\gamma\rangle \quad = \begin{cases} \langle n'|1_\gamma\rangle & \mu = \nu = \gamma \\ \langle n'|1_\mu\rangle & \nu = \gamma\ ,\ \mu \neq \nu\,, \end{cases} \tag{4.73}$$

$$\langle n'|\,\hat{a}_\mu^\dagger \hat{a}_\nu^\dagger\,|1_\gamma\rangle = \begin{cases} \sqrt{6}\,\langle n'|3_\gamma\rangle & \mu = \nu = \gamma \\ \sqrt{2}\,\langle n'|2_\gamma, 1_\mu\rangle & \nu = \gamma\ ,\ \mu \neq \nu, \gamma \\ \sqrt{2}\,\langle n'|2_\gamma, 1_\nu\rangle & \nu \neq \gamma,\ \mu = \gamma \\ \sqrt{2}\,\langle n'|1_\gamma, 2_\mu\rangle & \nu \neq \gamma\ , \mu \neq \gamma, \mu = \nu \\ \langle n'|1_\gamma, 1_\mu, 1_\nu\rangle & \nu \neq \gamma\ , \mu \neq \nu, \gamma \neq \mu\,. \end{cases} \tag{4.74}$$

Depending on the final MBD state n' and vibrational state b, the product between the V coefficient and the MBD energy difference $\Delta E_{mbd}^{1_\gamma, n'} = E_{mbd}^{n'}(\boldsymbol{R}) - E_{mbd}^{1_\gamma}(\boldsymbol{R})$ is (final MBD states will be labeled by indices γ, α, β):

$$V\left(0 \to b, 1_\gamma \to n'\right) \Delta E_{mbd}^{1_\gamma, n'} = \begin{cases} \Lambda_{b\gamma} & \text{if } \langle n'| = \langle 0| \\ \sqrt{2}\Lambda_{b\gamma} & \text{if } \langle n'| = \langle 2_\gamma| \\ \Lambda_{b\alpha} & \text{if } \langle n'| = \langle 1_\gamma, 1_\alpha| \text{ and } \alpha \neq \gamma \\ 2\Pi_{b\gamma\alpha} & \text{if } \langle n'| = \langle 1_\alpha| \qquad \text{and } \alpha \neq \gamma \\ \sqrt{6}\Pi_{b\gamma\gamma} & \text{if } \langle n'| = \langle 3_\gamma| \\ 2\sqrt{2}\Pi_{b\alpha\gamma} & \text{if } \langle n'| = \langle 2_\gamma, 1_\alpha| \text{ and } \alpha \neq \gamma \\ \Pi_{b\alpha\beta} & \text{if } \langle n'| = \langle 1_\gamma, 1_\alpha, 1_\beta| \text{ and } \alpha \neq \beta,\ \alpha \neq \gamma,\ \beta \neq \gamma \\ \sqrt{2}\Pi_{b\alpha\alpha} & \text{if } \langle n'| = \langle 1_\gamma, 2_\alpha| \text{ and } \alpha \neq \gamma\,. \end{cases} \tag{4.75}$$

Among all possible transitions, Eq.4.75 does not report the one with $\langle n'| = \langle 1_\gamma|$, i.e. where the MBD state remains unchanged. At first sight, such term could seem divergent, due to the vanishing denominator (difference between identical energies). However, this singularity can be avoided. Discretizing the derivative of the MBD state $|n_r\rangle$ with respect to ionic coordinate r one has

$$\langle n_r'|\,\nabla_r\,|n_r\rangle \simeq \langle n_r'|\left[\frac{|n_{r+\Delta r}\rangle - |n_r\rangle}{\Delta r}\right], \tag{4.76}$$

the wave function $|n_{r+\Delta r}\rangle$ can be calculated by first-order perturbation thery, using as a perturbing potential the derivative of the MBD hamiltonian with respect to the ionic coordinates, and treating $|n_r\rangle$ as the unperturbed state.

$$|n_{r+\Delta r}\rangle \simeq |n_r\rangle + \sum_{m \neq n} \frac{\langle m_r|\,\Delta r \nabla_r H_{mbd}\ |n_r\rangle}{E_{mbd}^m(r) - E_{mbd}^n(r)}\,|m_r\rangle\ , \tag{4.77}$$

$$\langle n_r'|\,\nabla_{r_p}\,|n_r\rangle = \langle n_r'|\sum_{m \neq n} \frac{\langle m_r|\,\nabla_{r_p} H_{mbd}\ |n_r\rangle}{E_{mbd}^m(r) - E_{mbd}^n(r)}\,|m_r\rangle \tag{4.78}$$

$$= \sum_{m \neq n} \frac{\langle m_r|\,\nabla_{r_p} H_{mbd}\ |n_r\rangle}{E_{mbd}^m(r) - E_{mbd}^n(r)} \underbrace{\langle n_r'|m_r\rangle}_{\delta_{n'm}}\,. \tag{4.79}$$

When $n' = n$ the term $\langle n'_r| \nabla_{r_p} |n_r\rangle$ is zero, because the sum over the index m excludes the case $m = n$.

Unlike the SC model, the final states are characterized here by a vibrational state and a multiplicity of MBD states. Hence, it is necessary to first understand the total probability of reaching the target vibrational state, regardless of the final MBD state. Subsequently, one can discern which MBD states contribute most significantly to the active transitions. The transition amplitude from vibrational vacuum to a selected phonon mode b, is therefore:

$$P\left(|1_\gamma\rangle \otimes |\varphi_0\rangle\right) \rightarrow |\varphi_b\rangle) = \left|U_{1_\gamma}\left(0 \rightarrow b\right)\right|^2 + \sum_{allowed\ n'} \left|V\left(0 \rightarrow b, 1_\gamma \rightarrow n'\right)\right|^2. \tag{4.80}$$

In analogy with the SC term, transition amplitudes relative to the QC are presented in heatmaps. For the C_{60}-catcher, and the 11-cis-retinal molecule, transition amplitudes are accompanied by a graph illustrating the overlap between the final vibrational mode and the desired target geometrical configuration.

Reported data consistently demonstrate that the amplitudes due to the QC are not negligible with respect to the SC contributions, although the latter were naively expected to be the leading terms. Largest QC transition amplitudes are found when some vibrational excitations are accompanied by de-excitation of a given MBD mode and subsequent re-excitation of a second MBD mode with similar energy. In fact, computation of the V coefficient as from Eq. (4.58), implies that nearly-degenerate MBD energies can eventually lead to a quasi-vanishing denominator. The unexpectedly large QC terms shed light on the limits of the SC approximation, which may not accurately describe systems where quasi-degenerate electronic levels arise.

Transition amplitudes are related to the $\mathbf{\Lambda}$ and $\mathbf{\Pi}$ tensors (Eq.4.68). Here, the leading contributions are given by the latter, that account for the states of the kind $|1_\alpha\rangle$, as reported (fourth line) in Eq.4.75. For this type of transition, the first of the 3 indices of $\mathbf{\Pi}$ labels the phonon, while the second and third indicates the initial and final MBD states, respectively. Overall, the transition amplitudes are symmetric under the exchange of initial and final MBD states. This symmetry arises not only from the symmetry of $\mathbf{\Pi}$ with respect to the second and third indices, but also because the energy difference ΔE in Eq.4.80 is ultimately squared. This eliminates the sign dependence which distinguishes between the initial and final states.

Comparing Figs. 4.1a and 4.8a we observe that some QC transition amplitudes can be even larger than the SC. However, we recall that the approximation introduced in Eq. 4.46 could imply effective renormalization of V coefficients. Hence, the relatively large numerical values reported for QC rates should not be overemphasized. According to Eq. 4.46, the potential energy surface experienced by the ions is due to quasi-electrons, whose energy state is always referenced to oscillations around the positions of ionic equilibrium. This approximation is consistent with the spirit of the Born-Oppenheimer approximation, which posits that the electrons adiabatically follow the ions.

In the QC heatmaps we note a localization of the most-probable transitions, in analogy with the SC term. As evidenced also by Figs. 4.9a, 4.10a,4.11d here the localization is two-fold, i.e. it involves both normal vibrational modes and MBD modes. The localization with respect to normal vibrational modes indicates the presence of selection rules which can be attributed to geometrical constraints, in analogy to the SC case. Localization with respect to MBD modes, instead, is related to the presence of quasi-degeneracy in the spectrum.

Concerning C_{60}-catcher, and the 11-cis-retinal, we observe no significant overlap between the phonon modes that can be activated by the QC term, and the target configurational changes. However, closure of the clamp around the C_{60} fullerene remains possible through SC terms. On the other hand, interesting results are observed for PYP (Fig.4.11). In fact, the energies of those MBD states that exhibit largest coupling with vibrational modes are highly compatible with the photon energies that

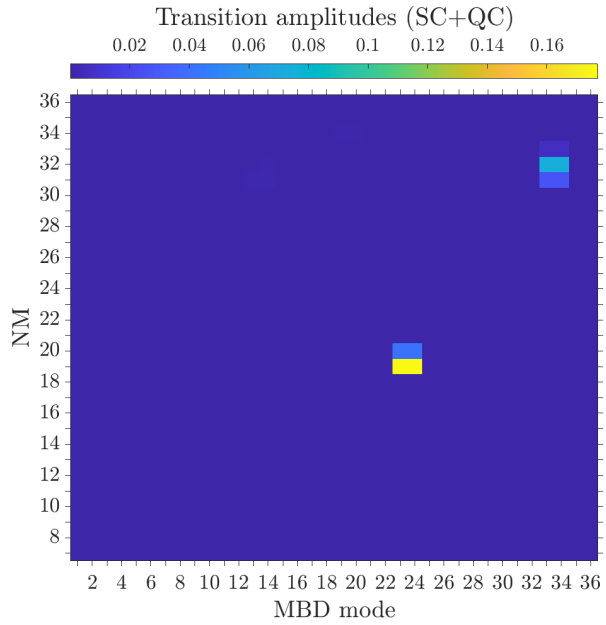

(a)

initial MBD	final MBD	final NM	P $(\times 10^{-1})$
23	24	19	1.77
24	23	19	1.77
34	33	32	0.73
33	34	32	0.73
23	24	20	0.41
24	23	20	0.41
34	33	31	0.26
33	34	31	0.26
34	33	33	0.06
33	34	33	0.06

(b)

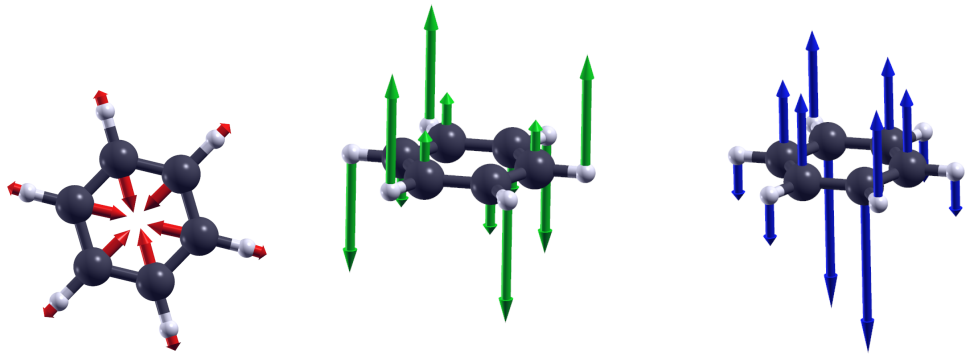

(c) (d) (e)

Figure 4.8: Transition amplitudes for benzene molecule (SC + QC). Semiclassical term and quantum correction contributions to the transition amplitudes for C_6H_6 molecule **(a)** and higher probability transitions **(b)**. Geometrical visualization of the modes involved in the preferred transition. MBD mode 23: vdW forces **(c)** and directions of dipole oscillations **(d)**; phonon displacements for final vibrational mode 19 **(e)**.

can induce isomerization of the p-coumaric acid, (i.e. ∼2.77 eV). It is thus possible that the excitation of the corresponding vibrational modes may play a role in the biological phenomena that interest this protein. Moreover, this also suggests that a broader study of rhodopsin (not limited to retinal) may also lead to similar conclusions. In summary, the non-locality of both vdW forces and phonon modes implies that large and seemingly inert structures can collectively participate to phenomena that are conventionally believed to be localized only on small molecular fragments.

We also remark that the aforementioned localization of the transition rates – also observed in SC contributions – appears compatible with the experimental observations [21] by Nardecchia et al., which reveal macroscopic occupation of a collective phonon mode, after some animal proteins undergoes light absorption. In practice, after light absorption, the photon energy is efficiently transferred into excitation of a single vibrational mode. In the presence of two-fold localization of the admitted transitions, this scenario is easier to interpret: if the frequency of the incoming photons matches a quasi-degenerate electronic excitation that exhibits high coupling with a given vibrational state, the observed effect can be easily obtained.

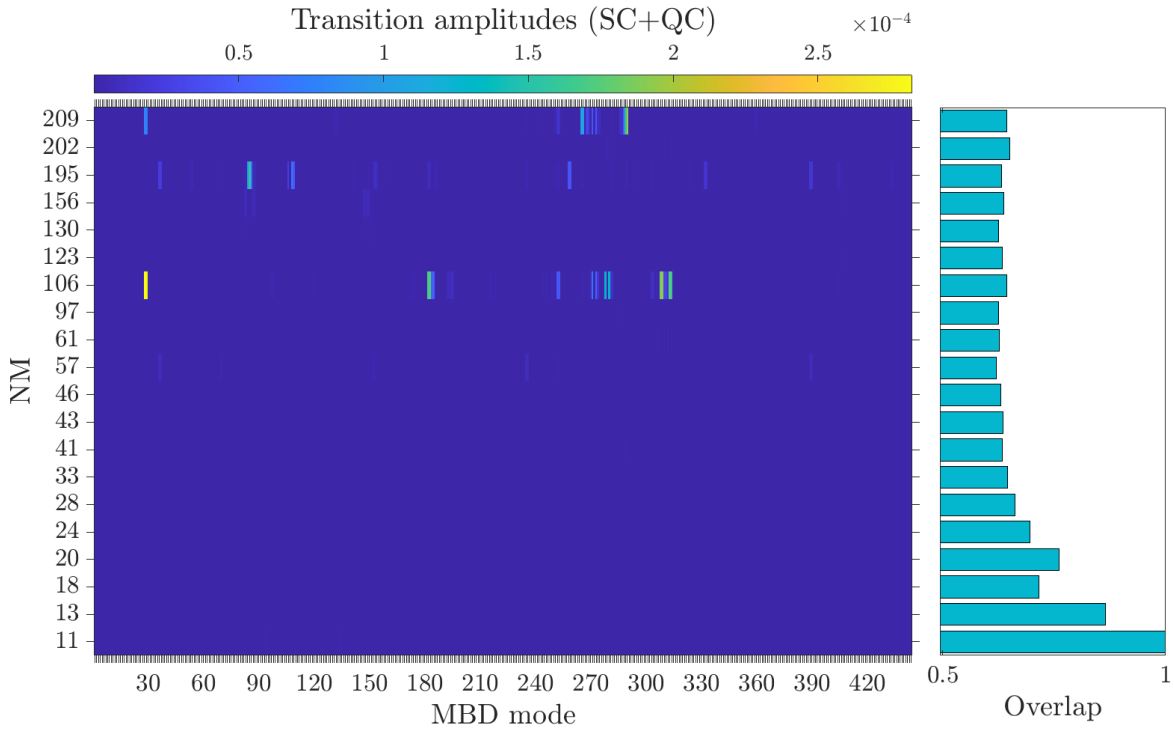

(a)

initial MBD	final MBD	final NM	P ($\times 10^{-4}$)
29	28	106	2.81
28	29	106	2.81
194	193	37	2.43
193	194	37	2.43
308	309	106	1.90
309	308	106	1.90
182	183	106	1.71
290	289	209	1.51
289	290	209	1.51
148	147	220	1.35

(b)

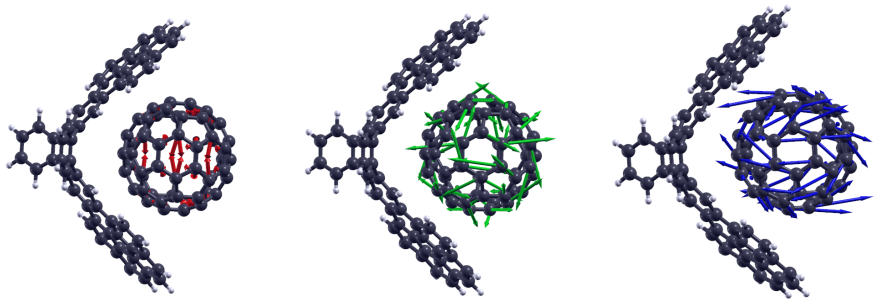

(c) **(d)** **(e)**

Figure 4.9: Transition amplitudes for Buckminsterfullerene-clamp complex (SC + QC). Semi-classical term and quantum correction contributions to the transition amplitudes for C_{60}-clamp complex, and overlap parameter for phonon-closed clamp configuration **(a)**. Higher probability transitions **(b)** and geometrical visualization of the modes involved in the preferred transition. MBD mode 29: vdW forces **(c)** and dipole oscillation directions **(d)**; phonon displacements for vibrational final mode 106 **(e)**.

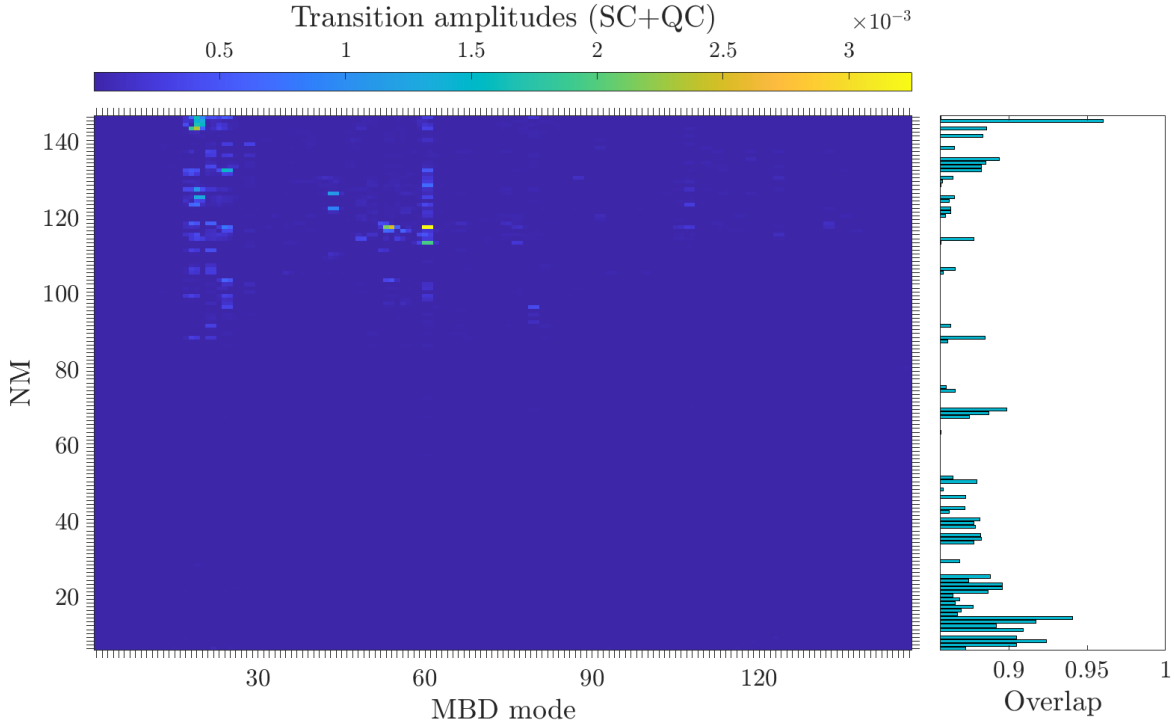

(a)

initial MBD	final MBD	final NM	P $(\times 10^{-3})$
60	61	118	3.23
61	60	118	3.23
54	53	118	1.91
53	54	118	1.91
18	19	144	1.79
19	18	144	1.79
61	60	114	1.76
60	61	114	1.76
20	19	145	1.39
19	20	145	1.39

(b)

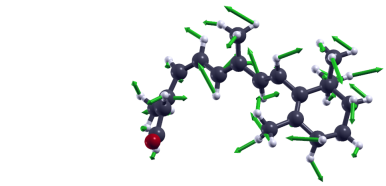

(c)

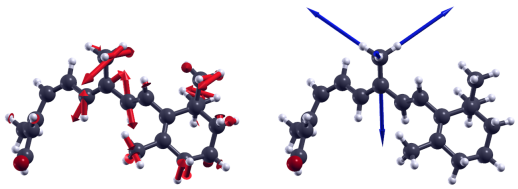

(d) **(e)**

Figure 4.10: Transition amplitudes for 11-cis-retinal (SC + QC). Semiclassical term and quantum correction contributions to the transition amplitudes for isolated 11-cis-retinal molecule, with overlap parameter for phonon modes and intermediate structure (Fig.4.4b) **(a)**. Higher probability transitions **(b)** and geometrical visualization of the modes involved in the preferred transition. MBD mode 60: dipole oscillations directions **(c)** and vdW forces **(d)**; phonon displacements for final vibrational mode 118 **(e)**.

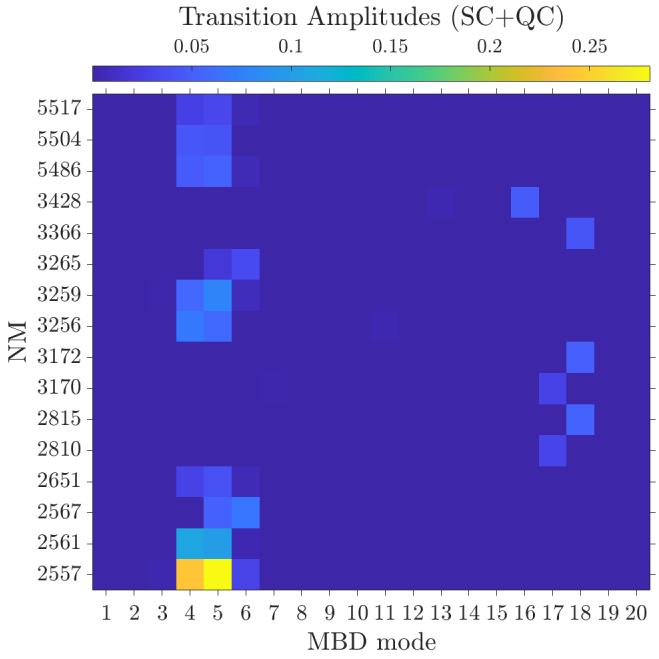

(a)

initial MBD	eV	final MBD	final NM	P
4	2.752	5	2557	0.24
5	2.753	4	2557	0.24
4	2.752	5	2562	0.09
5	2.753	4	2562	0.09
5	2.753	4	3256	0.06
4	2.752	5	3256	0.06
4	2.752	5	3259	0.06
5	2.753	4	3259	0.06
5	2.753	6	2567	0.05
6	2.754	5	2567	0.05

(b)

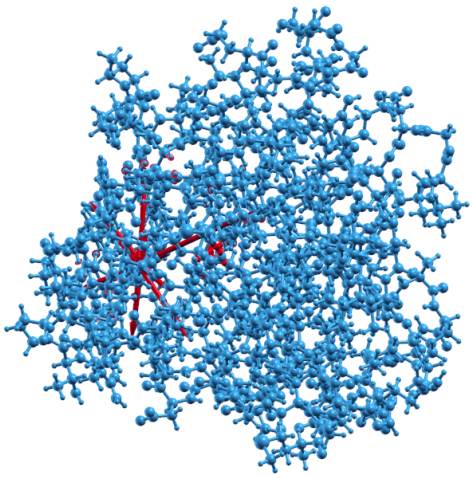

(c)

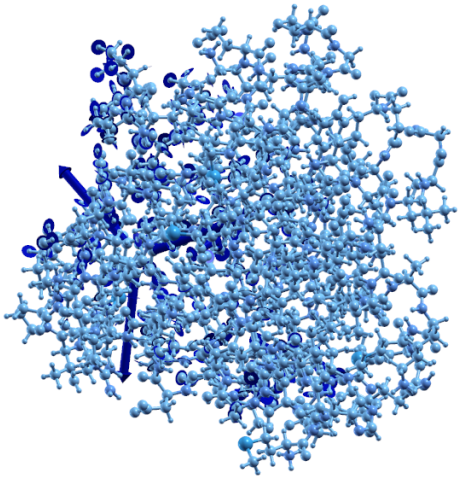

(d)

Figure 4.11: Transition amplitudes for PYP (SC + QC). Semiclassical term and quantum correction contributions to transition amplitudes for PYP. Only few MBD modes, the twenty normal modes with the lowest energy, are reported. Since they cover an energetic range (2.7 to 4.08 eV) compatible with visible and ultraviolet light. Higher probability transitions **(b)** with initial energy reported in eV. High amplitude transition involves MBD mode 4 (vdW forces directions **(c)**) and final vibrational mode 2557 (phonon displacements **(d)**).

Chapter 5

Conclusions

This thesis addresses the excitation of vibrational modes of large molecules due to absorption of optical photons. The coupling between optically-induced collective charge displacements and mechanical vibrations is mediated here by non-covalent optical vdW forces, described by the MBD model. Short-range optical interactions due to chemical bondings are instead neglected. Our model is thus specifically designed for addressing long-range collective phenomena, rather than local changes of single chemical bonds.
Two different approaches based on perturbative time-evolution of a suitable initial wavefunction are proposed, in order to estimate the transition amplitudes from the vibrational groundstate to a singly excited target mode. Within the first approach, optical vdW forces caused by excitation of a given MBD mode, are treated as a perturbation to the ion dynamics, according to a semi-classical approach. The second strategy involves a rigorous description of the full Hamiltonian beyond the Born-Oppenheimer approximation. Interestingly, this approach recovers the above semi-classical term, and further introduces a quantum correction that enables for quantum-mechanical transitions between quasi-electron MBD states. Both quasi-electron and phonon Hamiltonians are quantized by suitable ladder operators, that provide an intelligible description of the transition between different states. To guide intuition, the many-body wavefunction is accordingly expanded into products of quasi-electron (MBD) and ionic (phononic) wavefunctions. Within the quantum correction term, multi-mode excitation is allowed, and phonon excitation is accompanied by a multiplicity of possible final MBD states. However, the transitions between singly-occupied MBD quasi-degenerate states tend to be dominant, due to inverse proportionality of the transition matrix with respect to MBD energy differences.
Analyzing the transition amplitudes, a remarkable selectivity of the electron-phonon coupling emerges: many vibrational modes are essentially inert, and can hardly be excited. Geometrical analysis suggests a major role of molecular symmetries in determining the permitted transitions. Although the semi-classical term is naively expected to provide dominant coupling contributions, the quantum correction introduces a few strongly preferred transitions, whose transition amplitude can dominate over the semi-classical. This is qualitatively compatible with the 'phonon condensation', [25] experimentally evidenced in photo-excited bovine proteins. In fact, macroscopic occupation of a single vibrational state was observed after photoexcitation.
Future studies, will analyze the role and significance of the approximation in Eq.4.46. In fact, transition amplitudes between quasi-degenerate MBD states may undergo renormalization. As mentioned, the present results provide an indication of active and inert vibrational modes, but the numerical values of the transition amplitudes should not be overemphasized.

Chapter 6

Appendix

Appendix A

Derivation of MBD forces within a Hellman-Feynman framework

In the following lines, the detailed calculations required to evaluate the spatial derivative of the eigenvalues of the matrix $\boldsymbol{C}$ are presented, using a procedure analogous to the demonstration of the Hellmann-Feynman theorem.

Given λ_i the i-th eigenvalue of the symmetric matrix $\boldsymbol{C}$, and $\boldsymbol{M}$ the matrix whose columns are its eigenvectors, using index notation it holds that

$$\lambda_i = \sum_{jk} M_{ij}^T C_{jk} M_{ki} \,. \tag{A.1}$$

The derivative is explicitly evaluated:

$$\frac{\partial \lambda_i}{\partial r_{lc}} = \sum_j \sum_k \left\{ C_{jk} M_{ki} \frac{\partial M_{ij}^T}{\partial r_{lc}} + M_{ij}^T M_{ki} \frac{\partial C_{jk}}{\partial r_{lc}} + M_{ij}^T C_{jk} \frac{\partial M_{ki}}{\partial r_{lc}} \right\} \tag{A.2}$$

$$= \sum_j \left(\frac{\partial M_{ij}^T}{\partial r_{lc}} \right) \lambda_i M_{ji} + \sum_j \sum_k M_{ij}^T M_{ki} \frac{\partial C_{jk}}{\partial r_{lc}} + \sum_k \left(\frac{\partial M_{ki}}{\partial r_{lc}} \right) \lambda_i M_{ki} \tag{A.3}$$

$$= \lambda_i \sum_j \left(\frac{\partial M_{ji}}{\partial r_{lc}} \right) M_{ji} + \lambda_i \sum_k \left(\frac{\partial M_{ki}}{\partial r_{lc}} \right) M_{ki} + \sum_j \sum_k M_{ij}^T M_{ki} \frac{\partial C_{jk}}{\partial r_{lc}} \tag{A.4}$$

$$= \lambda_i \frac{\partial}{\partial r_{lc}} \sum_j M_{ij}^{-1} M_{ji} + \sum_j \sum_k M_{ij}^T M_{ki} \frac{\partial C_{jk}}{\partial r_{lc}} \tag{A.5}$$

$$= \lambda_i \frac{\partial \delta_{ii}}{\partial r_{lc}} + \sum_j \sum_k M_{ij}^T M_{ki} \frac{\partial C_{jk}}{\partial r_{lc}} \tag{A.6}$$

$$= \sum_j \sum_k M_{ij}^T M_{ki} \frac{\partial C_{jk}}{\partial r_{lc}} \,, \tag{A.7}$$

where eigenvalue relation ($\boldsymbol{A}\vec{v} = \lambda\vec{v}$) and properties of orthogonal matrices have been used:

$$\sum_k C_{jk} M_{ki} = \lambda_i M_{ji} \,, \tag{A.8}$$

$$\sum_j M_{ji}^2 = 1 \quad \forall i \,. \tag{A.9}$$

Appendix B

First derivative of the dipole-dipole matrix T

In the following lines the mathematical details for the derivative of $\boldsymbol{T}$ matrix elements, with respect to atomic coordinates, are reported. Dipole-dipole tensor reads:

$$T_{ij}^{ab} = \underbrace{-\frac{3r_a r_b - d_{ij}^2\delta_{ab}}{d_{ij}^5}}_{f}\underbrace{\left(erf\left(\frac{d_{ij}}{\sigma_{ij}}\right) - \frac{2}{\sqrt{\pi}}\frac{d_{ij}}{\sigma_{ij}}e^{-\left(\frac{d_{ij}}{\sigma_{ij}}\right)^2}\right)}_{g} + \underbrace{\frac{4}{\sqrt{\pi}}\frac{1}{\sigma_{ij}^3}\frac{r_a r_b}{d_{ij}^2}e^{-\left(\frac{d_{ij}}{\sigma_{ij}}\right)^2}}_{h}, \tag{B.1}$$

In order to evaluate the derivative with respect to position of atom l along coordinate $c = x, y, z$

$$\frac{\partial T_{ij}^{ab}}{\partial r_{lc}} = g\frac{\partial f}{\partial r_{lc}} + f\frac{\partial g}{\partial r_{lc}} + \frac{\partial h}{\partial r_{lc}}, \tag{B.2}$$

$$\frac{\partial g}{\partial r_{lc}} = \frac{\partial erf\left(\frac{d_{ij}}{\sigma_{ij}}\right)}{\partial r_{lc}} - \frac{2}{\sigma_{ij}\sqrt{\pi}}\left(d_{ij}\frac{\partial\, e^{-\left(\frac{d_{ij}}{\sigma_{ij}}\right)^2}}{\partial r_{lc}} + e^{-\left(\frac{d_{ij}}{\sigma_{ij}}\right)^2}\frac{\partial d_{ij}}{\partial r_{lc}}\right), \tag{B.3}$$

$$\frac{\partial f}{\partial r_{lc}} = -3\frac{\delta_{ab}}{d_{ij}^4}\frac{\partial d_{ij}}{\partial r_{lc}} - \frac{3}{d_{ij}^5}\left(\frac{\partial r_a r_b}{\partial r_{lc}} - 5\frac{r_a r_b}{d_{ij}}\frac{\partial d_{ij}}{\partial r_{lc}}\right), \tag{B.4}$$

$$\frac{\partial h}{\partial r_{lc}} = \frac{4}{\sigma_{ij}^3\sqrt{\pi}}\left(\frac{r_a r_b}{d_{ij}^2}\frac{\partial e^{-\left(\frac{d_{ij}}{\sigma_{ij}}\right)^2}}{\partial r_{lc}} + \frac{e^{-\left(\frac{d_{ij}}{\sigma_{ij}}\right)^2}}{d_{ij}^2}\frac{\partial r_a r_b}{\partial r_{lc}} - 2\frac{r_a r_b}{d_{ij}^3}e^{-\left(\frac{d_{ij}}{\sigma_{ij}}\right)^2}\frac{\partial d_{ij}}{\partial r_{lc}}\right). \tag{B.5}$$

While the not-already evaluated derivatives inside the latters are explicitly

$$\frac{\partial r_a r_b}{\partial r_{lc}} = (\delta_{li} - \delta_{lj})(\delta_{ca} r_b + \delta_{cb} r_a), \tag{B.6}$$

$$\frac{\partial d_{ij}}{\partial r_{lc}} = (1 - \delta_{ij})\left(\frac{r_c}{d_{ij}}\right)(\delta_{li} - \delta_{lj}) \text{ with } r_c = r_{ic} - r_{jc}, \tag{B.7}$$

$$\frac{\partial e^{-\left(\frac{d_{ij}}{\sigma_{ij}}\right)^2}}{\partial r_l^c} = -\frac{2e^{-\left(\frac{d_{ij}}{\sigma_{ij}}\right)^2}}{\sigma_{ij}^2} r_{ij}\frac{\partial d_{ij}}{\partial r_l^c}, \tag{B.8}$$

$$\frac{\partial\, erf\left(\frac{d_{ij}}{\sigma_{ij}}\right)}{\partial r_{lc}} = \frac{2}{\sigma_{ij}\sqrt{\pi}}e^{-\left(\frac{d_{ij}}{\sigma_{ij}}\right)^2}\frac{\partial d_{ij}}{\partial r_{lc}}. \tag{B.9}$$

Appendix C

NM analysis methods comparison

In this appendix, reference, Quantum Espresso (QE) and GROMACS (GRO) frequencies are reported for water, ammonia, propane, benzene, napthalene and buckminsterfullere molecules.
Reference values from NIST database [28] for each molecule except naphtalene [24] and C_{60} [23].

Ref	QE	GRO
3756	4075.86	3319.61
3657	3956.67	3276.31
1595	1316.09	1579.86

Table C.1:
H_2O vibrational frequencies.

Ref	QE	GRO
3444	3037.84	3370.50
3445	3029.48	3365.65
3337	2920.97	3283.88
3336	1612.72	1745.68
1627	1599.60	1744.43
1626	1154.14	1396.00
968	306.54	138.57
933	291.26	134.22

Table C.2:
NH_3 vibrational frequencies.

Ref	QE	GRO
2977	2801.53	3037.98
2973	2794.07	3031.02
2968	2792.00	3016.08
2968	2783.72	3013.50
2967	2743.23	3010.87
2962	2729.22	2972.51
2887	2725.83	2916.61
2887	2722.14	2909.87
1476	1410.64	1765.59
1472	1398.83	1740.81
1464	1396.97	1705.27
1462	1380.84	1701.00
1451	1380.18	1680.47
1392	1346.90	1679.95
1378	1340.58	1668.87
1338	1283.56	1502.03
1278	1225.66	1245.99
1192	1141.96	1181.49
1158	1120.23	1179.88
1054	1106.65	1078.16
940	913.10	1058.28
922	868.61	1033.80
869	838.97	943.76
748	688.75	797.44
369	359.14	382.41
268	225.19	258.34
216	212.42	213.45

Table C.3:
C_3H_8 vibrational frequencies.

Ref	QE	GRO
3068	3141.97	2998.57
3063	3131.68	2997.39
3063	3125.61	2994.25
3062	3115.38	2993.70
3047	3110.25	2986.22
3047	3099.55	2974.54
1596	1603.75	1692.46
1596	1599.71	1691.73
1486	1470.33	1670.92
1486	1467.48	1597.63
1326	1357.15	1592.48
1310	1330.69	1502.80
1178	1162.68	1251.92
1178	1161.84	1179.09
1150	1139.39	1177.49
1038	1039.54	1132.86
1038	1039.54	958.03
1010	1001.70	952.66
995	999.68	900.44
992	982.46	848.99
975	955.31	769.09
975	955.05	754.72
849	834.60	544.44
849	834.12	542.63
703	713.19	498.93
673	665.29	477.25
606	609.38	456.32
606	607.16	359.89
410	409.99	318.63
410	409.52	302.63

Table C.4:
C_6H_6 vibrational frequencies.

Ref	QE	GRO
3230	2996.43	3000.56
3180	2983.69	3000.40
3098	2983.17	2999.17
3076	2975.18	2998.13
3060	2971.78	2991.22
3027	2959.30	2990.94
3010	2948.52	2987.60
2987	2938.46	2987.38
2968	1418.37	1816.40
2851	1403.49	1747.22
2256	1363.14	1724.08
2114	1353.74	1672.95
1939	1344.84	1589.11
1908	1338.72	1562.75
1896	1316.87	1554.63
1830	1211.78	1536.13
1804	1125.08	1472.78
1770	1121.52	1324.16
1715	1095.91	1260.41
1669	1060.08	1256.55
1652	1054.47	1234.04
1592	1044.44	1188.26
1506	1027.68	1178.25
1458	978.34	1140.16
1419	974.13	1125.97
1387	960.83	1003.71
1361	946.73	845.58
1295	939.93	778.58
1267	891.81	761.98
1238	876.62	757.73
1210	862.47	730.44
1163	861.63	705.04
1138	820.08	697.05
1128	818.45	603.32
1011	793.04	534.74
958	769.11	511.97
943	722.29	488.66
877	654.71	480.97
825	623.47	445.48
782	587.08	440.94
753	561.88	417.59
739	541.51	359.82
717	468.74	348.07
689	455.68	345.17
655	440.82	337.07
618	383.15	294.62
562	293.96	179.88
476	283.79	93.60
359	186.42	10.23

Table C.5:
$C_{10}H_8$ vibrational frequencies.

Deg	Ref	GRO				
5	272	215.96	216.06	216.11	216.18	216.22
3	343	290.52	292.27	294.87		
4	353	298.09	300.69	301.15	302.72	
5	403	322.90	323.92	326.09	328.72	329.51
5	433	349.21	355.06	362.28	370.58	376.72
4	485	386.61	392.61	429.87	431.67	
1	496	439.23				
3	526	442.91	448.08	457.30		
5	534	469.89	471.76	483.16	493.81	496.13
3	553	501.65	504.33	511.42		
4	567	514.52	519.33	521.17	533.67	
3	568	539.08	539.55	542.56		
3	575	551.29	581.66	597.53		
5	668	625.20	628.32	639.76	649.59	661.49
5	709	674.84	677.10	680.18	686.18	698.18
4	736	706.02	710.24	712.39	714.60	
5	743	715.45	717.12	726.09	735.39	738.84
3	753	740.70	746.46	749.98		
3	756	763.60	772.54	776.10		
4	764	776.90	789.95	797.64	817.01	
5	772	829.89	842.93	853.05	859.31	870.89
4	776	882.08	891.06	898.25	908.33	
3	796	920.42	928.92	934.14		
3	831	962.09	968.83	974.14		
4	961	980.00	1023.44	1036.31	1038.97	
3	973	1041.37	1051.68	1056.00		
1	984	1068.38				
4	1079	1103.91	1108.53	1111.49	1115.22	
5	1099	1118.47	1130.25	1135.02	1149.46	1151.17
3	1182	1227.59	1230.50	1235.19		
3	1205	1243.80	1246.88	1255.96		
5	1223	1261.65	1262.05	1339.52	1339.56	1340.73
5	1252	1355.10	1355.39	1356.16	1357.01	1358.58
3	1289	1385.95	1393.24	1400.52		
4	1309	1498.73	1499.99	1501.36	1505.62	
4	1310	1508.43	1519.95	1522.10	1523.04	
5	1344	1525.94	1554.21	1555.60	1556.05	1557.07
3	1345	1573.41	1586.42	1586.84		
4	1422	1589.81	1595.89	1596.07	1596.12	
5	1425	1620.74	1620.94	1621.22	1621.46	1621.72
3	1429	1638.62	1639.58	1643.75		
1	1470	1674.34				
4	1482	1674.95	1677.25	1678.11	1679.21	
3	1525	1680.20	1681.12	1682.96		
5	1567	1725.25	1726.36	1728.04	1728.44	1729.17
5	1575	1729.71	1730.08	1731.43	1732.29	1733.37

Table C.6: Buckminsterfullerene (C_{60}) vibrational frequencies. Since the high number of frequencies (174), is reported the frequencies degeneracy (**Deg**) in the first column, and all the GROMACS-computed frequencies belonging to the same reference value.

Appendix D

Kinetic MBD spatial derivative

In this appendix, typical second quantization methods are employed to demonstrate that the derivative of the kinetic term of the MBD Hamiltonian, with respect to ionic coordinates, is zero. It's convenient to express H_{mbd} in normal form, clearly showing the dependence on ionic positions $\boldsymbol{r} = \{r_1, \ldots, r_{3N}\}$.

$$\hat{H}_{mbd}(\boldsymbol{r}) = -\frac{1}{2}\sum_q \nabla^2_{\chi_q(\boldsymbol{r})} + \frac{1}{2}\sum_q \chi_q^2(\boldsymbol{r})\tilde{\omega}_q^2(\boldsymbol{r}) \tag{D.1}$$

$$= \hat{T}_{mbd}(\boldsymbol{r}) + \hat{V}_{mbd}(\boldsymbol{r}) \tag{D.2}$$

where $\chi_q(\boldsymbol{r}) = \sum_\mu M^T_{q\mu}(\boldsymbol{r})\,(\tilde{r}_\mu - r_\mu)$ is the q-th collective MBD displacement coordinate.

Kinetic and potential terms are respectively equal even if expressed in the basis of the collective coordinates or of the atomic ones, thus the term $\frac{\partial \hat{V}_{mbd}}{\partial r_p}(\boldsymbol{r})$ is the one evaluated in Eq.4.63. With regard to the kinetic term, its operatorial nature emerges by employing an auxiliary function φ:

$$\left(\frac{\partial \hat{T}_{mbd}}{\partial r_p}\right)\varphi = -\frac{1}{2}\left(\sum_q \nabla_{r_p}\nabla^2_{\chi_q(\boldsymbol{r})}\right)\varphi$$

$$= -\frac{1}{2}\sum_q \left(\nabla_{r_p} \circ \left(\nabla^2_{\chi_q(\boldsymbol{r})}\varphi\right) - \nabla^2_{\chi_q(\boldsymbol{r})} \circ \left(\nabla_{r_p}\varphi\right)\right). \tag{D.3}$$

Symbol $\circ$ denotes the composition of operators. Recalling the cartesian to MBD collective coordinates transormation for the derivative

$$\nabla_{r_p} = \sum_j \frac{\partial}{\partial \chi_j(\boldsymbol{r})}\frac{d\chi_j(\boldsymbol{r})}{dr_p} = -\sum_j M^T_{jp}(\boldsymbol{r})\frac{\partial}{\partial \chi_j(\boldsymbol{r})}\,, \tag{D.4}$$

Eq.D.3 reads:

$$\left(\frac{\partial \hat{T}_{mbd}}{\partial r_p}\right)\varphi = \frac{1}{2}\sum_{qj} M^T_{jp}(\boldsymbol{r})\left(\nabla_{\chi_j(\boldsymbol{r})} \circ \left(\nabla^2_{\chi_q(\boldsymbol{r})}\varphi\right) - \nabla^2_{\chi_q(\boldsymbol{r})} \circ \left(\nabla_{\chi_j(\boldsymbol{r})}\varphi\right)\right)$$

$$= \frac{1}{2}\sum_{qj} M^T_{jp}(\boldsymbol{r})\frac{\tilde{\omega}_q}{2}\sqrt{\frac{\tilde{\omega}_j}{2}}\left(\left(\hat{a}_j - \hat{a}_j^\dagger\right)\left(\hat{a}_q - \hat{a}_q^\dagger\right)^2 - \left(\hat{a}_q - \hat{a}_q^\dagger\right)^2\left(\hat{a}_j - \hat{a}_j^\dagger\right)\right)\varphi$$

$$= \frac{1}{2}\sum_{qj} M^T_{jp}(\boldsymbol{r})\frac{\tilde{\omega}_q}{2}\sqrt{\frac{\tilde{\omega}_j}{2}}\left[\left(\hat{a}_j - \hat{a}_j^\dagger\right), \left(\hat{a}_q - \hat{a}_q^\dagger\right)^2\right]\varphi\,. \tag{D.5}$$

In the latter, $[\hat{A}, \hat{B}]$ is the commutator for bosonic operators $\hat{A}$ and $\hat{B}$.
Since $\left(\hat{a}_q - \hat{a}_q^\dagger\right)^2 = -1 + \hat{a}_q\hat{a}_q - 2\hat{a}_q^\dagger\hat{a}_q + \hat{a}_q^\dagger\hat{a}_q^\dagger$, commutator in Eq. D.5 is explicitly evaluated.

$$\begin{aligned}
\left[\left(\hat{a}_j - \hat{a}_j^\dagger\right), \left(\hat{a}_q - \hat{a}_q^\dagger\right)^2\right] &= \left[\left(\hat{a}_j - \hat{a}_j^\dagger\right), -1 + \hat{a}_q\hat{a}_q - 2\hat{a}_q^\dagger\hat{a}_q + \hat{a}_q^\dagger\hat{a}_q^\dagger\right] \\
&= \left[\left(\hat{a}_j - \hat{a}_j^\dagger\right),\ \hat{a}_q\hat{a}_q - 2\hat{a}_q^\dagger\hat{a}_q + \hat{a}_q^\dagger\hat{a}_q^\dagger\right] \\
&= \left[\hat{a}_j - \hat{a}_j^\dagger, -2\hat{a}_q^\dagger\hat{a}_q\right] + \left[\hat{a}_j, \hat{a}_q^\dagger\hat{a}_q^\dagger\right] - \left[\hat{a}_j^\dagger,\ \hat{a}_q\hat{a}_q\right] \\
&= -2\left[\hat{a}_j, \hat{a}_q^\dagger\hat{a}_q\right] + 2\left[\hat{a}_j^\dagger, \hat{a}_q^\dagger\hat{a}_q\right] + \left[\hat{a}_j, \hat{a}_q^\dagger\hat{a}_q^\dagger\right] - \left[\hat{a}_j^\dagger,\ \hat{a}_q\hat{a}_q\right] . \qquad \text{(D.6)}
\end{aligned}$$

Each term in the latter is computed:

$$\begin{aligned}
\left[\hat{a}_j, \hat{a}_q^\dagger\hat{a}_q\right] &= \underbrace{\hat{a}_j\hat{a}_q^\dagger}_{\delta_{jq} + \hat{a}_q^\dagger\hat{a}_j}\ \hat{a}_q - \hat{a}_q^\dagger\hat{a}_q\hat{a}_j = \delta_{jq}\hat{a}_q + \hat{a}_q^\dagger\hat{a}_j\hat{a}_q - \hat{a}_q^\dagger\hat{a}_q\hat{a}_j \\
&= \delta_{jq}\hat{a}_q\,, \qquad \text{(D.7)} \\
\left[\hat{a}_j^\dagger, \hat{a}_q^\dagger\hat{a}_q\right] &= \hat{a}_j^\dagger\hat{a}_q^\dagger\hat{a}_q - \hat{a}_q^\dagger\hat{a}_q\hat{a}_j^\dagger = \hat{a}_q^\dagger\ \underbrace{\hat{a}_j^\dagger\hat{a}_q}_{-\delta_{jq} + \hat{a}_q\hat{a}_j^\dagger}\ - \hat{a}_q^\dagger\hat{a}_q\hat{a}_j^\dagger \\
&= -\delta_{jq}\hat{a}_q^\dagger + \hat{a}_q^\dagger\hat{a}_q\hat{a}_j^\dagger - \hat{a}_q^\dagger\hat{a}_q\hat{a}_j^\dagger \\
&= -\delta_{jq}\hat{a}_q^\dagger\,, \qquad \text{(D.8)} \\
\left[\hat{a}_j^\dagger,\ \hat{a}_q\hat{a}_q\right] &= \hat{a}_j^\dagger\hat{a}_q\hat{a}_q - \hat{a}_q\hat{a}_q\hat{a}_j^\dagger = -\delta_{qj}\hat{a}_q + \hat{a}_q\hat{a}_j^\dagger\hat{a}_q - \delta_{qj}\hat{a}_q - \hat{a}_q\hat{a}_j^\dagger\hat{a}_q \\
&= 2\delta_{jq}\hat{a}_q^\dagger\,, \qquad \text{(D.9)} \\
\left[\hat{a}_j^\dagger,\ \hat{a}_q\hat{a}_q\right] &= \hat{a}_j^\dagger\hat{a}_q\hat{a}_q - \hat{a}_q\hat{a}_q\hat{a}_j^\dagger = -\delta_{qj}\hat{a}_q + \hat{a}_q\hat{a}_j^\dagger\hat{a}_q - \delta_{qj}\hat{a}_q - \hat{a}_q\hat{a}_j^\dagger\hat{a}_q \\
&= -2\delta_{qj}\hat{a}_q\,. \qquad \text{(D.10)}
\end{aligned}$$

Hence it holds that

$$\left[\left(\hat{a}_j - \hat{a}_j^\dagger\right), \left(\hat{a}_q - \hat{a}_q^\dagger\right)^2\right] = -2\delta_{jq}\hat{a}_q - 2\delta_{jq}\hat{a}_q^\dagger + 2\delta_{jq}\hat{a}_q^\dagger + 2\delta_{qj}\hat{a}_q = 0\,. \qquad \text{(D.11)}$$

Bibliography

[1] ATB - atomic simulation environment. `https://atb.uq.edu.au/`. Accessed: June 23, 2023.

[2] Legacy pseudopotentials. `http://pseudopotentials.quantum-espresso.org/legacy_tables`. Accessed: 22/06/2023.

[3] A. Ambrosetti, Paolo Umari, Pier Silvestrelli, Joshua Elliott, and Alexandre Tkatchenko. Optical van-der-waals forces in molecules: from electronic bethe-salpeter calculations to the many-body dispersion model. *Nature Communications*, 13:813, 2022.

[4] Alberto Ambrosetti, Dario Alfè, Robert A. Jr. DiStasio, and Alexandre Tkatchenko. Hard numbers for large molecules: Toward exact energetics for supramolecular systems. *The Journal of Physical Chemistry Letters*, 5:849–855, 2014.

[5] Alberto Ambrosetti, Anthony M. Reilly, Jr. DiStasio, Robert A., and Alexandre Tkatchenko. Long-range correlation energy calculated from coupled atomic response functions. *The Journal of Chemical Physics*, 140:18A508, 2014.

[6] Williams D.R. Getzoff E.D. Borgstahl, G.E. A structure of photoactive yellow protein, a cytosolic photoreceptor: unusual fold, active site, and chromophore. *Biochemistry*, 34:6278–6287, 1995.

[7] A. G. Donchev. Many-body effects of dispersion interaction. *The Journal of Chemical Physics*, 125:074713, 2006.

[8] Saul T. Epstein. Time-Dependent Hellmann—Feynman Theorems for Variational Wavefunctions. *The Journal of Chemical Physics*, 45:384–384, 2004.

[9] H. Fröhlich, H. Pelzer, and S. Zienau. Properties of slow electrons in polar materials. *The London, Edinburgh, and Dublin Philosophical Magazine and Journal of Science*, 41:221–242, 1950.

[10] Feliciano Giustino. Electron-phonon interactions from first principles. *Rev. Mod. Phys.*, 89:015003, 2017.

[11] Matteo Gori, Philip Kurian, and Alexandre Tkatchenko. Second quantization approach to many-body dispersion interactions, 2023.

[12] Lev Gribov. Vibrations of molecules and isomerization. *Russian Journal of Physical Chemistry*, 75:1494–1497, 2001.

[13] Stefan Grimme. Semiempirical gga-type density functional constructed with a long-range dispersion correction. *Journal of Computational Chemistry*, 27:1787–1799, 2006.

[14] Z. Feng G. Gilliland T.N. Bhat H. Weissig I.N. Shindyalov P.E. Bourne H.M. Berman, J. Westbrook. The protein data bank. *Nucleic Acids Research*, 28:235–242, 2000.

[15] W. D. Hoff, P. Dux, K. Hard, B. Devreese, I. M. Nugteren-Roodzant, W. Crielaard, R. Boelens, R. Kaptein, J. Van Beeumen, and K. J. Hellingwerf. Thiol ester-linked p-coumaric acid as a new photoactive prosthetic group in a protein with rhodopsin-like photochemistry. *Biochemistry*, 33(47):13959–13962, 1994.

[16] The MathWorks Inc. Matlab version: 9.13.0 (r2022b), 2022.

[17] Werner Jaross. The possible role of molecular vibration in intracellular signaling. *Journal of Cellular Signaling*, 1:180–186, 2020.

[18] P. W. Langhoff, S. T. Epstein, and M. Karplus. Aspects of time-dependent perturbation theory. *Rev. Mod. Phys.*, 44:602–644, 1972.

[19] Du D. Li H, Lantz R. Vibrational approach to the dynamics and structure of protein amyloids. *National library of medicine*, 2019.

[20] Steven G. Louie and Sohrab Ismail-Beigi. Excited-state forces within a first-principles green's function formalism. *Physical Review Letters*, 90:076401, 2003.

[21] A.G Markelz, A Roitberg, and E.J Heilweil. Pulsed terahertz spectroscopy of dna, bovine serum albumin and collagen between 0.1 and 2.0 thz. *Chemical Physics Letters*, 320:42–48, 2000.

[22] F. Marsiglio. Eliashberg theory: A short review. *Annals of Physics*, 2020.

[23] José Menéndez and John B. Page. *Vibrational spectroscopy of C60*, pages 27–95. Springer Berlin Heidelberg, 2000.

[24] S. Mitra and H. Bernstein. Vibrational spectra of naphthalene-d0, --d4, and -d8 molecules. *Canadian Journal of Chemistry*, 37:553–562, 2011.

[25] Ilaria Nardecchia, Jeremie Torres, Mathias Lechelon, Valeria Giliberti, Michele Ortolani, Philippe Nouvel, Matteo Gori, Yoann Meriguet, Irene Donato, Jordane Preto, Luca Varani, James Sturgis, and Marco Pettini. Out-of-equilibrium collective oscillation as phonon condensation in a model protein. *Phys. Rev. X*, 8:031061, 2018.

[26] Kumasaka T. Hori T. Behnke C.A. Motoshima H. Fox B.A. Le Trong I. Teller D.C. Okada T. Stenkamp R.E. Yamamoto M. Miyano M. Palczewski, K. Crystal structure of rhodopsin: A g protein-coupled receptor. *Science*, 289:739–745, 2000.

[27] Sofia F. Prazeres, Carmen García Ruiz, and Gemma Montalvo García. Vibrational spectroscopy as a promising tool to study enzyme-carrier interactions: A review. *Applied Spectroscopy Reviews*, 50:797–821, 2015.

[28] T. Shimanouchi. Tables of molecular vibrational frequencies consolidated. *National Bureau of Standards*, I:1–160, 1972.

[29] Pier Luigi Silvestrelli and Alberto Ambrosetti. Including screening in van der Waals corrected density functional theory calculations: The case of atoms and small molecules physisorbed on graphene. *The Journal of Chemical Physics*, 140:124107, 2014.

[30] Alexandre Tkatchenko and Matthias Scheffler. Accurate molecular van der waals interactions from ground-state electron density and free-atom reference data. *Phys. Rev. Lett.*, 102:073005, 2009.

[31] E. Bright Wilson, J. Charles Decius, and Paul C. Cross. *Molecular Vibrations: The Theory of Infrared and Raman Vibrational Spectra, Chapter 3, Sec. 3-2*. Dover Publications, 1995.

[32] Guozhen Wu. Nonlinearity and chaos in molecular vibrations. pages 1–13. Elsevier, Amsterdam, 2005.